College of Aeronautics Report No. 9402
October 1994

Design Synthesis for Swept-Wing Combat Aircraft Incorporating Stealth Technology

F.Siegers

ISBN 1 871 564 76 X

£10

The investigation which is the subject of this report was carried out under the terms of Contract FRN1c/405 for the Manager of Aircraft System Performance Department, Defence Research Agency, Farnborough

Dept.of Aerospace Technology
College of Aeronautics
Cranfield University
Cranfield
Bedford MK43 0AL
England

ABSTRACT

The College of Aeronautics has been involved in several research contracts funded by the Defence Research Agency of the United Kingdom to investigate the design synthesis and optimization of military aircraft. This report presents the results of the latest such investigation into the enhancement of a swept-wing combat aircraft design synthesis to incorporate stealth technology.

In the light of the current changes in the method of procurement of airborne weapons systems it has become necessary to develop combat aircraft which are effective against a wide range of threats whilst meeting the requirements of both navy and air force. One way of doing this is to incorporate into combat aircraft those features which make it stealthy, in other words reducing their detectability by means of radar, infrared, visual and acoustic identification methods. Although the full benefits of stealthy aircraft may only become apparent when such systems are deployed within an appropriate strategic and tactical environment, it is important to define the features inherent to the aircraft at the conceptual design stage.

This report briefly describes those features of stealthy aircraft incorporated into the design synthesis, leading to the definition of a baseline aircraft, followed by a full description of the design synthesis methodology. Finally, the development of the design synthesis computer code is outlined, rounded off by plans for future work.

TABLE OF CONTENTS

List of Figures

List of Tables

1. INTRODUCTION AND PROJECT BACKGROUND

Reductions in the levels of government spending on defence brought about in part by the ending of the cold war have forced a rethinking of the priorities behind the procurement of many military systems, including that of combat aircraft. Bearing in mind that modern versions of these types of aircraft have reached an extremely high level of complexity, the implications for both manufacturers and purchasers are far-reaching. For example, it may no longer be feasible to have at the disposal of the armed forces a large variety of aircraft each optimized or designed for a specific mission. Rather, it will become more and more common to have one aircraft type employed in a variety of roles. Also, reduced procurement budgets mean that fewer aircraft numbers will be purchased, increasing the need for systems which must reconcile the sometimes conflicting objectives of high cost effectiveness and high lethality.

One way of achieving the goal of developing highly efficient and effective airborne systems within ever tighter budgetary constraints is to ensure that a designer has at his finger tips a design synthesis tool which will allow him or her to evaluate a wide range of potential candidate solutions. The solution space defined in this manner can be used to perform trade-off studies, in which the effects of making modifications to the design parameters upon the outcome of the design can be assessed, or it may be used to choose the best possible solution for the given design requirements. The Defence Research Agency has developed such a numerical design synthesis for combat aircraft based upon aircraft state-of-the-art in the late 1970s and early 1980s (Ref. 3), and is only one of many such tools in use both in government and industry research and development institutions. As part of a wider-ranging program to maintain the technology base included in the synthesis while catering for an ever more diverse range of aircraft types, Cranfield University has been awarded a series of research contracts to undertake modifications or enhancements to the original code (Ref. 2 and 4). The current research program has as its overall objective an initial investigation and the inclusion into the design synthesis process of those features which give an aircraft low-observable characteristics, also known as stealth technology.

In the past 15 years there have been several examples of stealthy aircraft, the first of which was the Lockheed F-117 Stealth Fighter unveiled in 1988. This was followed by the first bomber designed explicitly as a stealthy aircraft, the Northrop B-2. More recently, the United States Department of Defense sponsored a competition to develop an advanced tactical fighter, the result of which was the design, construction and demonstration of the YF-22 and YF-23 by Lockheed and Northrop, respectively. Despite the impression that interest in stealth is a fairly recent phenomenon, the history of low-observable aircraft in fact goes back to the years before World War II, when aircraft designers attempted to come up with a way of defeating the then emerging threat to airborne missions posed

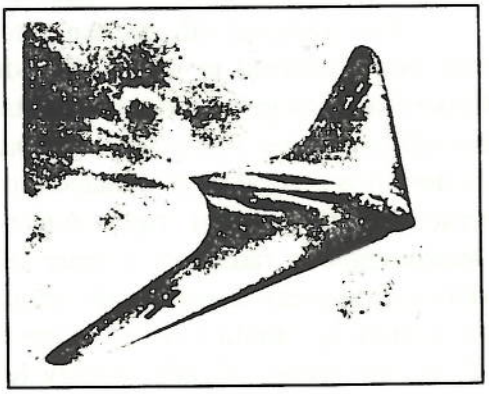

Fig. 1: Germany's Ho IX

by radar (Ref. 34). Besides using chaff, electronic jamming and beacons as countermeasures, German engineers were working on the use of radar absorbing and radar transparent materials in the construction of aircraft. A first prototype of a flying wing powered by jet engines called the Ho IX actually flew in January of 1945, but crashed after only two hours flying (see Fig. 1).

One of the problems with the design of stealthy aircraft was and still is the prediction of the radar cross section. Not until the development of computational codes based upon experience with computational fluid dynamics was it possible to accurately predict the reflective characteristics of geometrically complex objects, which allowed designers to simultaneously tailor the aerodynamic and stealthy characteristics of their aircraft at an early stage in the design. Another obstacle to the development of aircraft with unconventional shapes has been the availability of suitable design tools at the conceptual and preliminary aircraft design stages. The applicability of existing ones has generally been limited to known aircraft types, and new designs can usually be considered only in terms of extensions or extrapolations of the state-of-the-art.

Thus, for the purpose of this research program, it was decided to investigate the possibilities of modifying existing computer codes to cater for a larger variety of aircraft, whose key characteristics in addition to the conventional design descriptors will be given in Sections 1.1 and 3 below. Furthermore, an initial analysis of the validity of current aerodynamic and mass prediction methods in the conceptual design of stealthy aircraft was undertaken. This work was preceded by an extensive literature search and by the definition of the research program objectives, outlined in Sections 1.1 and 1.2 below. Section 1.2 also briefly describes the layout of this report.

1.1. Requirements of Stealthy Aircraft

A wide range of literature is available on the more general aspects of stealthy aircraft. Some books provide only a summary of the operational and technical characteristics of current stealth aircraft such as the F-117 stealth fighter (Ref. 32) or the B-2 stealth bomber (Ref. 33). The authors have usually done nothing more than to collect and compile the publicly available aircraft specification data, which does not significantly differ from that available through other references such as Jane's All the World's Aircraft (Ref. 1). Nevertheless, these references tend to be highly illustrated, offering images of the aircraft in question from a variety of viewing angles and they are thus a valuable source of information.

More detailed information can be gleaned from papers written by authors who have been involved in stealth aircraft projects. Thus, J.W. Burns (Ref. 35) and Prof. Howe (Ref. 36) give an extensive introduction to the important features which a stealthy aircraft must have. For example, in order to reduce an aircraft's reflectivity or radar cross section, it is a good idea to shape the fuselage in such a way as to avoid surfaces which present themselves at right angles to the expected direction of illumination by electromagnetic radiation. Corner reflectors, which consist of two or more surfaces joining at a ninety degree angle, should be avoided at all costs. Finally, the alignment of the leading and trailing edges of the flying surfaces is recommended so that the number of discrete spikes of radar energy reflected by the aircraft is kept to a minimum. The overall aim is not only to reduce the reflectivity itself, which can be a very difficult and, in terms of the mass of the aircraft, costly exercise, but also to direct any incident electromagnetic energy away from the receiving radar antenna.

Other important stealthy features are related to the aircraft visual, infrared and acoustic characteristics. While an aircraft's optical reflective characteristics may be relatively easily controlled by the use of appropriate paint schemes, its overall size is also an important determinant of detectability, and is usually more directly related to the outcome of the design process, which takes into account mission requirements to arrive at the projected size of the aircraft. Sources of infrared energy whose emissions intensity should be reduced or shielded are the engines including the exhaust and local heat sources such as the avionics equipment. Finally, important acoustic sources are the powerplant as well as the aerodynamic noise of the airframe itself.

While the abovementioned aspects of stealthy aircraft may be important at an early stage of the design process, a more detailed quantification of the aircraft characteristics will be needed for an effective optimization. A survey of the available literature shows that radar cross section, considered perhaps the most significant of all features related to stealth, is extremely difficult if not impossible to calculate analytically. A variety of books, such as Refs. 27, 28 and 29 as well as a plethora of papers, for example Refs. 30 and 31, are available which delve deeply into the theory of electromagnetic scattering and on methods of calculating it numerically. None of this is much good at the preliminary design stage, because on the one hand computational methods are not sufficiently fast to deal with complex codes, and on the other hand the aircraft geometry may not be known in sufficient detail. However, it can be useful at least to investigate the effects upon the optimum aircraft sizing of changing the aircraft shape to match stealthy requirements.

The development of stealthy aircraft has been justified in a number of ways, most of which share the common idea that such aircraft will be able to operate for a significantly longer period of engagement in combat without being detected by an opponent. Thus, a stealthy aircraft may be able to approach much nearer to a radar transmitter because its low radar cross section decreases the detection range while at the same time increasing the radar data processor's search volume. However, very few studies attempt to correlate the advantages and disadvantages of employing a fleet of such aircraft together with other elements in a much more comprehensive, tactical and strategic context. G. Lindsey (Ref. 37) has pointed out the various mechanisms by which the individual armed forces and the technology they employ interact with one another, and the influence of stealth on this interaction.

In a tactical context, the effect of stealth upon the operation and conduct of armed hostilities is considered quite significant. For example, reduced aircraft infrared signatures mean that the detection ranges of air-to-air and ground-to-air missiles using infrared homing devices will be reduced, making countermeasures more effective and increasing the time available to a target under threat to take evasive action. This logic applies equally to detection and tracking by radar. Also, much of an aircraft's stealthiness depends upon its operational tactics, such as low level flying or maintaining radar silence until reasonably close to the target.

The benefits seem to be less clear in terms of strategic deterrence, which depends mainly upon the portrayed ability of delivering a devastating retaliatory strike against an adversary, even after suffering a surprise first attack. Such action may generally necessitate the involvement of many different military systems in order to be effective, but the involvement of aircraft is often limited both by speed and range. Fleets of aircraft also require sophisticated logistics for their operational support, not to mention the

availability of suitable airfields, quite frequently located near the engagement area. This makes them much more vulnerable to attack than ballistic missiles, another important element of strategic deterrence. Missiles can be located either in underground, hardened silos or on nuclear submarines, which are by nature highly mobile and can remain submerged and undetected for long periods of time. In contrast to aircraft, missiles are much less likely to benefit from stealth technology because of the enormous amount of infrared radiation emitted during the launch and boost phases, which is also when they are most easily detected by satellites.

After taking into consideration the various roles of ships and aircraft as well as ballistic, cruise and short-range missiles, Lindsey concludes that effective stealth will

- cause some deterioration in the certainty of detecting a first strike,
- strengthen the certainty of retaliation from submarines,
- complicate active defence against ballistic missiles, and
- increase the probability of success for a surprise attack by aircraft and missiles.

In other words, from a tactical point of view, weapons systems which successfully employ stealth technology are a necessary addition to the inventory of the armed forces. While the strategic benefits may not be immediately obvious, they nevertheless warrant consideration during the design and development phase of the systems when the acquisition of new technology within the framework of future defence spending is being considered. It can therefore be said that the inclusion of stealthy features into the aircraft design process as early as possible has become a necessity for all military designs.

1.2. OBJECTIVES

The objectives of this research program were agreed to in consultation with the Defence Research Agency. Based upon the aircraft design synthesis code developed by David Lovell (Ref. 3), an analysis of the existing aerodynamic and mass estimation methods was to be undertaken. Its aims were to ensure that they represented the current state-of-the-art and were applicable to the types of aircraft under consideration. The results are described in Section 2.

Then, based upon the information obtained during the initial literature search, a methodology for the inclusion of features which give an aircraft stealth characteristics was to be defined and developed. Because of the difficulty of modelling aircraft emissions, no consideration was to be taken of radar cross section, infrared, visual or acoustic signatures. However, the definition of the aircraft geometry was to be undertaken in such a manner as to leave parameters which influence the aircraft emissions under the control of the designer. A resulting baseline aircraft configuration is described in Section 3. Finally, the results were to be combined into a design synthesis tool for swept-wing combat aircraft. A summary of the research program milestones and the amount of time allocated to each one is given in Table 1. Detailed descriptions of the design relationships developed during the course of this work are presented in Section 4.

Milestone	Months
Initial Literature Search	3
Assess Mass and Aerodynamics Estimation Methods	3
Define Fuselage Synthesis Method	3
Define Fin and Thrust Vectoring Synthesis Method	3
Produce Synthesis Code	3

Table 1: Summary of Research Program Objectives

2. ASSESSMENT OF PREDICTION METHODS

The accuracy of any numerical aircraft design synthesis will depend to a large extent on the validity of the relationships employed to estimate the properties of the design under consideration. Usually, the methods are derived from any one of or a combination of historical data, analytical formulae and empirical studies. Historical data is used to validate the current design in the light of past experience. Analytical formulae may be available for aircraft characteristics which are easily quantified or which are fairly simple dependencies on the design parameters. More often than not, however, empirical data must be used, obtained either from very accurate, numerical methods such as computational fluid dynamics, or from experiments, such as free-flight measurements or wind tunnel experiments, or from an analysis of existing aircraft design data. The objective is to minimize the computational effort involved in the preliminary design phase while maintaining as high a degree of accuracy and validity as possible.

In the light of this background, one of the objectives of this research program was to analyse the existing aerodynamics and mass estimation methods as presented by Lovell (Ref. 3). Using the comparison between the respective method and known data or other, tested methods, recommendations were made as to the probability of obtaining accurate results if the existing methods were to be employed for the current analysis. Also, an initial evaluation into the desirability of including more complex aerodynamic or mass estimation methods than currently available from Lovell's report was carried out. One example was the suggested use of simplified panel or computational fluid dynamics methods for the prediction of aerodynamic characteristics. However, as will be shown below, the development of alternative methods could not be justified, both because of the time frame available for this research as well as the fact that the existing methods, with a few exceptions, proved to be sufficiently accurate for the purposes of this design synthesis.

2.1. AERODYNAMICS

At the beginning of the analysis, a literature search was conducted to find experimental data for aircraft configurations to which the aerodynamics estimation methods would be applicable. Results of the search were limited to combat aircraft which had trapezoidal or delta wings and aft-mounted control surfaces. A variety of fuselage shapes were considered, ranging from circular to highly blended ones similar to those found on stealthy aircraft. The aim was to obtain a correlation between the aircraft aerodynamic characteristics and criteria which would define the stealthiness of a particular configuration without using an analysis of aircraft infrared, radar and acoustic emissions data, as well as to analyse the validity of the methods.

The experimental configurations used are described in Section 2.1.1. Some of the geometric parameters considered were ratios of fuselage fineness ratio to wing chord thickness and fuselage width to wing span. However, work on this problem was limited both by the time scale and by the insufficient availability of experimental data to provide any meaningful correlations, so that no conclusive results could be obtained.

2.1.1. EXPERIMENTAL CONFIGURATIONS

Figure 3 shows a configuration which closely resembles the one found in Lovell's report (Ref. 3), having a straight tapered wing, conventional fuselage shape, tailplane and fin. It is described in Ref. 14. The difference is mainly in the intake position, which in Lovell's design synthesis is located at the fuselage side. Also, this configuration is not area ruled. Although it is not a stealth aircraft, the configuration shown in Fig. 2 (Ref. 16) has a highly blended shape, which would be expected of aircraft designed with a low radar cross section in mind.

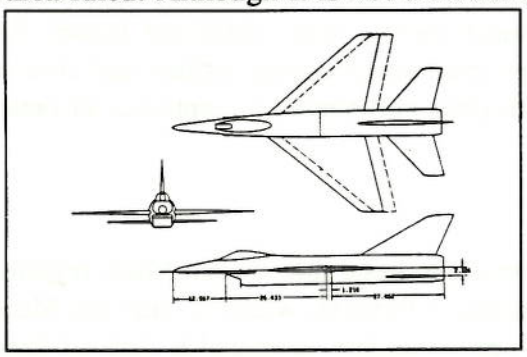

Fig. 3: NASA TM X-3078

The configuration in Fig. 4 (Ref. 15) was developed from a supersonic transport configuration and has a fairly well defined fuselage with a significant degree of blending between it and the wing. The cambered shape of the fuselage and the wing will significantly affect the aerodynamic characteristics.

Figure 5 (Ref. 18) shows a similarly blended shape, characterized by chin mounted intakes and a wing leading edge which extends

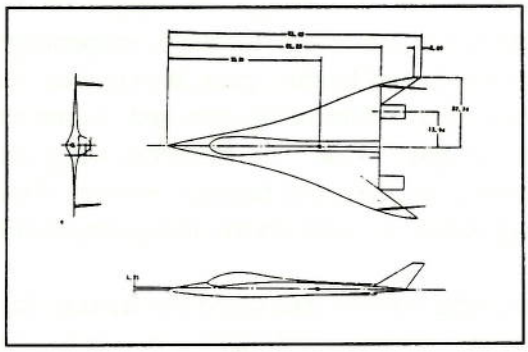

Fig. 2: NASA TM 78764

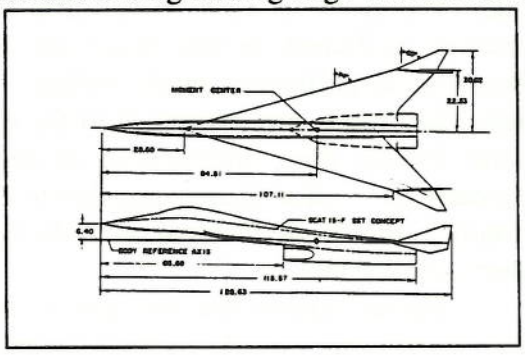

Fig. 4: NASA TM X-3530

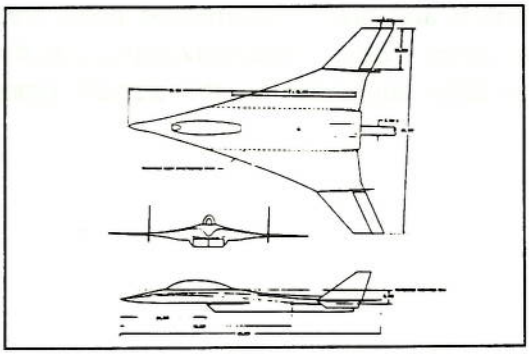

Fig. 5: NASA TM X-3559

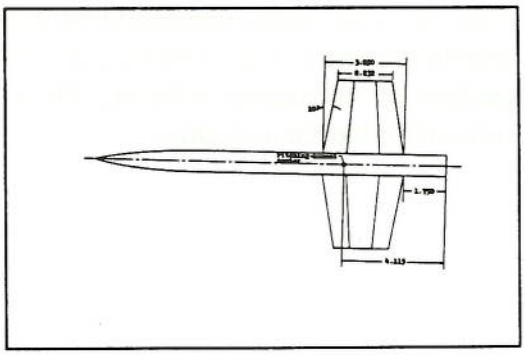

Fig. 6: NASA TN D-2236

until the nose of the aircraft. Finally, Fig. 6 (Ref. 17) is a simple trapezoidal wing mounted on a fuselage with circular cross-section.

2.1.2. ZERO-LIFT DRAG ESTIMATION

The estimation of drag within Lovell's design synthesis consists of three elements: the subsonic zero lift drag, the transonic and supersonic zero lift drag, and the drag due to lift. The drag curve as a function of Mach number is estimated separately for the major components of the aircraft, these being wing, fuselage and tailplane. Allowances are made for items such as landing gear, cockpit canopy, external stores and gun ports. The drag components are then added, assuming linear theory, with additional factors for interference between components and for losses from surface irregularities and control surface gaps and leaks. The assessment of each drag component is explained in detail below.

2.1.2.1. SUBSONIC FRICTION DRAG

This component of the drag estimation forms the basic drag for all Mach regions, including the transonic and supersonic. The estimation method, which is valid for Mach numbers of less than 0.8, assumes a fully turbulent boundary layer and is derived from Prandtl's skin friction drag formula for flat plates. It is modified using two form factors, one to cater for the Reynolds number variation across the lateral dimensions of the body and the other to account for the thickness of the body compared with a flat plate. An additional factor is used to calculate the effect of the skin roughness height on the friction coefficient. Having found the drag values for the wing, fuselage, empennage, boundary layer diverter, intake spillage, external stores and landing gear, if extended, the individual values are referenced to the gross wing area before being summed to find the total friction drag. Interference amongst aircraft parts (such as between wing and fuselage) as well as increments due to the presence of gaps and fairings between flight control surfaces are factored on to the basic drag values defined above, using empirically derived constants.

Figure 7 shows how for each of the eight configurations examined the friction drag calculated using Lovell's method compares with the experimental values. It can be seen that very good agreement exists between the experiment and the estimation without interference factors. This is due to the fact that in all cases the wind tunnel models do not contain control surfaces or other excrescences which might cause an increase in drag. Moreover, the good agreement between experiment and prediction method holds true despite the fairly wide variation in configuration types. Thus, it was concluded that the method of estimating subsonic friction drag is fully applicable to the aircraft types currently under investigation.

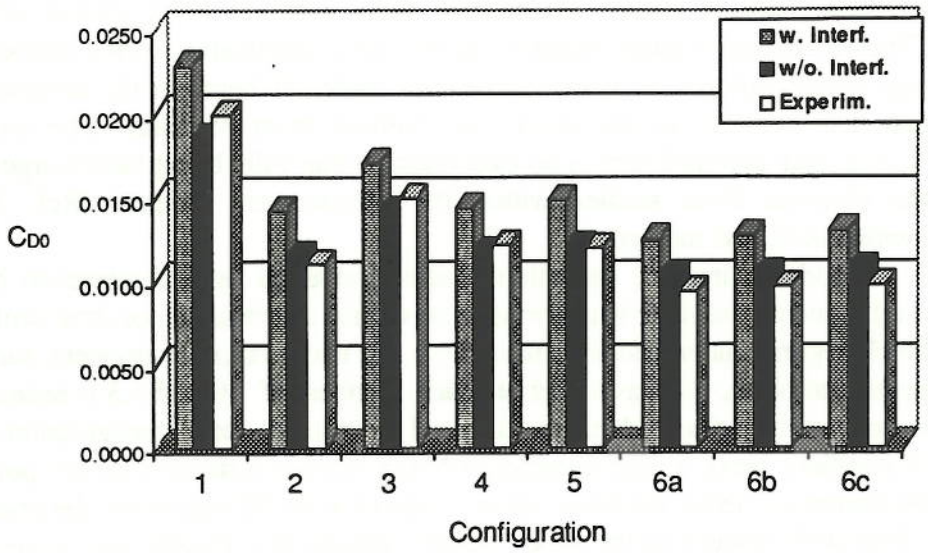

Fig. 7: Comparison of Experimental with Estimated C_{D0}

2.1.2.2. TRANSONIC AND SUPERSONIC FORM DRAG

The development of a method for the estimation of aircraft wave drag is a difficult task since the validity of the results is highly dependent upon the individual configuration. Although there are a range of wave drag theories available, they seldom apply to anything more than basic aircraft components such as bodies of revolution, as opposed to the necessity of and complications involved in catering for a realistic fuselage or even a complete aircraft shape.

Nevertheless, it is possible to identify several rules about the supersonic form drag. Firstly, if the geometry of a given body conforms to slender theory, i.e. if its cross-sectional area distribution along the longitudinal axis is a smooth curve as defined by Eminton (ref. 5), then the wave drag appears to depend only upon said distribution. Secondly, if a configuration has been shaped according to the area rule for a given Mach number, then it will have minimum wave drag only at that Mach number, but not necessarily at any other Mach number. Finally, according to Lord and Eminton (ref. 5) as well as Barger (ref. 6), there is no strict mathematical proof for the fact that the use of area ruling will result in a valid calculation of wave drag, but verification by a number of experiments has shown that application of this method is usually successful in further reducing the wave drag of a given configuration. In theory, then, the wave drag of a slender aircraft can be calculated by considering the wave drag of an equivalent body of revolution.

Despite the availability of this apparently relatively simple method of wave drag estimation, most handbook methods to be used for conceptual design, i.e. DATCOM (Ref. 7) or Nicolai (ref. 22), rely on methods derived from experimental data correlated with major aircraft geometric parameters. More often than not, they are valid for a

certain, well defined class of aircraft rather than being available for a general aircraft design case. Therefore, great caution must be used in their application to the conceptual and preliminary design process, in which a constant trade-off between the accuracy of calculation and the simplicity of the estimation method must be made. The method proposed by Lovell and analyzed here is no exception to that rule, being based largely on empirical data obtained from studies within the Ministry of Defence (Ref. 3) in combination with DATCOM methods.

Lovell's method requires the definition of drag values at several reference Mach numbers through which a curve fit is undertaken to obtain the variation of drag with the rest of the Mach regime under consideration First, for each major component such as wing, fuselage and tailplane, the wave drag at Mach numbers of 1.0 and 1.3 is estimated. Thereafter, the component drag values are summed to give the total configuration drag at these Mach numbers. Next, a drag divergence Mach number is defined for the point at which the drag increment above the basic value at M=0.8 is 0.002 and where the gradient of the wave drag with respect to the Mach number equals 0.1. Finally, the wave drag above Mach=1.3 is assumed to remain constant. Using the values thus defined in combination with an estimation of the gradient of the drag curve at M=1.0, a cubic variation is assumed between the drag divergence Mach number and M=1.0. From M=1.0 to M=1.3, an empirically derived formula is given.

The analysis of the above method was begun in a manner similar to the analysis of the subsonic drag. However, it was soon found that its application to the experimental configurations would be very difficult due to the fact that Lovell derived his method by using aircraft geometric parameters not available from the experimental configurations. For example, calculation of the fuselage wave drag required knowledge of the cross sectional area distribution, which was available only from one of the configurations. Also, a knowledge of the intake stream tube geometry for the calculation of the maximum net cross sectional area is required. Even if an attempt had been made to derive this information from the aircraft drawings, considerable inaccuracy would have to have been accepted.

Not least because of the limited time available to complete the analysis, it was decided to try a slightly simpler approach to validate the curve fitting method for the sum of the component drag values between the drag divergence Mach number and M=1.3. Firstly, using Lovell's method of calculating supersonic friction drag, described in the previous section, the supersonic wave drag increment of the models was estimated by subtracting the subsonic, calculated value from the experimental, total supersonic drag. Figure 8 shows the result of this analysis.

It can be seen that the aircraft in NASA TM X-3078 (ref. 14) and, to a lesser extent, NASA TN D-2236 (ref. 17) have a very strong drag peak as compared with the other configurations. Also, the lack of experimental data for several models at transonic Mach numbers should be noted.

The next step in the analysis consisted of estimating the total aircraft wave drag using the curve fitting methods proposed by Lovell. To do this, the drag values at M=1.0 and M=1.3 were extracted from the data, which was only possible for NASA TM X-3078 and NASA TM X-3559 (Ref. 18). The results are plotted in Figures 9 and 10, respectively. For NASA TN D-2236, it was possible to linearly interpolate between M=1.1 and M=1.4 in order to obtain a value for M=1.3.

It can be seen that a good fit is obtained for NASA TM X-3559, whereas for NASA TM X-3078, the estimation is considerably in error. This is assumed to be a result of the fact that the area rule was not used for the design of the model in NASA TM X-3078 as opposed to NASA TM X-3559. Although not shown, the results for NASA TN D-2236 are similar to NASA TM X-3078. This configuration also has a wing-body configuration which has not been area-ruled. A similar analysis for the other configurations was not deemed possible, due to the lack of data at transonic and low supersonic speeds.

Based upon what has been said above, it is safe to conclude that there was not enough data available to obtain any meaningful results about possible modifications to the methods proposed by Lovell. The assumption of constant wave drag at Mach numbers greater than 1.3 is correct, but it holds true only for area ruled configurations. In addition, some of the methods described in Lovell's report are derived from DATCOM, which itself is based upon a large-scale study of available data coupled with the relevant theory, and therefore may be considered valid. In summary, although the experimental data used to derive Lovell's method is most likely valid, caution must be used in applying it because it is based upon a class of aircraft not known to the author.

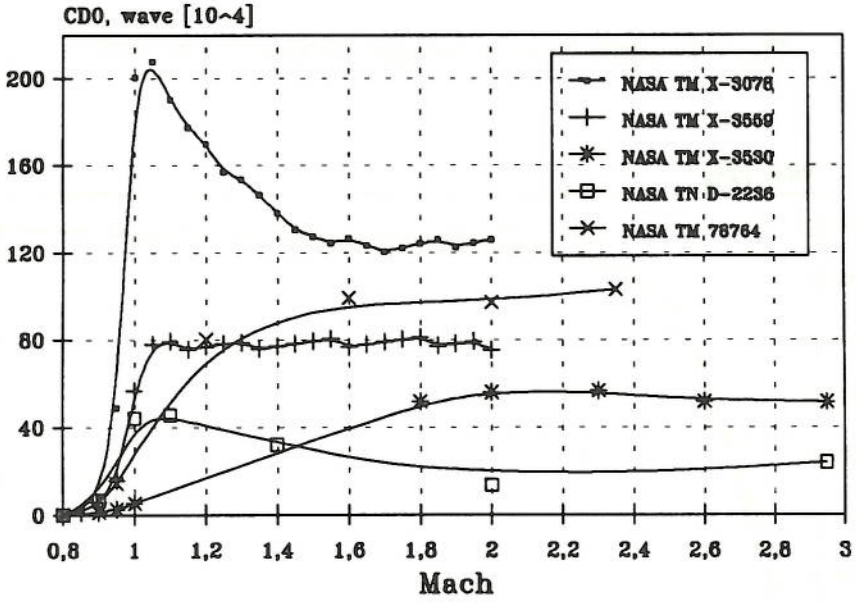

Fig. 8: Comparison of Experimental Wave Drag

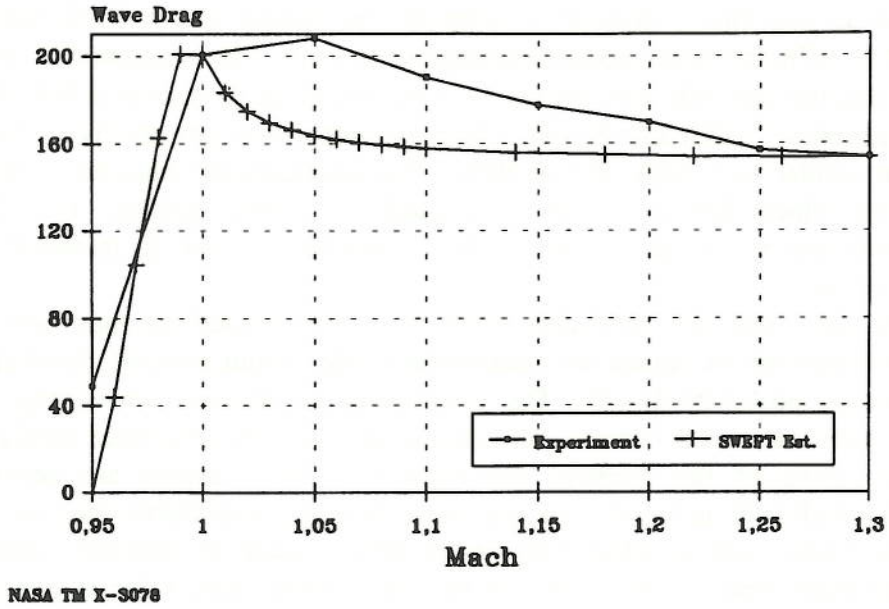

Fig. 9: Experiment vs. estimation, NASA TM X-3078

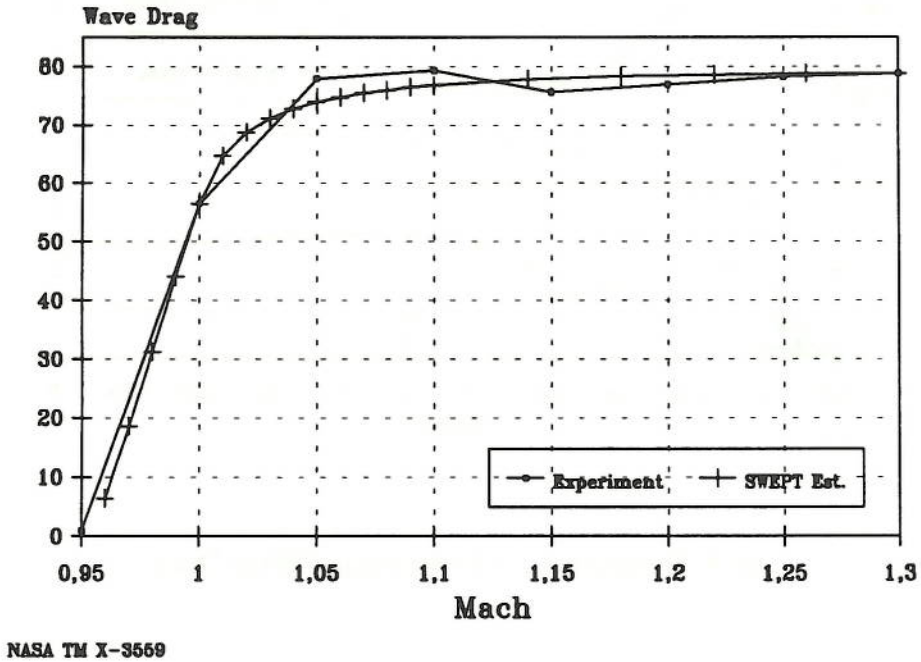

Fig. 10: Experiment vs. estimation, NASA TM X-3559

2.1.3. LIFT-DEPENDENT DRAG ESTIMATION

The drag due to lift in the design synthesis by Lovell (Ref. 3) is assumed to have a parabolic shape. The curve is defined by three parameters: two factors, K1 and K2, which govern the shape of the parabola and a critical lift coefficient, CLC, which determines the point of transition between the two regions of the drag polar. The transition region is determined by fitting a cubic to the values of the drag polar at points slightly above and below the critical lift coefficient.

The factor K1 was derived empirically from a series of curve fits to aerodynamic data, as described by Lovell. It is estimated separately for subsonic ($0.8 \leq M$) and supersonic ($M \geq 1.20$). In the subsonic regime, K1 is dependent upon the quarter-chord sweep of the wing, the aspect ratio and taper ratio of the gross wing as well as the wing thickness-to-chord ratio. In the supersonic regime, K1 depends upon the trailing and leading edge sweep angles, the Mach number, the taper ratio and aspect ratio of the gross wing, the mid-chord sweep, the geometric mean chord and the distance between the mean quarter-chord point of the tail and the mean quarter-chord point of the wing. The factor K2 and the critical Mach number are provided to the synthesis code in tabular form and are valid only for a given class of aircraft.

In the initial analysis of Lovell's method, the aforementioned geometric parameters were extracted from the model configurations available in the reports. The drag polars for selected Mach numbers were then calculated and compared with the experimental results. Figures 11 and 12 below show a few of these correlations.

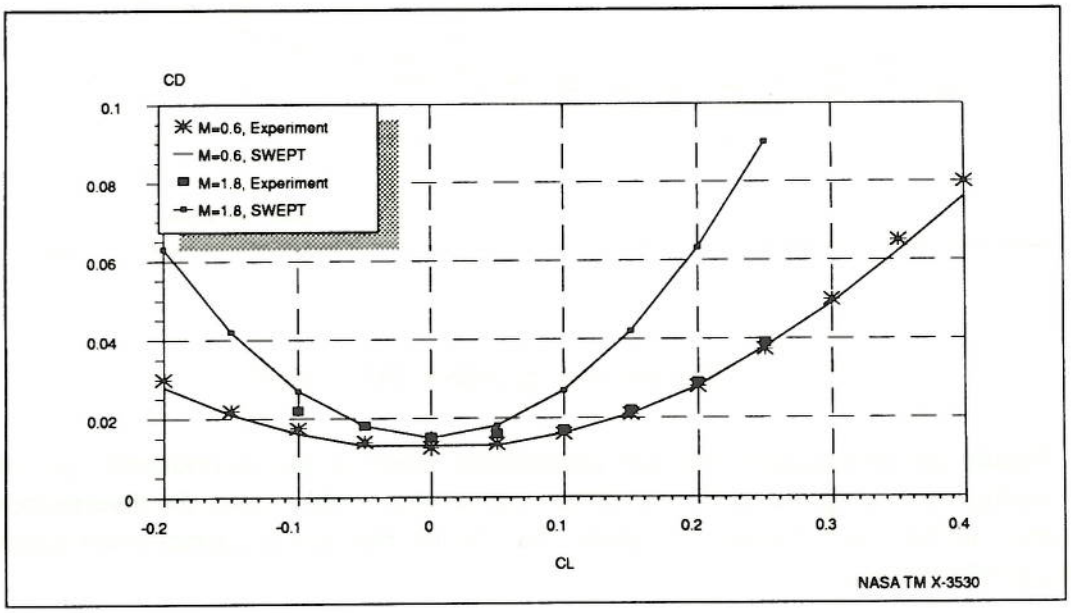

Fig. 11: Drag due to Lift, NASA TM X-3530

Three conclusions can be drawn from this investigation. First, at Mach numbers less than 0.8, the subsonic regime, Lovell's method appears to underestimate the drag due to lift. Second, at supersonic speeds greater than M=1.2, the drag values at lifting

conditions are overestimated. Finally, it appears that, at transonic conditions, particularly at Mach numbers close to 1.0, Lovell's method provides good estimations of the drag polar.

It must be noted that the aspect ratio of the wing has a similarly direct effect upon the shape of the estimated drag curve. Therefore the extraction of this geometric parameter must be handled with care if the introduction of errors into the regression is to be avoided.

An additional source of uncertainty lies in the estimation of the critical Mach number and the factor K2, both of which are provided to the synthesis code in tabular form versus Mach number. These factors are provided based upon assumptions relating to a particular class of aircraft, which unfortunately are not referenced in the report. In the absence of further information, it must be assumed that they are correct.

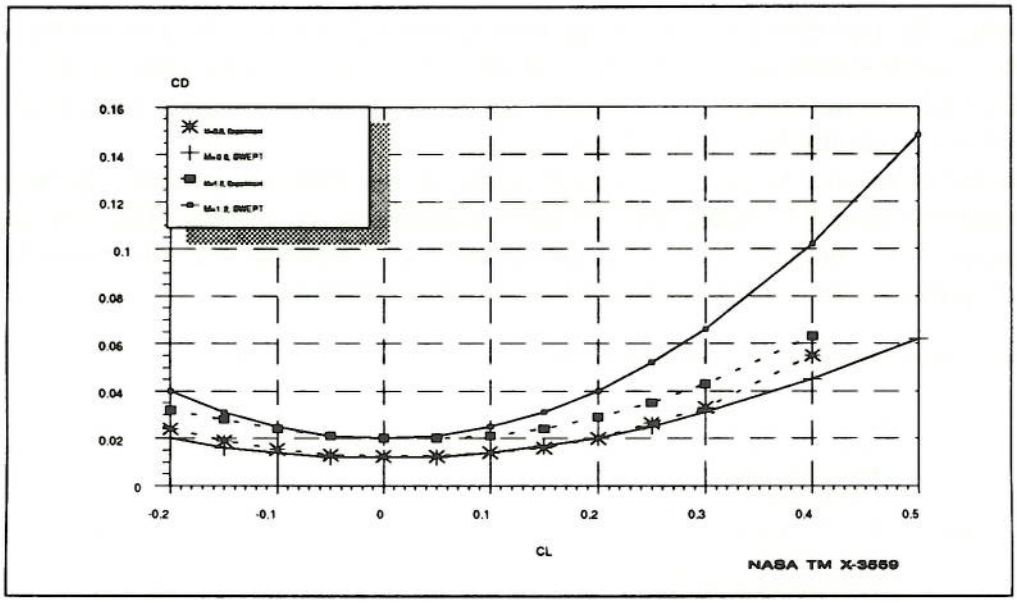

Fig. 12: Drag due to Lift, NASA TM X-3559

Finally, an investigation into the interference effect of the components upon the total configuration drag due to lift should be made as this could explain the divergence of the curves in the above figures. It appears that the interference is currently not catered for in Lovell's method.

2.1.4. LIFT ESTIMATION

The estimation of aircraft lift is divided into two parts: the estimation of the variation with Mach number of the slope of the lift curve as a function of angle of attack at zero lift, and the prediction of maximum lift. Whereas the former is calculated using methods developed by Lovell, the latter is provided to the design synthesis in tabular form as external constants versus Mach number. According to Lovell (Ref. 3), the original proposal of using DATCOM methods for the prediction of maximum usable lift

was discarded after a correlation and comparison with data from real combat aircraft produced undesirable results.

The estimation of the lift curve slope is based on the assumption that it is linear in the angle of attack range in which aircraft performance will be evaluated. For the purposes of this investigation, this premise was retained, since the investigation of maneuverability, specifically at high angles of attack in the non-linear part of the lift curve, was not a requirement of this research program. In Lovell's method, the lift curve slope is calculated for the zero-lift condition as a function of Mach number separately in the subsonic, transonic and supersonic regimes. In order to ensure a match between the three areas, the subsonic and supersonic lift curve slopes are used to determine a cubic fit for estimation of the lift in the transonic regime. Initially, a critical Mach number is defined for the point at which the wing leading edge becomes supersonic. The values of the lift curve slope at this Mach number and at M=0.8 as well as the respective gradients at these points are used to fit the abovementioned cubic, using Skrobanski's method (Ref. 21).

The subsonic lift gradient, at Mach numbers less than 0.8, is estimated by first calculating the gradient for the airfoil section using a DATCOM method (Ref. 7), and then calculating the aircraft lift curve slope using a formula given by Lovell, the origin of which is not known. For the supersonic regime above the critical Mach number, linear theory is used to estimate the lift curve slope.

The analysis of Lovell's method has again concentrated on a comparison of empirical estimations with experimental data available from the references. A few of the results are shown in Figure 13.

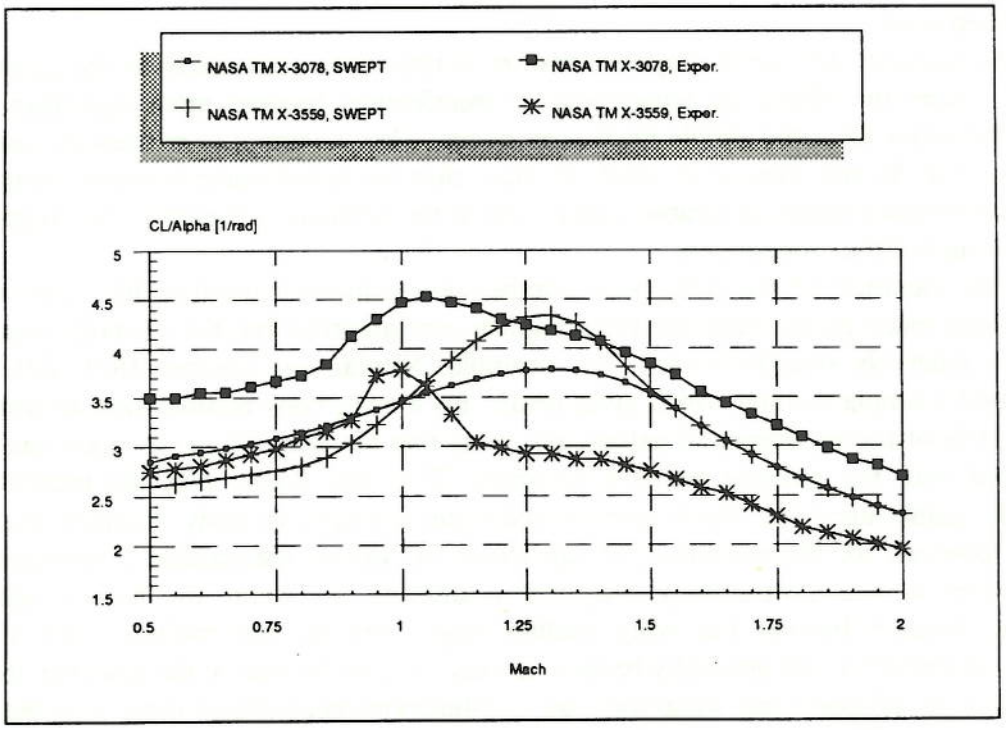

Fig. 13: Gradient of the Lift Curve vs. Angle of Attack

The comparison shows that the method given by Lovell is completely inadequate for a reasonable prediction of the lift characteristics of a swept-wing combat aircraft. Only in the subsonic regime is there a result which could be adapted to a new method by the inclusion of a factor to cater for the differences in geometry of the trial configurations. In fact, the correlation of a configuration in NASA TN D-2236 conforms nearly exactly to Lovell's method. The inclusion of a tailplane in the experimental investigation of NASA TM X-3078 causes a considerable divergence in the lift curve slope values as compared with Lovell.

In the supersonic regime Lovell's estimations are very inaccurate. This is due primarily to the shortcomings of linear theory, which is valid for the two-dimensional case of a wing alone. Schlichting and Truckenbrodt (Ref. 19) show how the supersonic lift curve slope of a three dimensional wing can indeed be approximated by linear theory, however only for relatively slender wings and at Mach numbers such that the wing leading edge is supersonic. For Mach numbers less than the critical Mach number a factor is defined which is a function of Mach, wing leading edge sweep and gross wing aspect ratio to correct the lift curve slope.

Due to the inadequacy of the linear theory, the cubic fit for the transonic region is also significantly in error. Apart from not following the shape of the experimental curve, the peak value for the lift curve slope is also predicted to be much greater.

In summary, then, it can be said that Lovell's method of estimating the lift curve slope as given in Ref. 3 is insufficient because it applies the wing lift alone to the entire aircraft and is really valid only for lower subsonic or higher supersonic speeds as well as low angles of attack. The configuration should also have a large wing when compared with the fuselage. Also, the effects of a tailplane upon the lift curve slope are not considered at all.

An accurate lift curve slope estimation is important particularly in the transonic region, where the effects of wing-body-tail interference become more significant and large deviations from the simple model can occur. Also, a variety of references, such as Nicolai (Ref. 8) and Pitts et.al. (Ref. 9) state that the interference between wing and body can produce quite favourable effects, that is the combined lift curve slope is greater than the sum of the components.

Consideration of the wing-body combination alone will produce lift curve slope estimations much greater than for the complete configuration, but the methods available are also relatively straightforward. For example, Nicolai and Sanchez (Ref. 22) have developed a simple method which gives results for a wing-body combination accurate to within 10% of the experimental values, assuming that the wing lift curve slope has been estimated with the greatest possible accuracy. They also found that the interference depends mainly upon the Mach number and upon the ratio of body diameter to wing span. However, for the estimation of supersonic lift values, the method is restricted to those cases in which wing-body carryover is present, i.e. where the body extends a suitable distance beyond the wing trailing edge. Because the trailing edge of the horizontal stabilizer will generally be located very close to the rear of the fuselage, the lift estimation of tail-body and wing-body-tail combinations necessitates more detailed data on supersonic lift when no tail-body carryover is present. Ref. 10 provides some information about this problem.

While wing-body and tail-body lift carryover have only a small influence on the overall lift, the major influence on wing-body-tail lift curve slopes is the interference

between wing and tail. First, the downwash generated by the wing causes unfavourable angles of attack at the tailplane, reducing its effectiveness. Second, the vortices shed by the wing tips will also cause significant interference with the tail flow field. Small ratios of wing span to tail span will exacerbate this problem, as will the aerodynamics at higher angles of attack because the vortex will tend to move inboard. A tail that was not in an area of wing vortex influence at low angles of attack may find its airflow disrupted as the aircraft pitch attitude increases.

The method presented in DATCOM (Ref. 7) is based upon a consideration of the abovementioned interference effects. After quantifying the lift of wing, fuselage and tail separately, the individual interference effects between wing and body and tail and body are considered. Finally, the interference effect between wing and tail is catered for by including an estimation of the effect of wing downwash and vortex flow upon the tailplane. If the ratio of wing span to tail span is large enough, this latter effect may be small enough to be disregarded.

One of the limitations to the DATCOM method is that the estimation of fuselage lift applies only to fuselage shapes with a more or less circular cross section. In most cases, a stealthy aircraft may have a non-circular cross section. Refs. 11 and 12 give some guidance for simple modifications applicable to such bodies. Erickson and Brandon (Ref. 11) found that the addition of chines to a circular fuselage does not significantly affect the lift curve slope at low angles of attack. At angles of attack greater than 10°, the chines will give higher lift curve slopes while at the same time increasing the instability in pitch.

Jorgensen (Ref. 12) carried out measurements on bodies of non-circular cross section and presents some simple correlations of the lift of a body with a given width to height ratio to a body with a circular cross section. In general, with rising width to height ratio the lift also increases. However, the circular body generally has the lowest zero lift drag. This is attributed to its lower wetted area when compared with the bodies with non-circular cross section as well its higher proportion of laminar flow.

During the course of the investigation into suitable lift curve slope estimation methods, two questions were addressed. One, would the method be sufficiently simple to implement in a numerical design synthesis of the type demanded by this research program? While a certain degree of accuracy is desired, a highly complicated calculation would mean a corresponding rise in computer code complexity and hence computation time. Since the total computation time for the design synthesis is to be kept as low as possible, the available resources need to be divided more or less equally among several tasks, and a given estimation method should not take up the greatest share.

The DATCOM method, probably one of the most accurate methods available for conventional configurations, proved to be fairly cumbersome to implement numerically, since a significant portion of the data must be read from graphs. On the other hand, the method of Nicolai gives fast results for wing-body combinations having lift-carryover, but is not necessarily applicable to tail-body combinations, let alone complete aircraft.

The difficulty of deciding between a simple and a more complex method based upon their respective merits alone led to the second question: does the significance of the lift curve slope for the preliminary aircraft design process warrant a sufficiently detailed and complex estimation? In other words, how important is the accuracy of the lift curve slope estimation for the overall design synthesis?

A closer look at Lovell's report showed that the lift curve slope is employed extensively in the performance analysis of the synthesized aircraft. Its first application is in an iteration to find the maximum usable lift and the angle of incidence that the aircraft can sustain under full power, for example during combat turns. The maximum angle of incidence is used to estimate the maximum sustainable normal acceleration, in a second iteration. Finally, in a third iteration, the lift curve slope is used in determining the mass of fuel required for a given leg. This can be considered the main part of the sortie analysis, since the results of the fuel calculation for each leg to be flown are used to find the total mission fuel and to perform a variety of further aircraft performance analyses. These include the field performance, sustained turn rate, attained turn rate, specific excess power, acceleration at constant altitude, and ride quality. Of these, the calculations of the attained turn rate and the ride quality both make direct use of the lift curve slope, while the angle of attack figures in most of the other calculations.

The use of the lift curve slope forms an important part of the overall optimization routine. Its value is used extensively in the estimation of aircraft performance, in particular those elements related to the aircraft mass, and the convergence of the optimization is directly influenced by the accuracy with which it is calculated. Therefore, it is surprising that such little effort went into the development of a method for the estimation of the lift curve slope, particularly in the light of the complexity of some of the other aerodynamic calculations in SWEPT. In order to recommend solutions for possible implementation in the SWEPT design synthesis, a more detailed analysis of existing methods was carried out and compared with some experimental results.

Fig. 14 shows a comparison of experimental results from a report by Dollyhigh (Ref. 14) with results obtained by applying the DATCOM method to the estimation of the wing alone lift curve slope and using the method of Nicolai to find the wing-body lift curve slope. Fig. 15 shows the same calculation, but using the DATCOM method for the prediction of the wing-body combination lift. It can be seen that the two methods produce similar results. This is not surprising, since both rely in part upon data and methods produced by Pitts et.al. (Ref. 9).

An estimation of the wing-body-tail lift curve slope was also attempted. This proved to be a very difficult task, and due to the limited time scale it could not be completed. For all subsonic Mach numbers, the calculations are fairly simple, but for supersonic Mach numbers they are much more complicated. An examination of the work done by Serghides (Ref. 4) showed that he also replaced the SWEPT method with the DATCOM method, but he stayed away from the wing-body-tail problem, preferring to implement his own version after an analysis of aerodynamic data relating to Canard-Delta configurations.

Fig. 16 shows another example of a lift curve slope estimation done using the method of Nicolai. The correlation is very good. This is thought to be due in part to the well defined geometry of the experimental configuration, which consists of a trapezoidal wing joined to a body of revolution (Ref. 17).

For the purposes of implementing a suitable lift curve slope estimation method, it is suggested that the DATCOM method be adopted for the prediction of the wing lift curve slope. The method of Nicolai and Sanchez could easily be implemented in the form of a curve fit to the charts given in Ref. 22 in order to predict the wing-body interference effects. The calculation of the tail-body interference effects would need further investigation, because the data given in DATCOM and also by Nicolai are valid only for

those instances in which wing-body or tail-body lift carryover is present. Finally, the problem of predicting the interference between wing and tail needs to be investigated further, possibly by examining experimental data or by attempting an implementation of the DATCOM method. The advantage of this approach is that maximum use can be made of existing, proven methods while new developments need only to be done in very few areas. Nevertheless, these developments would require a significant amount of work to be implemented.

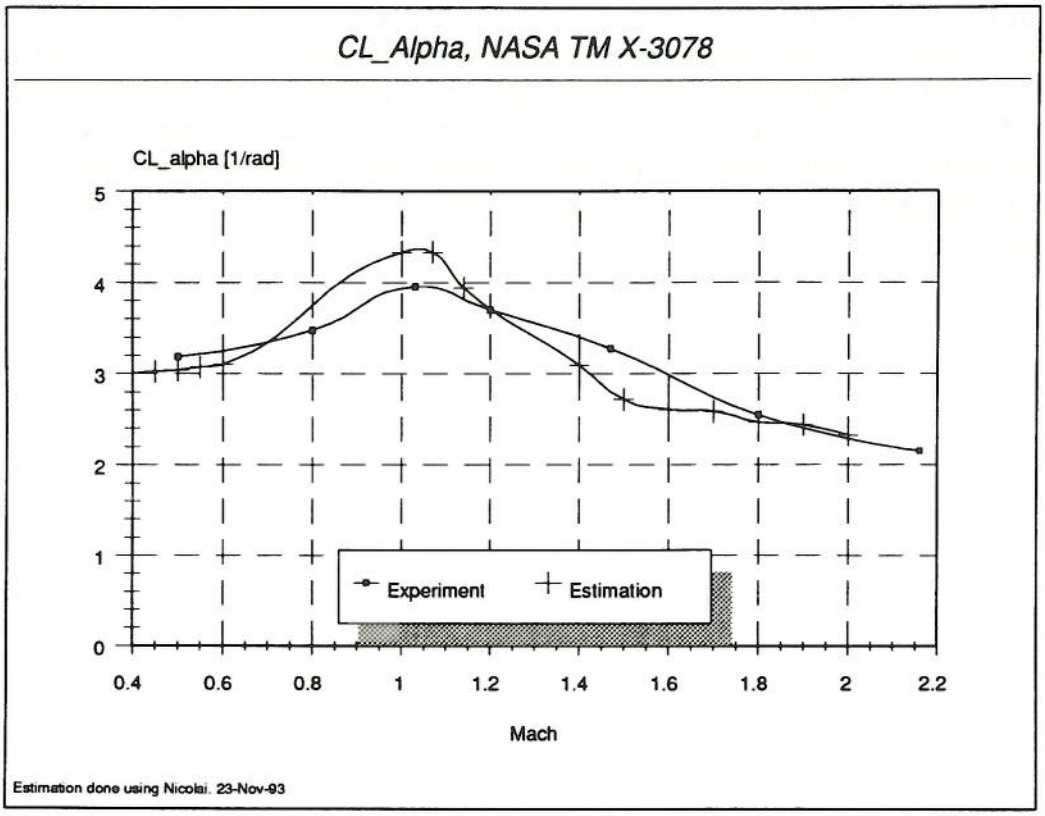

Fig. 14: Lift Curve Slope Estimation using Nicolai

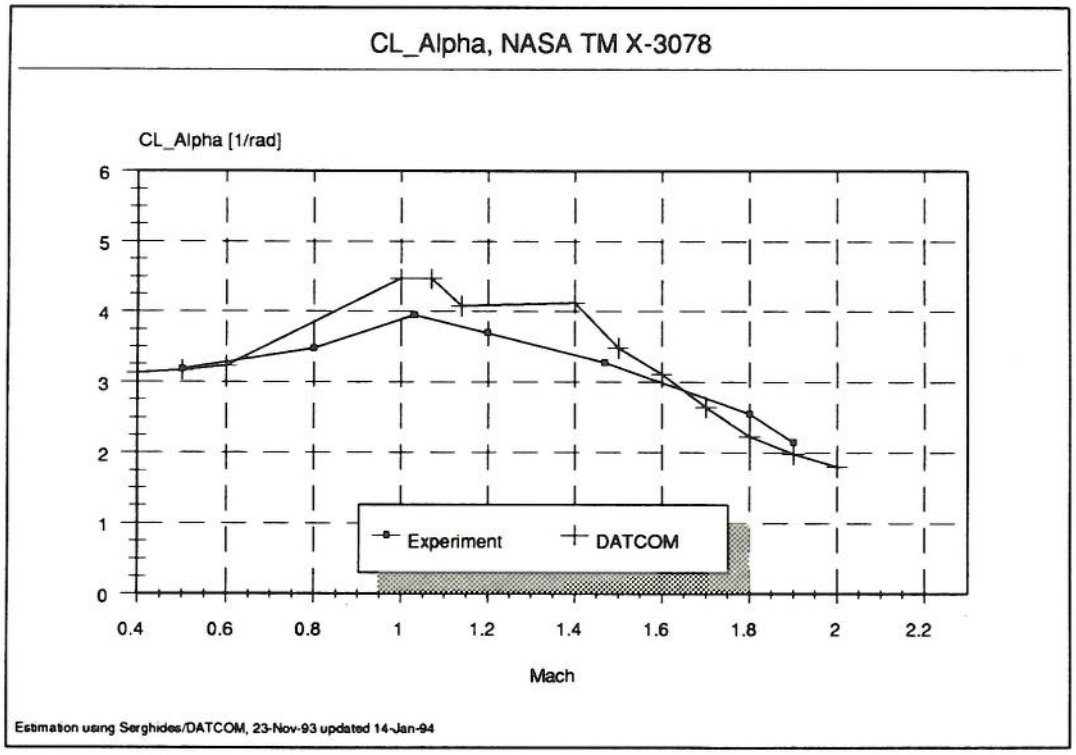

Fig. 15: Lift Curve Slope Estimation using Serghides/DATCOM

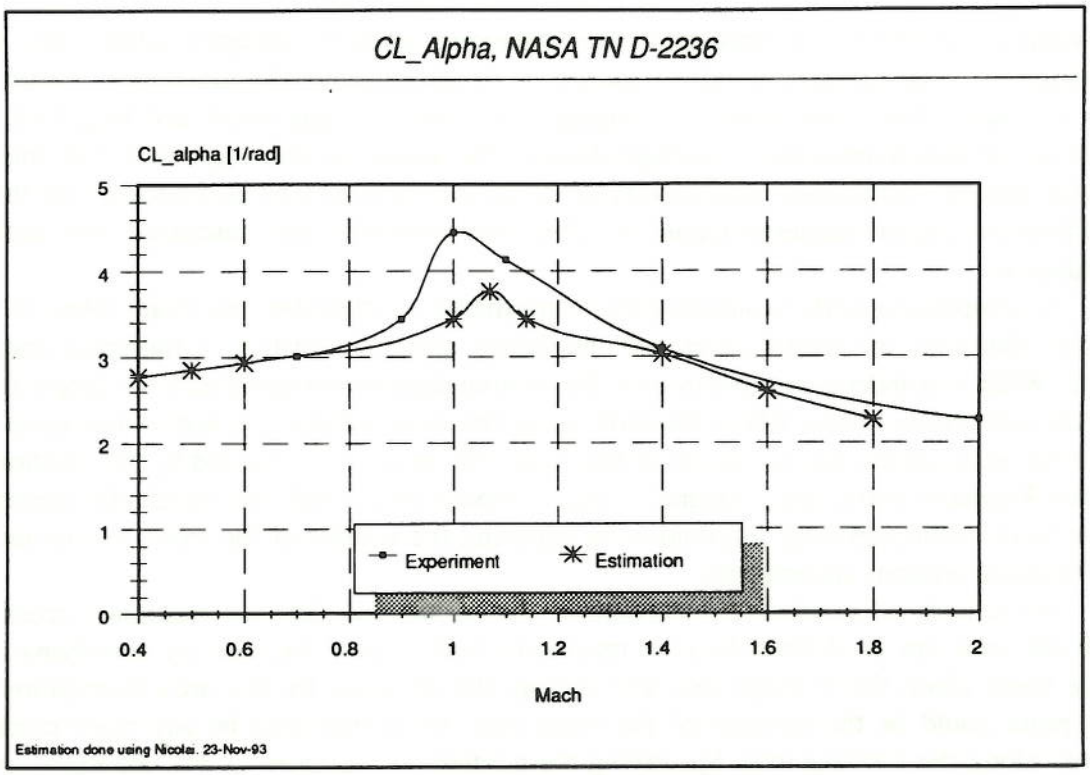

Fig. 16: Lift Curve Slope Estimation using Nicolai

2.1.5. FAIRING CURVE ANALYSIS

The fairing curve is a mathematical description of the longitudinal distribution of cross-sectional area and is designed to ensure a continuous value of the first and second derivatives. It is defined by several independent variables[1] which essentially describe a forebody, a centre section with constant cross-sectional area, and an afterbody using their respective fineness ratios, as well as a radome section, this latter item having a fixed geometry.

In order to determine the maximum cross-sectional area, the independent variables describing the forebody are used in conjunction with the cross-sectional area at the rear of the radome as well as the gradient of cross-sectional area with respect to the fuselage longitudinal axis to define a cubic function. The maximum occurs at the rear of the front section. The point at which the increment in fuselage cross-sectional area is one-half of the total increment is defined as a ratio to the length of the front section minus the radome. The rear section is similarly described by its foremost point and the point at which the decrease in cross-sectional area reaches one-half the total decrease. Thus, the shape of all three sections and in particular the maximum cross-sectional area are defined mainly by the lengths of the first two parts of the fuselage: the radome and the front section.

During the course of the analysis several questions were asked: does the mathematical description described above conform to a minimum drag area distribution

[1]Independent variables are put at the disposal of an optimization routine and may be varied in order to achieve a minimum of a given objective function. For more details see Ref. 3.

and what is the effect of a variation in each parameter upon the design relationships, in particular the mass prediction and the estimation of aerodynamic characteristics? Finally, does the method of transforming the required area into fuselage width and height at a given station lead to reasonable fuselage shapes? The answer to these questions provided insights into the functionality and validity of the fairing curve as well as guidelines for the modification and/or implementation of alternative methods for describing the area distribution.

A comparison with minimum area distributions as described by Sears (Ref. 20) showed that only in specific cases will the fairing curve conform to a minimum drag shape. While it is indeed possible to describe an area distribution using only the length of a body and certain points whose location along the longitudinal axis and whose cross-sectional areas are known, the shape of this body will be uniquely defined by the solution to von Kármán's wave drag integral. Thus, it would be possible to match the fairing curve to the minimum drag distribution by adjusting the lengths of the front, centre and rear fuselage sections accordingly.

For a body of revolution according to Sears, we find that the maximum cross-sectional area can be defined both in magnitude and in axial location by specifying a single point along the fuselage axis and solving the equation for the area distribution. This point could be the position of the radar dish, yet it may also be any other cross section along the fuselage axis. Specifying the gradient at that point is not necessary, as this computation is implicit in the solution of the minimum drag integrals. In analogy to this simple case of a minimum drag body with given length and whose area curve passes through a given point, it is possible to define several points along the body axis and therefrom find the area distribution which gives minimum drag. However, this calculation involves the solution of a set of integral equations, and the solutions are not given by Sears.

Although Lovell (Ref. 3) gives no background information as to the origin of the fairing curve, the most likely reasons for describing the area distribution as a series of sections whose lengths can be varied seem quite clear. Firstly, the definition of a centre section with constant cross section seems to conform to a large number of combat aircraft designs whose fuselage cross sections are either circular, rectangular or of some intermediate shape such as rectangular with rounded corners. The provision of area ruling in SWEPT is then achieved by subtracting from the fuselage cross-sectional area the cross-sectional area of the flying surfaces.

Secondly, the estimation of the wave drag and of the mass depends upon the fineness ratios of the various sections. The wave drag estimation is accomplished in part by considering the effects of the forebody on the afterbody and by considering the effects of truncating an initially defined, equivalent, pointed afterbody. For each section, the respective fineness ratio of length to diameter is used in the drag estimation. In accordance with linear theory, a reduction in wave drag within limits can be achieved by increasing the fineness ratio. Thus, during the optimization process the aircraft should tend to become longer and/or thinner.

This trend is counteracted by the mass of the aircraft, which will tend to increase with aircraft length. The main factors other than the design speed affecting the mass estimation are the length and width as well as the surface area and internal volume of the fuselage. While an increase in length also increases the fineness ratio and hence may reduce the wave drag, the corresponding increases both in surface area and in volume

will tend to increase the mass of the aircraft. Other factors affecting this optimization are the skin friction drag, which increases with increasing surface area but decreases with increasing Reynold's number, and the geometry of the flying surfaces, especially if their cross-sectional area is subtracted from that of the fuselage.

Finally, the provision of a large number of independent variables for the mathematical definition of the fairing curve provides the design synthesis with a very flexible method of finding the area distribution which, in order to satisfy the theory, must have a continuous value for the second derivative. It is clear that, in order to achieve a reasonable fuselage shape, the designer must provide a good initial estimate of the independent variables defining the curve.

It has been mentioned by J. Kirk of the Defence Research Agency (DRA) that he felt a definition and optimization of the cross sections based upon width and height rather than purely cross-sectional area would be more appropriate to the design process. According to his evidence, use of the optimizer will occasionally tend to produce designs which have excessive cross-sectional area at positions along the fuselage length where they should not, in theory, occur. In other words, the given cross sections are forced to fit a defined area distribution. Therefore, the detailed analysis of the methodology as given by Lovell was a prerequisite to the redefinition of the fuselage cross sections. The author feels that the failure of Lovell's method to produce reasonable fuselage shapes is the result of the procedure employed.

In order to define a cross section for the fuselage, the dimensions at a given fuselage station are fixed by certain minimum values. For example, the minimum width for the fuselage station located at the pilot's design-eyepoint may be fixed by the minimum cockpit width as specified in MIL-STD-1333B and MS33574 (Refs. 23 and 24). From these minimum dimensions, a minimum allowable cross-sectional area is defined. This area is compared with the required value, obtained from the fairing curve. By dividing the required area by the minimum area and forming the square root, a factor is derived by which the minimum width and height are multiplied to obtain the desired dimensions. Essentially, a scaling process based on the cross-sectional area ratios is carried out.

There are three problems with this procedure. The first is that, for some stations, the ratio of width to height is given by the minimum dimensions, while at other stations, one of the dimensions is scaled from a minimum while the other is calculated from the required area. This transformation of an area into a linear dimension does not take into account the desired ratio of width to height. For example, if the required area is used to first calculate the fuselage width, the corresponding height must be derived from an expression satisfying not only a number of geometrical constraints but also driven by so-called area factors. The combination of large numbers of variables does not seem to be a very robust method of calculating the dimensions at a given station. In some cases, an excessive height may result, while in other cases, the area ruling by removal of the flying surface areas leads to extremely small fuselage heights.

The second problem seems to have been unwittingly built into the design process. In some cases, the scaling of the cross sections is based upon a gross area, while in other cases only the net area is used. As an example, the scaling factor for the fuselage cross section at the pilot's eyepoint is determined after subtracting the canopy area from both the minimum and the required dimension. The reasoning seems to be that the canopy area must remain fixed and therefore should not be scaled. At the subsequent cross

section, however, no account whatsoever is taken of the canopy and the dimensions are simply scaled using the width and height of the section, ignoring the canopy dimensions.

Finally, the method of defining the area curve itself seems to be a significant source of distortions. The only cross section which is essentially fixed throughout the design process is the radar dish. In combination with the engine nozzle, which defines the base area, the independent variables defining the fairing curve determine the maximum cross-sectional area. If this combination produces an excessively high maximum, then the cross sections fitted to the curve will be excessively scaled. Finally, if the cross-sectional areas of the flying surfaces are subtracted from those of the fuselage, the result may be some highly unusual fuselage shapes. The problem with the method is that each iteration, during which the shape of the fairing curve may be adjusted to fit the aerodynamics or mass estimations, does not take into account the amount of scaling on the cross sections during the previous iteration.

The following conclusions can be drawn from the above analysis:

- The fairing curve as defined in the SWEPT design synthesis is not, in general, an area distribution for a minimum drag body. However, the method results in continuous second derivatives, and therefore meets a requirement of the supersonic slender body theory.
- The fairing curve, by appropriate choice of variables, can be made to approximate a minimum drag area distribution.
- A bad choice of the independent variables in combination with inappropriate minimum dimensions will lead to excessively large or distorted cross sections.
- The only driver for the independent variables defining the fairing curve are the results of the aerodynamics and mass estimations. The aerodynamics modules should tend to drive the area distribution towards that for minimum drag.

It can be seen that the problem of initially specifying and subsequently optimising the area distribution is no simple task and may well require a significant amount of research to arrive at a satisfactory solution. Several avenues of approach are suggested:

One would be to carry out a design analysis of existing combat aircraft by deriving area distributions from drawings or other sources. The existing fairing curve would be compared with the obtained data, which could be used either to define area distributions for a given design goal or to derive a standard area distribution as the basis for all designs.

Another approach would involve a redefinition of the fairing curve based upon a minimum drag distribution of cross-sectional area. The existing specification, using the radome as the fixed portion of the aircraft, might be retained. However, in view of the need for a more realistic distribution of area and because of the advanced computing power available to the mathematical optimizer, an expansion to include more than one fixed area may be feasible. By solving the integral equations for a given number of cross sections located at known positions along the longitudinal axis, the magnitude of excessive cross-sectional areas may be reduced. This redefinition would be independent of the method employed to transform the area into linear dimensions and may be too

restrictive in terms of the number of independent variables available to describe the fuselage.

Lastly, the transformation of required areas into linear dimensions could be reassessed. This approach was used by Serghides (Ref. 4). While the definition of the fairing curve was retained, it was generally assumed that the vertical dimensions remained either constant or varied linearly from station to station. Scaling of dimensions to fit each cross section to the area distribution was applied only on horizontal dimensions. Alternatively, aspect ratios could be specified for each fuselage section, in order to preserve a defined cross-sectional shape. Finally, in a completely different approach, one could define a layout for aircraft components, fit fuselage cross-sections around them and subsequently move the components about during the optimization phase until the desired area distribution is achieved. This approach would not necessitate a direct comparison of the actual with the required area distribution and may lead to more realistic aircraft shapes.

In general, considerations for a stealthy aircraft should be the driver for any such development. It may be that a cross section with the lowest possible vertical profile is required, in which case the method of Serghides could be adapted. On the other hand, a more realistic minimum wave drag area distribution might be obtained using a curve fit according to Sears for a number of fixed cross sections. Also, care must be taken during the scaling process in order not to distort angular dimensions, for example the angle of the fuselage size with the vertical, since they are fundamental to preserving the radar, infrared or optical reflectivity characteristics.

While perhaps not conclusively solving the problem of defining an area distribution, it seems that any of the methods to be chosen involves a compromise between two opposite requirements: should the flexibility of a design process with many independent variables be sacrificed in favour of a more rigid but perhaps also more accurate definition using just a few variables? It is an area which will certainly require careful consideration.

2.2. MASS

The mass estimation methods in Lovell's design synthesis (Ref. 3) have been developed at British Aerospace. An analysis of the methods was not carried out due to the limited time available. An examination of the work of Serghides, which is also based upon Lovell's work, showed that no major modifications were made. However, their validity remains to be proven.

One suggestion for further work would involve an analysis of existing, similar configurations using the mass estimation methods available in the references. The results would be compared with estimations using Lovell's equations. An area of prime importance is the fuselage. Estimating its mass is difficult because of the sometimes highly irregular geometry and because of the high loads required to be carried through it. The British Aerospace method solves the problem by providing two estimations: one for the fuselage shell and another for the internal structure.

J. Donaldson of the Ministry of Defence has said that one of the best methods available in the open literature which considers stealth mass penalties due to to the addition of features such as radar absorbent material is a report by Burns (Ref. 35). Work is also apparently underway to obtain a more up-to-date mass estimation method from British Aerospace.

A different way of estimating fuselage shell weight is presented in Ref. 26. First, a fuselage loading is defined. Then, based upon the cross section shape a differential shell mass is calculated at each fuselage station which is included in the analysis. Finally, the individual station masses are integrated over the fuselage length to provide the overall fuselage mass. It is suggested that this procedure also could form the basis for further work on the mass estimation module.

One of the most important objectives of this stage of the research program was to find a method of estimating the mass effect of locating weapons internally in a weapons bay as opposed to externally on pylons. This work is presented in Section 4.2.

3. BASELINE CONFIGURATION

Before beginning with the detailed coding of the design synthesis, a baseline configuration was defined. The features included in the aircraft were partly the result of the literature survey, and partly the result of the initial project specification, which was defined in consultation with the DRA. As such, the new aircraft was limited to be an extension of the previous design synthesis used by Lovell, having side mounted intakes, the option of twin or single engines, and a straight-tapered, trapezoidal wing. The additional requirements were defined to be a choice amongst

- Axisymmetric or two-dimensional, vectoring nozzles
- Single or twin, canted fins,
- Single or twin, tandem cockpit, and
- Internal weapons carriage.

Moreover, several features were included which relate to the aircraft stealth characteristics as found during the literature search. These were

- Alignment in the planform of leading and trailing edges of wing, tailplane and vertical stabilizer, if canted,
- Wing and tailplane in the same plane
- Canting of fuselage side to match fin canting,
- Curved intake ducts to shield engine face, and
- Complex definition of fuselage geometry using splines and ellipses.

Table 2 lists the major aircraft components and summarizes the options which were included in the synthesis code along with the principal geometry descriptors.

Component	Options	Main Sizing Drivers
Cockpit	– Single or twin tandem	Mil. Standards
Engines	– Twin or single	Scaling factor Nozzle types Separation distance
Fins	– Twin or single – Canted or uncanted	Wing leading edge sweep Cant angle
Flying surfaces	– Wing alone – Wing and horizontal stabilizer – Wing and complete empennage	Align leading and trailing edges Wing and horizontal stabilizer in one plane Intake geometry
Nozzles	– Two-dimensional or axisymmetric	Aspect Ratio (width to height)
Weapons Bay	– Choice of one, two, three or none	Weapons load

Table 2: Summary of Baseline Aircraft Characteristics

A detailed description of the reasoning which lead to the above choices being made is given in the sections below.

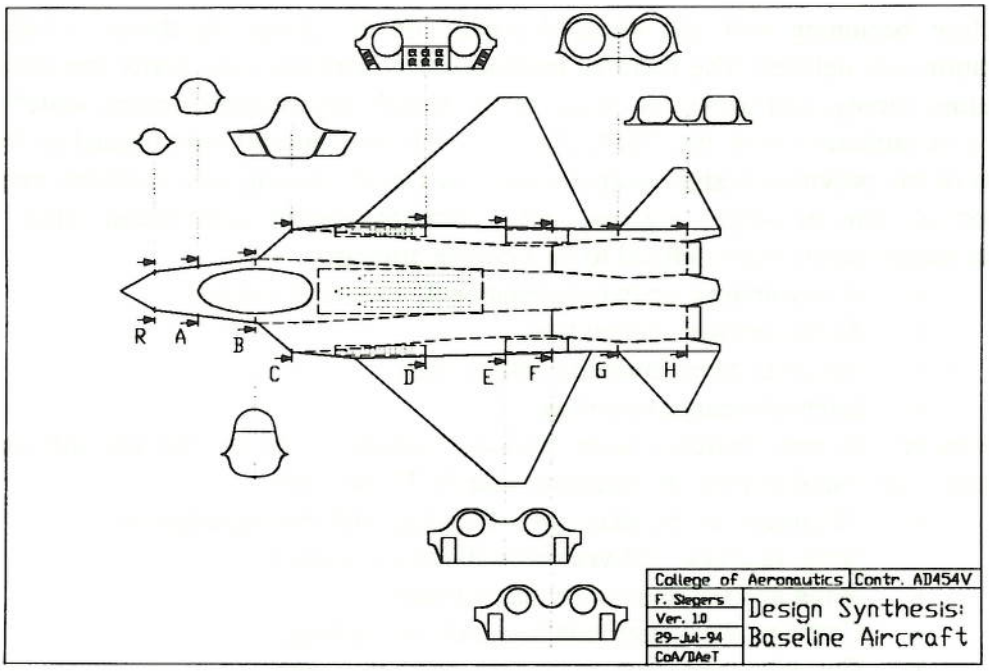

Fig. 17: Baseline Aircraft Concept

3.1. Single or Twin, Canted Fins

In many aircraft design cases, the layout of the vertical tail may require using twin fins. The reasons for such a step are quite varied, and the study of reference material reveals that the conclusions are often far from straightforward, particularly when an attempt is made to address aerodynamics and stability and control issues simultaneously.

Aerodynamically, the main argument in favor of twin fins is the fact that one fin will always be in relatively undisturbed flow during sideslip. Also, by locating the fins in proximity to the horizontal stabilizer, they may act as endplates, increasing its effective aspect ratio. On the other hand, twin fins will have a larger wetted area than an aerodynamically equivalent single fin, increasing the subsonic friction drag. Also, their performance may be degraded by mutual interference effects if insufficient fin lateral separation distance is not provided for. It has been stated that twin fins may guarantee directional stability at high angles of attack, as in the case of the F/A-18. During the design evolution of the F-16, on the other hand, twin fins were found to show unstable characteristics at the same flight conditions due to adverse interference from the forebody vortices (Ref. 48).

The apparently contradictory data on twin-fin aerodynamics can be supplemented with more straightforward considerations of other design aspects. From a stealth point of view, twin fins are desirable for a number of reasons. First, they will diminish the signature of the aircraft when viewed side-on by reducing the visual cross-section as well as by shielding the engine and exhaust infrared radiation. Twin fins can be canted out of

the vertical plane and thus reduce the radar cross section both by reflecting incident energy away from the receiver and by eliminating the corner reflector formed by fin and wing on single-fin aircraft. Finally, the canting of the fins will enable the projections of the leading and trailing edges of the fin into the horizontal plane to be aligned with the corresponding edges of the wing.

From a structural point of view, twin fins are less susceptible to flutter because of their reduced dimensions. Also, they can be located further from the engines and thus suffer less form thermal and acoustic stress. On the other hand, overall aircraft mass will increase not only because of the greater mass of twin fins, but also because of the additional structure required to react the fin loads on either side of the engine bay.

P. Mangold (Ref. 49) presents a detailed analysis of the aerodynamics of twin-fins as compared with single fins. Throughout the angle of attack range investigated (0° to 70°), twin fins canted outward at 25° generally improved the yawing and rolling moment stability while a single fin has a more constant rudder effectiveness. Within the limits posed by the tail-fin interference, increasing the cant angle seems to improve the lateral characteristics. In general, modifications to the fins produce changes only to the magnitude of the lateral derivative curves, but not to their shape.

In this respect the forebody seems to have a much more significant influence. For example, flattening the nose means that the aircraft will have better restabilization characteristics at high angles of attack but will tend to lose roll stability. The rolling moment coefficient due to sideslip is the predominant factor affecting spin departure tendency. Strakes located on the aircraft forebody are a good way to improve all lateral stability coefficients, including the tendency for yaw departure. Mangold also found that a canard-configured aircraft may prove to be unstable at certain sideslip angles. This is because a canard must be fairly large in order to provide the desired pitch maneuver capability and would thus be larger than the optimum required for lateral stability.

In view of what has been said above, it is likely that the choice of single or twin fins will depend less upon aerodynamic considerations and more upon structural and stealth features, particularly for the type of aircraft under investigation here and if high angle of attack characteristics are a design driver.

Considerations in the design of stealth aircraft require the leading edge sweep of the wing and the fin leading edge sweep when projected into the horizontal to have an equal value. This is done to minimize the number of spikes of radar energy scattered towards the receiver. In other words, the fin leading edge sweep and cant angles must be chosen to conform to a given sweep of the horizontal projection.

The correct choice of the fin sweep angles highlights a design optimization problem for stealth aircraft. Referring to Fig. 21, it can be found that the relationship between fin cant angle (QEF), leading edge sweep (QEFL) and leading edge sweep of the horizontal projection (QEFLH) is

$$\sin(\mathrm{QEF}) \cdot \frac{\tan(\mathrm{QEFLH})}{\tan(\mathrm{QEFL})} = 1 \qquad (1)$$

The relationship is valid only if QEF is not equal to 0 and if QEFLH is greater than or equal to QEFL. Assuming therefore that QEFLH is fixed, there are two possible ways of finding the other two angles.

The first would be to fix QEFL according to aerodynamic requirements. Usually, it is important that the critical Mach number of the fin should be greater than that of the wing in order to maintain control capability in the critical Mach region. Alternatively, the sweep may be chosen to provide the fin with a subsonic leading edge at the design supersonic Mach number. In this case, the fin leading edge sweep must be greater than $\cos^{-1}\left(1/Ma\right)$. While the choice of fin leading edge sweep may in this case be aerodynamically correct, the resulting value for the fin cant angle may be unacceptable in terms of the overall radar reflectivity of the aircraft. Hence the other approach. By defining a cant angle to conform to some desired radar cross section, a fin leading edge sweep may be found by fixing QEF and QEFLH. In this case the resulting sweep will be less than that required for supersonic Mach numbers.

To resolve this predicament, it was decided to rely on stealth requirements as the principle design driver for the vertical tail cant angle. Although the supersonic drag of the vertical tail is not negligible, it can be argued that its magnitude is sufficiently small for it to play only a secondary role in the layout of the vertical fin of a stealthy aircraft. Therefore, designing a fin which is aerodynamically off-optimum is one of the penalties of stealth configured aircraft.

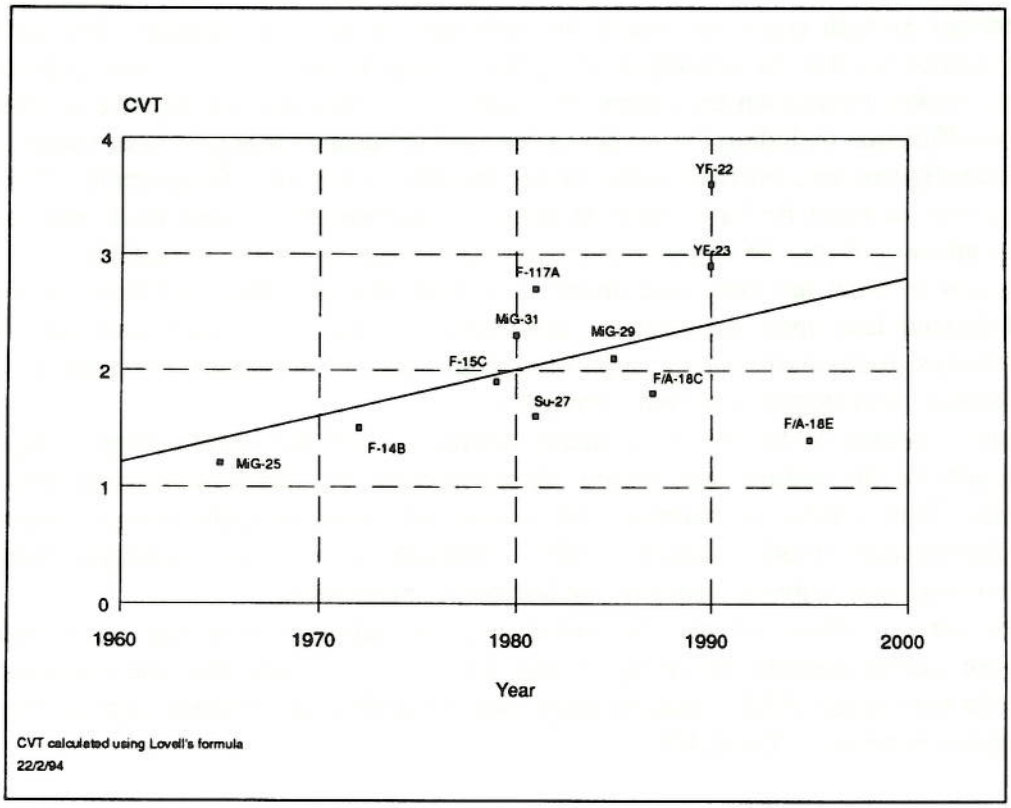

Fig. 18: Twin Vertical Tail Volume Trend

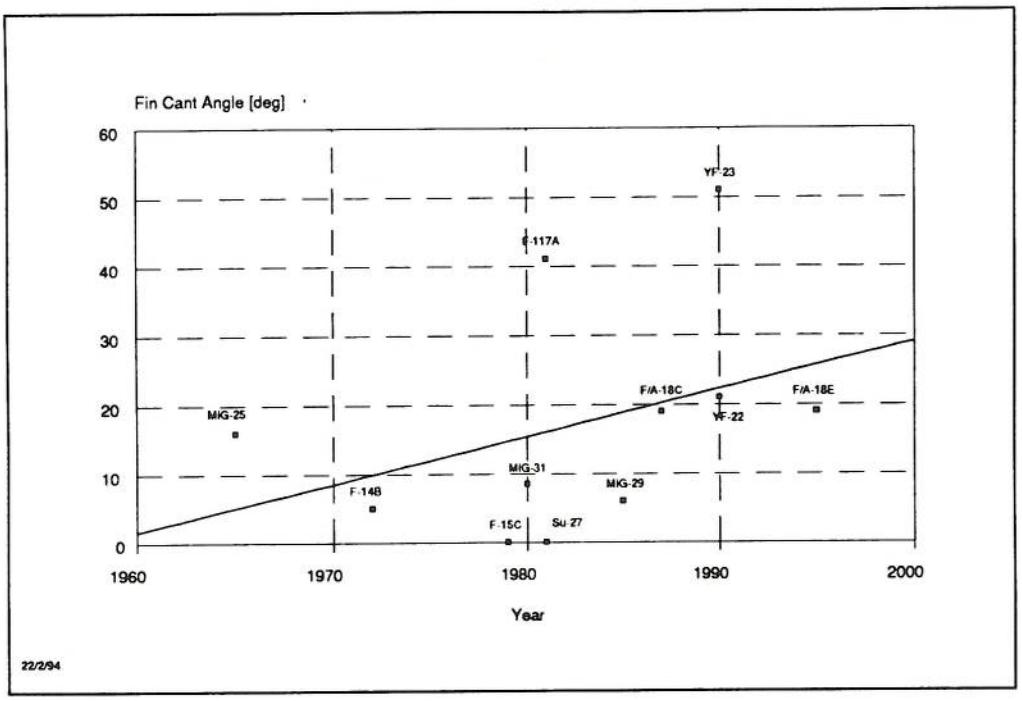

Fig. 19: Twin Vertical Tail Cant Angle Trend

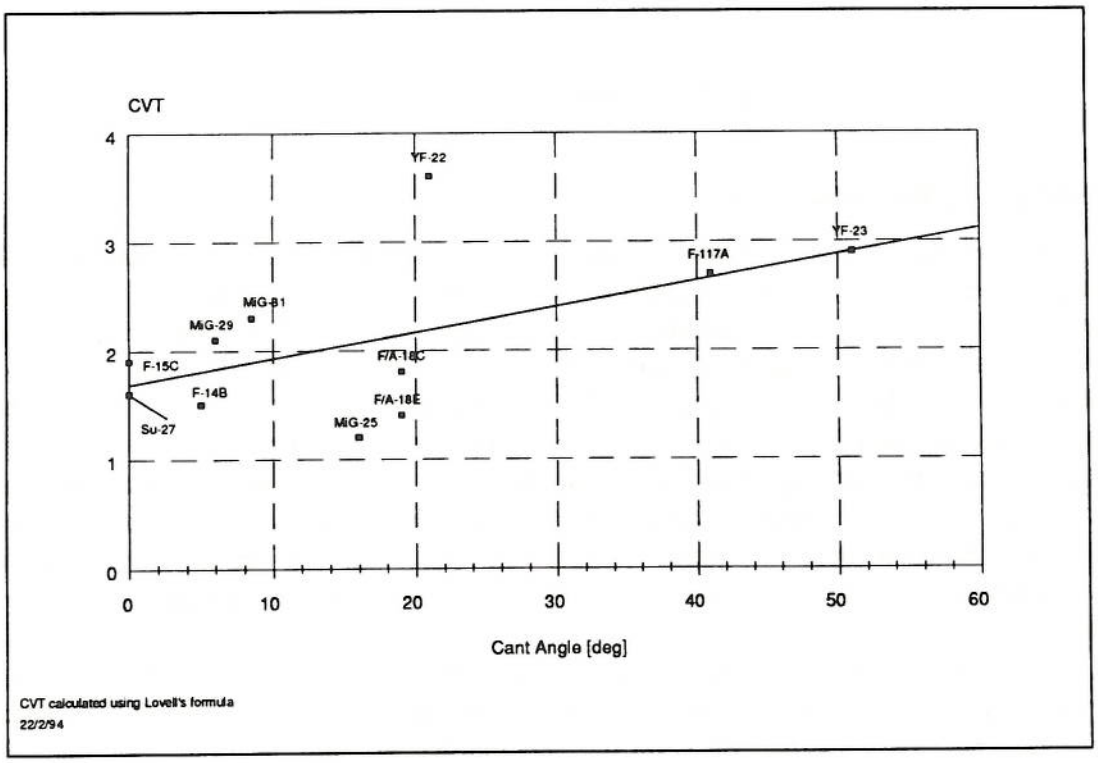

Fig. 20: Correlation of Vertical Tail Volume Coefficient with Cant Angle

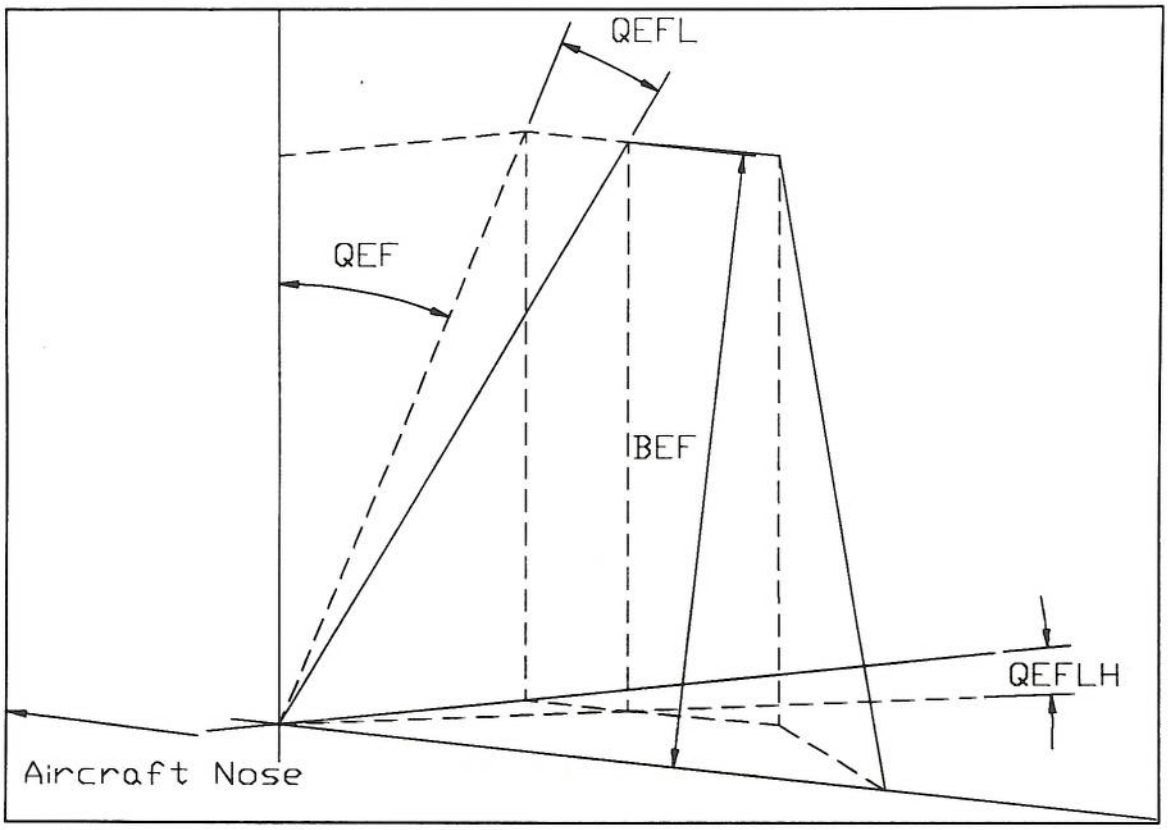

Fig. 21: Geometry of Canted Fin

3.2. Internal Weapons Bay

One of the greatest difficulties involved in the design synthesis of aircraft with internal weapons bays is the estimation of the mass effects. Because of the large dimensions of the opening in relation to the fuselage, the use of methods given in the literature for general fuselage cutouts such as doors and windows is not possible. Additionally complicating the issue is the fact that a weapons bay will normally be located in the region of the center fuselage, a highly stressed part of the structure which carries not only the fuselage longitudinal bending moments, but also the wing bending moments as well as all manners of shear and torsion loads. Moreover, other components which must be fitted near the center fuselage such as the engine stream tubes and the main landing gear compete with the weapons bay for space and load carrying structure to support them.

In combat aircraft, the structural and geometrical complexity of the fuselage generally leads to a layout in which the loads are carried to a large extent by mass booms, as opposed to a stressed skin, monocoque design common in simpler fuselage shapes on transport aircraft. The advantage of such a design is that a weapons bay can be located without too much difficulty in the cavities formed by the main wing box spars. The effect of the additional surrounds on the fuselage mass will not be quite as severe, since the skin itself is not as highly stressed. Also, modifications to frames may incur less

of a mass penalty if the doors are mounted to special ones already designed to carry large loads such as the wing bending moments.

On the other hand, the type of weapons bay to be implemented in a stealthy aircraft may necessitate the provision of quite a significant amount of structure for the launcher, which is subjected to highly dynamic loading as a result not only of the launch process itself, creating high inertial loads, but also because of the heavy aerodynamic forces experienced during the missile firing sequence. The literature available on the aerodynamics of cavities shows that the oscillations induced by the slipstream can be quite severe. Structural damage may occur if measures are not taken to control the flow in the cavity. Brian Wilson, in his lecture on the Navy Advanced Tactical Fighter (Ref. 50), mentioned the fact that the "noise of an open weapons bay at transonic speeds is quite horrendous".

Further mass penalties may arise from the doors themselves, because they must be able to open in flight and at all maneuvering conditions and can not carry any fuselage structural loads, consequently necessitating more fuselage structure to transmit the loads normally carried through the aircraft skin now replaced by the weapons bay cavity.

Internal weapon bays are not very common on conventional fighter aircraft. This fact is reflected in the lack of open literature available about such configurations. Despite the sometimes complicated aeroelastic effects during flight, stores, including tanks, have frequently been carried externally because of the simpler design of the supporting structure and ease of installation and maintenance, reducing turnaround time. External stores can also be added at a later stage in an aircraft's lifetime, although that is highly undesirable from an aircraft designer's point of view. Moreover, once an aircraft has dropped its external load, it has become relatively clean aerodynamically and is better suited for rapid egress from the combat area, aided by the fact that no excessive structural mass penalty is paid when compared with the essentially useless mass of an empty internal weapons bay.

On the other hand, external weapons create a significant amount of wave and interference drag, significantly degrading the aircraft range and performance. Also, they provide additional radar and visual reflection points, essentially reducing the stealthiness of the configuration, an argument which is the main driver behind the desire of locating weapons internally, not withstanding the penalties associated with such an arrangement.

For the purposes of this research program, it was decided to synthesize a weapons bay configuration which would allow a high degree of flexibility in the choice and arrangement of internal stores. During the optimization process, the size and initial mass of the weapons bay plus stores remains constant. Only the position may be varied by changing the value of two independent coordinates describing the positioning of the bays in the longitudinal and lateral directions. Internally, the arrangement of the weapons may be varied by specifying the number of store points in the vertical, longitudinal and lateral directions. Furthermore, a choice of none, one, two or three bays is possible, as summarized in Table 2.

3.3. Flying Surfaces

The overall synthesis methodology of the flying surfaces was retained from Lovell (Ref. 3). Modifications were made to the fin and tailplane sizing to allow the trailing edges to extend beyond the nozzle exit plane. Currently, the fin and taiplane moment arms are input as external variables, but it would be possible to include them as

independent variables for an optimizer. Also, a number of different configurations can be synthesized by choosing between no tail, a fin only, or a fin and tailplane arrangement, as well as deciding between one or two fins. A detailed description of the twin fins is given both in Section 3.1 and in Section 4.1.4.

3.4. Engine Bay and Intake Diffusers

The synthesis of the engine bay follows closely the approach given by Lovell (Ref. 3), modified by the author to cater for two-dimensional exhaust nozzles. A detailed description is given in Section 4.1.5.

The intake diffusers have a complicated, three dimensional geometry which arises mainly from the need to curve them around the internal weapons bay. In addition, flexiblility needs to be provided for three different arrangements. The geometry is slightly different for twin- or single-engined aircraft. In addition, there is an option for the weapons bay to be located either below the diffusers or between the diffusers. Finally, the three-dimensional curvature of the intakes is necessary in order to hide the engine face from the intake as much as possible. This will reduce the infrared, acoustic and radar emissions from the aircraft when viewed head-on.

3.5. Thrust Vectoring Exhaust Nozzles

Vectoring exhaust nozzles are attractive for installation on future combat aircraft for a number of reasons. They are most advantageous in the extremes of the aircraft flight envelope, namely during high speed combat maneuvers as well as in the low speed, high angle of attack range. Another application is in the reduction of take off and landing distances. In any case, the full potential of vectored thrust will only be achieved if it is included in the aircraft design process from the outset, rather than considering it as an addition to an existing airframe.

Vectored thrust works in essentially two ways. The first and most obvious one is the capability of pointing the thrust vector in a direction away from the engine centerline. Thus, the engine/nozzle combination ceases to be an instrument for the provision of simple forward thrust. Instead, it can provide additional lift and sideslip forces as well as pitch and yaw moments. If two engines are used, roll control may additionally be possible. Since the magnitude of the forces and moments is quasi independent of the speed of the aircraft, vectoring can be employed at any point within or even outside the conventional, aerodynamic flight envelope. Typical examples are the use of vectored thrust to influence the takeoff and landing distances as well as to control the high angle of attack, post-stall flight envelope (Ref. 39).

Vectored thrust can also affect the aerodynamics of the aircraft-nozzle combination by inducing supercirculation. Research into this phenomenon is quite old, and Poisson-Quinton (Ref. 40) gives a good summary of the physics of supercirculation. Thus, blowing a jet of air out of the trailing edge of a body at an angle will influence both the boundary layer, by delaying the separation point, as well as the circulation, but it will not affect the transition from laminar to turbulent flow. Siestrunck (Ref. 41) states that the resultant force upon an airfoil with a jet flap is a sum of the forces due to Kutta-Joukowski circulation around the whole configuration (airfoil plus jet) on the one hand and the additional momentum of the jet on the other. The additional lift is therefore due to the combination of an apparent increase in chord with a change in the camber.

The literature provides a large variety of experimental data and descriptions on different vectoring nozzle concepts, which can be broadly classified into two categories: axisymmetric and two-dimensional. Axisymmetric nozzles are an extension of conventional, round nozzles. Thrust vectoring is achieved either by rotating the entire nozzle about a gimbal or by appropriately deflecting a circumferential array of paddles. As the name implies, they are symmetrical about the longitudinal axis.

Two-dimensional nozzles have rectangular cross sections and may take on a number of different shapes. One extremely common type is known as convergent-divergent (CD). As with the axisymmetric CD nozzles, the internal contour consists of a fixed-geometry convergent section followed by a variable divergent part. In some cases, the rear portion of the nozzle is replaced by a single expansion ramp. Such nozzles were developed for use on aircraft with vertical or short take off and landing characteristics, the idea being that the ramp provides extremely efficient and effective vectoring at large angles in one direction only. An interesting side effect of this last nozzle type is that the infrared emissions are also highly directional, thus making them attractive for installation on stealthy aircraft.

Thrust vectoring can provide a number of benefits which must be seen in conjunction with a perceived shift in emphasis away from high energy maneuvering towards rotational-translational agility (Ref. 42). In addition to pitch/yaw thrust vectoring, some of the more important features of modern aircraft which lead in this direction are high thrust-to-weight ratios, rapid thrust onset, stall resistant engines and integrated flight controls.

For example, the F-14, F-18, F-16 and F-15 were designed with high turn rates as well as rapid climb and acceleration in mind. In contrast, their cruise efficiency is very low. However, by employing thrust vectoring nozzles from the outset of the design process, the aircraft can be aerodynamically designed for supercruise conditions while retaining very good maneuvering capabilities in the transonic and high subsonic regimes. Consequently, reducing the size of the flying surfaces and controls to reduce drag may also sharply reduce gross weight. Potential benefits for stealthy aircraft are the reductions both in visual signature as well as in radar cross section.

In spite of what has been said above, Kitowski (Ref. 43) raises a number of important points about the use of thrust vectoring. The key issue in its implementation appears to be the level of flying qualities expected upon failure of the nozzle vectoring system. Obviously, as in the case of active controls, a balance must be struck between the desired improvement in performance and the reduction in flying qualities when thrust vectoring is inoperative. If vectoring is flight essential, failure will result in loss of control of the aircraft. Other problems associated with highly agile aircraft are the increased maneuver and gyroscopic forces experienced by the pilot during combat. Also, inertia loads on aircraft components will increase because of the higher pitch and yaw rates expected.

Mace and Nyberg (Ref. 44) showed how the use of thrust vectoring provided more overall benefits than achievable with flight controls only. Because of the trend in development towards multi-role aircraft, advanced technologies should be employed to improve the performance in ground attack roles while not degrading combat maneuverability. In addition to the payoffs mentioned above, the use of thrust vectoring can lead to redundancy in flight controls, helping to increase aircraft survivability. Also, the improvements in mission performance seem to be larger if the external stores present

less drag, i.e. if air-to-air missiles are carried rather than air-to-ground. In other words, a stealthy configuration configured by necessity with an internal weapons bay would benefit to an even larger extent from such improvements.

The design of vectoring nozzles must take into account the usage of vectoring and its impact upon the durability of the nozzle materials. Not only the increased loads in the vectored position are of importance but also fatigue due to the nozzle vectoring rate and cycle. Cain and Doane (Ref. 45) reported on a study about the analysis and usage of vectored thrust. By simulating flight usage in an accelerated mission test, they were able to create a database defining the pitch and yaw vectoring rates and cycles. They found that average yaw deflections are close to zero while pitch deflections had a significant pitch up tendency.

The pitch cycles were also highly autocorrelated, whereas yaw cycles tended to be driven by short, independent events. This is thought to be a result of the way pitch and yaw vectoring are used in combat. While the former tends to be employed for longer periods of time, such as for nose pointing or trim, the latter is mainly used for directional control at high angles of attack and is thus very cyclic. Most vectoring was found to occur at rates of around 0.75 Hz. On the other hand, it is known that fatigue crack rates are increased by chemical reactions in conjunction with vibrations at frequencies below 1.5 Hz. Finally, it was found that there is very little correlation between pitch and yaw vectoring cycles.

The decision whether to use axisymmetric or two-dimensional nozzles depends largely upon the aircraft configuration under consideration. Both types of nozzle can be designed to have similar vectoring characteristics, although two-dimensional ones are generally less efficient because the axisymmetric engine airflow needs to transition to a rectangular duct. Capone (Ref. 46) has found that round nozzles produce more supercirculation lift than two-dimensional ones but exhibit more drag. The reason for this appears to be that two-dimensional nozzles integrate more readily with the aircraft afterbody. Also, as mentioned, two-dimensional nozzles can be made to have directional infrared and radar cross section characteristics. It appears, therefore, that they are more attractive for installation on stealthy aircraft than axisymmetric nozzles.

The literature provides very little concrete information about the mass effects of using vectoring nozzles compared with conventional ones. Stevens et. al. (Ref. 47) have shown that weight increases may result from using higher expansion ratios, from higher normal forces as a result of vectoring, as well as from an increase in the ratio of width to height because of the corresponding increase in transition section length. This section is necessary in order to change the flowfield from circumferential to rectangular. According to Stevens et. al., the design of the transition section for two-dimensional nozzles should minimize pressure losses and axial length. It should have a constant cross-sectional area, the corner radius should decrease linearly with length, the sidewalls should be straight and their divergence angle should be no greater than 45°. On the other hand, the reduction in size of the control surfaces now possible with the introduction of thrust vectoring nozzles may well offset the corresponding mass increase described above.

3.6. Design of Fuselage Cross-Sections

In the following paragraphs the development of cross sections to enclose the fuselage contents is presented. The definition of variables satisfies two essential constraints. The first, and most obvious one, is that the shape and size must not violate

minimum dimensions which are required to fit such items as cockpit, inlet diffuser or engines into the fuselage.

Secondly, and perhaps more importantly, the fuselage cross sections should have a shape which ensures that the synthesized aircraft will have stealthy characteristics. For example, the fuselage sides should not form a right angle with other aircraft parts such as the flying surfaces or with the horizontal plane. Also, the number of sharp edges should be minimised. Curved surfaces may be preferred over straight sides depending upon the philosophy of the designer, but the facility to chose between the two should be included.

With these points in mind it was possible to proceed to the detailed design of fuselage shapes. During the analysis of the existing method given by, it was found that the number of major cross sections would be insufficient to fully determine the fuselage shape. An additional station was therefore included between the intake and the front of the main wheel bay, increasing the total to nine. Also, in order to provide greater flexibility in the design process, the option of choosing either side intakes or underwing intakes was provided. Finally, the option of a twin cockpit and the combination of weapons bays referred to earlier was retained, with a few modifications.

In order to provide a smooth contour for the cross sections, the preferred method for fitting curves was the Bezier spline as described in Ref. 51. A Bezier spline is essentially a cubic which is calculated using the parametric form of representing curves. The shape of the curve is determined entirely by four control points, two of which form the endpoints while the other two are used to determine the slope of the curve at the endpoints. The slope is in the form of a tangent vector. Thus, the definition of the cubic avoids the usual problems encountered in curve fitting such as an infinite slope at an endpoint. Also, the method avoids unnatural overshoots of the cubic, because the control points constrain the curve to remain inside the polygon they define.

Fuselage station A is located at the front cockpit bulkhead, whose minimum dimensions are determined by the cockpit geometry. In addition, there is an underfloor area which houses the nose wheel and the gun. Bezier splines are used to fit the contours of the upper and lower fuselage parts, divided by the position of the chine.

Station B is located at the pilot's eyepoint. Based upon the cockpit geometry, minimum dimensions for the cockpit height and width are determined, and the resulting cross-section is scaled to fit the cross-sectional area as required by the fairing curve. In addition, account is taken of the cross-sectional area required to fit the nose gear and gun underneath the cockpit floor.

Fuselage station C is located at the intake position. The minimum width results from a summation of the width of the internal weapons bay, if present, and the width of both intakes, plus a clearance factor for structures. The outboard intake sides are not vertical, but are instead inclined at an angle to the vertical, given as an external variable. The minimum total height at station C is a sum of the fuselage height and a section of the canopy, which is assumed to extend rearward from the pilot's eyepoint with a fixed geometry. These dimensions are then scaled in order to match the fairing curve.

Station D is located at the front of the small internal weapons bays, which are located outboard of the intakes, as shown in the overall layout in Fig. 17. The minimum required dimensions are determined similarly to station C, with the addition of the outboard weapons bays to the fuselage minimum width. The height at D is determined from a curve fit joining the heights found at C and F and remains fixed throughout the synthesis.

Station E is located at the front of the main wheel bays and is assumed to contain additionally the intake diffusers and the internal weapons bay, if present. It can only be positioned after the main gear has been sized.

Fuselage station F is located at the engine face (engine station 1), while fuselage stations G and H correspond to engine stations 2 and 3, respectively. The minimum dimensions are determined using the engine geometry and, for station F, the size and layout of the main landing gear. Additionally, the synthesis method provides a more detailed description of the fuselage-tailplane junction geometry than originally given by Lovell.

3.7. Component Layout

The fuselage synthesis method developed by Lovell (Ref. 3) is characterized by a simple nose-to-tail procedure, in which the fuselage is defined by a number of stations located at predetermined positions on the longitudinal axis. For each fuselage station, a series of minimum dimensions are defined, using values obtained from the synthesis of the individual components which are required to be contained within the perimeter of the cross section at that station. Thus, as an example, the geometry of the station located at the front of the main landing gear bay is defined by the dimensions of the gear bay itself as well as the wing box and the intake diffusers. The minimum dimensions thus obtained are scaled to match the cross-sectional area required by the fairing curve (see Ref. 3 and Section 2.1.5 above). The fuselage stations are synthesized by proceeding along the fuselage from nose to tail.

The fact that the above procedure incurs several problems in terms of an accurate representation of the fuselage geometry was extensively discussed with the Defence Research Agency. Based upon the analysis of the fairing curve presented in Section 2.1.5 above, it was decided to slightly modify the order of the synthesis of the fuselage cross-sections in order to allow a more realistic transformation of required cross-sectional area into actual fuselage vertical and horizontal dimensions. Thus, station C and the radome are synthesized first. Curve fits then define the spine and the forebody chine of the fuselage between these stations, and the width and height thus defined are not changed during the scaling process. Similarly, a curve fit between stations C and F defines the fuselage spine, while the lower fuselage is flat, as defined by the size and vertical location of the weapons bay. A more detailed description of the method is given in Section 4.1 below.

3.8. General Design Considerations

The main driver for the type of aircraft under consideration is the design of a layout which will simultaneously minimize the emissions and/or reflections of electromagnetic (both radio and optical frequencies), infrared and acoustic energy. At the same time, the requirements of the aircraft role must be met, including the ability to carry a specified weapons load for a given distance. The weapons capacity is determined directly by the size of the internal weapons bay, which must be fixed at an early stage in the preliminary design. In effect, the aircraft must be designed around a weapons bay (Ref. 50).

In general, the initial layout will involve the definition of threat directions. Once the likelihood of a given system such as radar or heat-seeking missile to be used against the

aircraft has been determined, the direction from which this threat is most likely to be employed must be identified. As an example, the front and rear head-on views of the aircraft are extremely common threat directions. This is not only due to the fact that an aircraft attacking a target is most likely to do so in a head-on direction, but also because it is more likely to be illuminated head-on by surveillance radar or tail-on by airborne missile attack radar.

Once these threat directions have been agreed upon, their relative significance should be assessed. This is necessary in order to determine design priorities, since the aircraft emissions and reflections can generally not be minimized simultaneously for all threat directions. From an analysis of the available literature on stealth design, it was determined that the most likely threat directions needing attention are the head-on, rear and lateral ones. The following general design rules were derived from these requirements:

First, the overall fuselage height should be kept as low as possible. This will particularly reduce the optical signature of an aircraft when viewed from the side or head-on. It can also be said that the aircraft should be as small as possible, for the same reason. Second, the fuselage sides should be tilted away from the vertical. This will tend to scatter incident radiation, in particular the large reflective spikes associated with radar energy, away from the observer. Also, the joining of two surfaces at right angles must be avoided at all costs in order to prevent the creation of corner reflectors.

Second, the engines should be shielded as much as possible, both by burying them as far as possible within the fuselage and by hiding the intakes and exhausts. This can be accomplished by curving the ducts and by choosing a twin-fin arrangement.

Finally, any straight edges such as chines or wing and tailplane leading edges should be oriented in parallel to each other. This is done in order to reduce the number of reflective parts generating distinct spikes of radar energy to as few as possible. Wing and horizontal stabiliser should be located in the same plane. Surfaces should be treated in the same manner: the fuselage sides, as an example, must all reflect incident energy at the same angle.

The fact that the combined wing and fuselage horizontal surfaces may offer a large reflector is not considered to be of extreme importance, because the likelihood that an aircraft will be illuminated by a threat from directly above or directly below is extremely small.

Minimising the reflections and emissions will be the result of simultaneously juggling a large number of variables. The design of the fuselage for a stealth aircraft and in particular the provision of code for the numerical synthesis must reflect this. Thus, it may appear that some of the fuselage cross sections are excessively complicated. However, it is felt that only in this way can the desired design flexibility be achieved.

4. SYNTHESIS METHODOLOGY

The following sections describe in detail the design relationships developed as modifications to the method described by Lovell. The order in which the individual algorithms are called within the program code is shown in Fig. 22. It has been set up in order to facilitate the planned linking of the synthesis with the DRA's numerical optimizer. The code was designed to be highly modular, such that an incremental implementation of the algorithms described below could be undertaken.

A short description of the synthesis methodology follows. Then, in sections 4.1 and 4.2, a detailed description of the synthesis equations. They should be read in conjunction with Lovell's report (Ref. 3), in particular because no description is given below of the

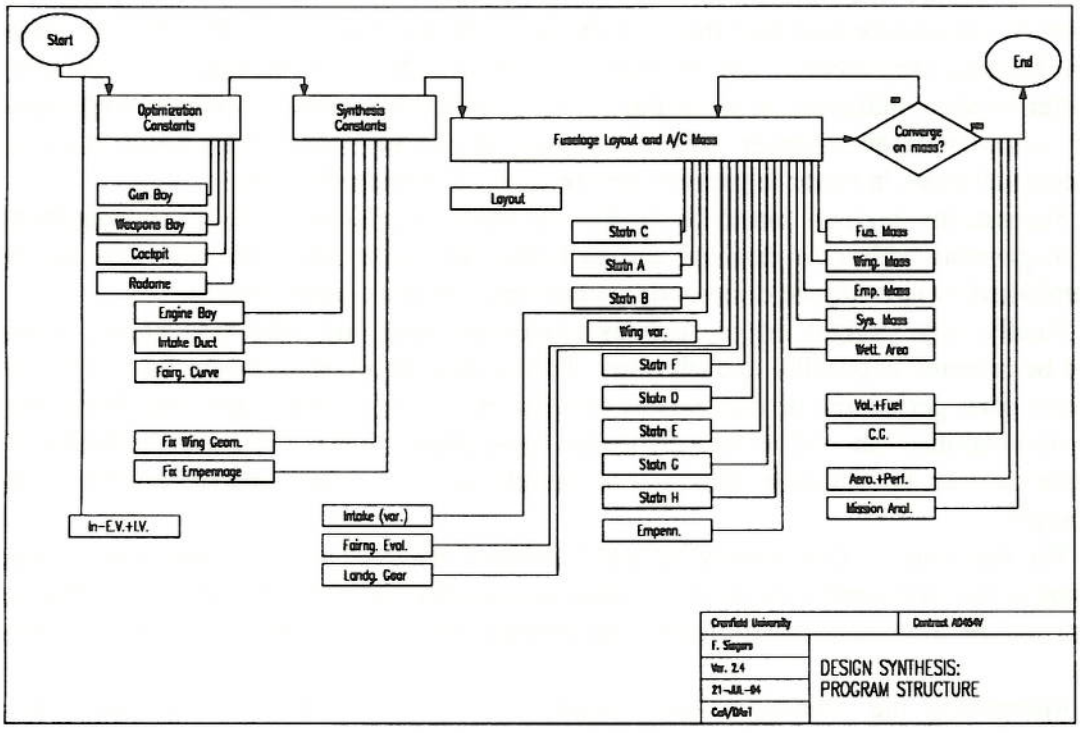

Fig. 22: Design Synthesis Flow Chart

aerodynamics and performance estimation methods, which have not been modified.

Firstly, those items which remain constant during the optimization process are synthesized. They include the radome, the gun bay, the weapons bay, and the cockpit. Initially, only the sizing is done, as their layout is a variable and is determined at a later stage. Then, all of those items which remain constant during one run through the design synthesis are defined, including the engine bay, the intake duct items not dependent upon the fuselage shape, and the fairing curve. Also, those items relating to the fixed parts of the wing geometry, i.e. not dependent upon the net wing, as well as the empennage variables such as the relationship between the fin cant angle and leading edge are calculated. Included in these modules are the fixed mass terms for the abovementioned components.

The central routines of the synthesis code are the ones performing the fuselage packaging and the mass estimation. Lovell's original code relied on just a few modules to accomplish these tasks, but it was decided to carry the modularization even further and separate the mass estimation, as much as possible, from the geometry layout. Also, a number of individual modules were written for the sizing of the fuselage cross-sections, one for each station, as shown in Fig. 22. An iteration is performed to find the aircraft mass, as described by Lovell, because the sizing of the fuselage is dependent upon a landing reference mass derived from the take-off mass, following which the aerodynamics and performance estimations are carried out.

4.1. GEOMETRY

4.1.1. RADOME

The diameter of the nose at the position of the radar dish is determined by an antenna diameter, DAR, and an increment, EDAR, to allow for clearances. It is assumed that the cross sectional area varies linearly from the front of the radome to the radar dish with a gradient given by GOF1. Referring to the Figure, a spline is fitted to the radome such that

$$\begin{aligned} PFRT(1,1) &= \frac{0.5 \cdot FFS \cdot (DAR + EDAR)}{\cos(QFS)} \\ PFRT(1,2) &= 0 \\ PFRT(4,1) &= 0.5 \cdot (DAR + EDAR) \cdot \cos(QFS) \\ PFRT(4,2) &= 0.5 \cdot (DAR + EDAR) \cdot \sin(QFS) \ , \end{aligned} \tag{2}$$

using the subroutine BEZFIT to calculate the remaining points of the spline. Subroutine BEZFIT is explained in detail in Appendix A.

The perimeter and cross-sectional area of the radome are found using BEZEVAL, described in Appendix A, as well as the relationships

$$PFR = 3.14 \cdot (DAR + EDAR) \cdot \frac{1}{1 - 2.0 \cdot \frac{QFS}{3.14}} \ , \text{ and} \tag{3}$$

$$\begin{aligned} OF1 = &\left(1 - 2.0 \cdot \frac{QFS}{3.14}\right) \cdot 0.785 \cdot (DAR + EDAR)^2 + \\ &+ 0.5 \cdot (DAR + EDAR)^2 \cdot \sin(QFS) \cdot \cos(QFS) + 4.0 \cdot area(PFRT) \ . \end{aligned} \tag{4}$$

The length, volume and wetted area of the radome are given by

$$XFR = \frac{OF1}{GOF1},$$

$$VFR = \frac{1}{3} GOF1 \cdot XFR^2, \text{ and}$$

$$WFR = \frac{2}{3} \cdot PFR \cdot XFR \tag{5}$$

respectively.

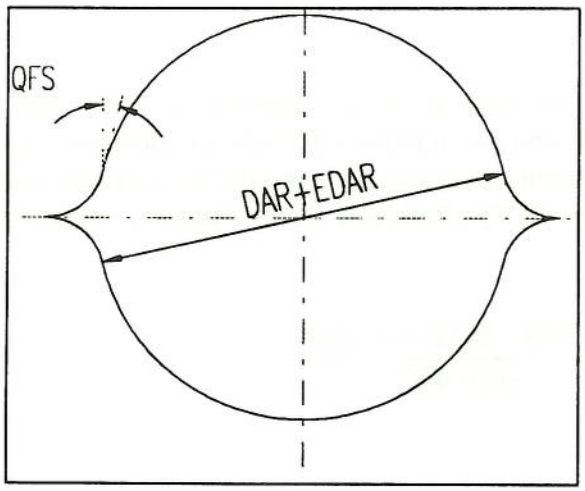

Fig. 23: Fuselage Cross-Section at Radar Dish

4.1.2. COCKPIT

The design synthesis of the cockpit follows closely the approach given by Lovell (Ref. 3), with modifications as proposed by J. Kirk of the Defence Research Agency to allow for the option of single or twin, tandem cockpits. The dimensions and arrangement of components wee based upon information obtained from MIL-STD-1333B (Ref. 23) and MS33574 (Ref. 24) as well as DEF STAN 00-970 (Ref. 25). If a one-seat cockpit is chosen, the layout is as given by Lovell. Fig. 24 shows the layout for a two seat arrangement. Thus, we have

$$QCFOOT = \sin^{-1}\left[\frac{HC3 \cdot \sin(QCSEAT) + HCSEAT \cdot \cos(QCSEAT)}{HC2}\right], \tag{6}$$

$$HCEYE = HC1 \cdot \cos(QCSEAT) + HC3 \cdot \sin(QCSEAT) + HCSEAT \cdot \cos(QCSEAT), \tag{7}$$

$$LCEYE1 = HC1 \cdot \sin(QCSEAT) + HC2 \cdot \cos(QCFOOT) + LCFOOT \quad , \tag{8}$$

$$LCFL1 = HC2 \cdot \cos(QCFOOT) + LCFOOT + HC3 \cdot \cos(QCSEAT) - \\ - HCSEAT \cdot \sin(QCSEAT) + \frac{EHC5}{\cos(QCSEAT)} \quad , \tag{9}$$

$$HC5 = HCEYE - LCEYE1 \cdot \tan(QCEYE1) \quad , \tag{10}$$

$$HCWSC = (HCSEAT + HC1) \cdot \cos(QCSEAT) + HC6 \cdot \sin(QCEYE2) \tag{11}$$

$$LCWSC = LCEYE1 - (HC6 - HC3) \cdot \cos(QCSEAT) \tag{12}$$

$$HC7 = 0.5 \cdot BCH \cdot \tan(QCEYE3) \quad . \tag{13}$$

The vertical coordinate of the canopy top centreline is described by a cubic, with a front and rear section the size of which depends upon whether a single or two-seat configuration is chosen. The gradient used to define the forward section is the same as that of windscreen inclination angle, and is found from

$$QCWSC = \tan^{-1}\left(\frac{HCWSC - HC5}{LCWSC}\right) \tag{14}$$

For a single seat cockpit, LCT=LCFL1, and the following additional relationships apply:

$$HCCANS = HCEYE + HC4 \tag{15}$$

$$LCCANS = LCEYE1 - LCWSC \tag{16}$$

The values for LCWSC, HCWSC, QCWSC, LCEYE1, and HCCANS are used to fit the cubic for the front part of the canopy, and stored in the array FZCF. At the rear of the canopy, the vertical coordinate used to define the cubic is calculated from

$$ZCCANR = HCEYE - HC7 + LCCAN \cdot \tan(QCCAN) \ , \tag{17}$$

which makes use of QCCAN, the cockpit side inclination angle, and the canopy length, LCCAN, both of which are external variables. The gradient of the canopy top centreline is given by

$$GCCANR = 2 \cdot \frac{ZCCANR - HCCANS}{LCCANS - LCEYE1} \ . \tag{18}$$

Should a twin-seat cockpit have been chosen, then

$$LCT = LCFL1 + ELCT \ , \tag{19}$$

$$HCT = HC4 + ELCT \cdot \tan(QCEYE4) \ , \tag{20}$$

$$LCFL2 = ELCT - HCT \cdot \tan(QCSEAT) \ , \tag{21}$$

$$LCEYE2 = ELCT + LCEYE1 \ , \tag{22}$$

$$HCCANS = HCEYE + HC4 + HCT \ , \text{ and} \tag{23}$$

$$LCCANS = LCEYE2 - LCWSC \ . \tag{24}$$

Using the values calculated above, the front cubic is fitted between the rear of the windscreen and the point at which the canopy is assumed to reach its maximum height, located above the eyepoint of the rear seat. For the aft portion of the canopy cubic,

$$ZCCANR = HCEYE - HC7 + (LCCAN - LCEYE1) \cdot \tan(QCCAN) \text{ and} \tag{25}$$

$$GCCANR = 2 \cdot \frac{ZCCANR - HCCANS}{LCCAN - LCEYE2} \ . \tag{26}$$

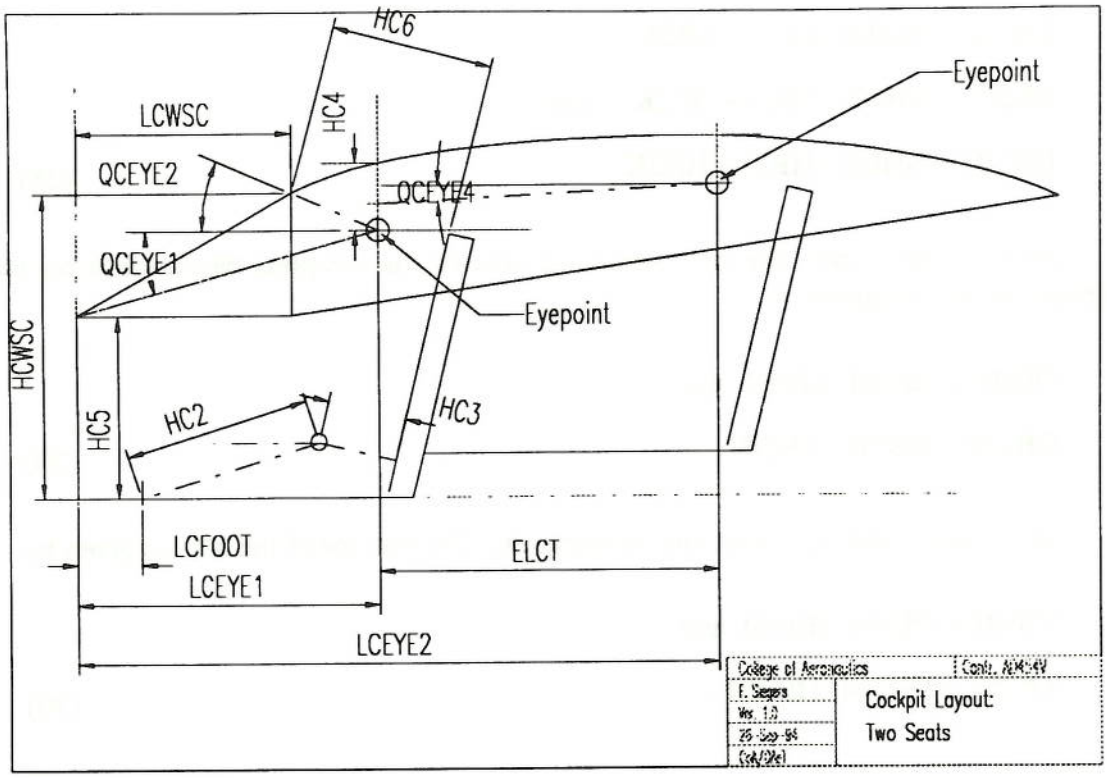

Fig. 24: Cockpit Layout for Twin-Seat Arrangement

4.1.3. WEAPONS BAY

The synthesis methodology of the weapons bay was designed to allow a great deal of flexibility for the specification of the weapons load while maintaining an overall simple algorithmic structure. An external variable, NWEPB, chooses the number of weapons bays to be synthesized. Thus, if NWEPB=1, a single bay located on the centreline is chosen. If NWEPB=2, two bays outboard of the diffusers are selected. Finally, if NWEPB=3, then both an inner and two outer bays are implemented. Alternatively, NWEPB=0 allows the implementation of no weapons bay.

A group of external variables, NLBI, NBBI, and NHBI control the number of store stations lengthwise, in width, and in height, respectively. Using some clearance factors, LB1K, BB1K and HB1K for the inboard ones and LB2K, BB2K and HB2K for the outboard ones, the bay dimensions are found as

$$\begin{aligned} LB1BI &= NLB1I \cdot LB1I + LB1K \ , \\ BB1BI &= NBB1I \cdot BB1I + BB1K \ , \text{ and} \\ HB1BI &= NHB1I \cdot HB1I + HB1K \end{aligned} \tag{27}$$

for the inner bay, and

$$LB2BI = NLB2I \cdot LB2I + LB2K \ ,$$

$$BB2BI = NBB2I \cdot BB2I + BB2K \ , \text{ and}$$

$$HB2BI = NHB2I \cdot HB2I + HB2K \tag{28}$$

for each outer bay. The cross-sectional area of the weapons bay cavities on the fuselage surface are given by

$$OB1BI = BB1BI \cdot LB1BI \text{ and}$$

$$OB2BI = BB2BI \cdot LB2BI \tag{29}$$

for the inner and each outer bay, respectively. The volume of the bays is given by

$$VB1BI = OB1BI \cdot HB1BI \text{ and}$$

$$VB2BI = OB2BI \cdot HB2BI \ . \tag{30}$$

4.1.4. EMPENNAGE

The initial sizing of the vertical tail is accomplished using the vertical tail volume coefficient, REFSW, but with a slightly different approach as compared to that of Lovell (Ref. 3). It is given by the following expression:

$$REFSW = \frac{SEFNV \cdot LEFCQM}{0.5 \cdot XWCQM \cdot DFC^2} \ , \tag{31}$$

in which SEFNV is the projection of the fin area into the vertical plane containing the aircraft longitudinal reference axis. By specifying LEFCQM as an external variable, the calculation of SEFNV is simplified. In addition, it allows the fin trailing edge to extend beyond the nozzle exit plane. The cant angle of the fins is QEF, measured from the vertical plane, and thus the fin area is found from

$$SEFN = \frac{SEFNV}{\cos(QEF)} \ . \tag{32}$$

Similarly, the projection of the fin area into the horizontal plane, SEFNH, is found from

$$SEFNH = SEFN \cdot \sin(QEF) \ . \tag{33}$$

Once a fin volume coefficient has been chosen and the fin areas have been calculated, the rest of the fin dimensions may be determined. Thus, the length of the fin root chord is found from

$$CEFB = \frac{2}{1+UEFN}\sqrt{\frac{AEFN \cdot SEFN}{NFIN}}, \tag{34}$$

where NFIN is the number of fins. The mean aerodynamic chord of the fin is given by

$$CEFM = \frac{2}{3} \cdot CEFB \cdot \frac{1+UEFN+UEFN^2}{1+UEFN} \tag{35}$$

and its vertical location above the root chord is found from

$$ZEFM = \cos(QEF) \cdot \sqrt{\frac{AEFN \cdot SEFN}{NFIN}} \cdot \frac{CEFB - CEFM}{1-UEFN} . \tag{36}$$

The mean quarter chord point is located a distance

$$XEFM = \sqrt{\frac{AEFN \cdot SEFN}{NFIN}} \cdot \frac{CEFB - CEFM}{1-UEFN} \cdot \tan(QEFL) + 0.25 \cdot CEFM \tag{37}$$

aft of the leading edge of the fin.
The distance of the fin leading edge at the root aft of the nose is given by

$$XEFLB = XWCQM + LEFCQM - XEFM . \tag{38}$$

The volume of the fin is given by

$$VEFF = 0.15 \cdot UEFF \cdot RTEF \cdot CEFB^2 \cdot BEFN \cdot \left(1+UEFN+UEFN^2\right). \tag{39}$$

For the horizontal stabilizer,

$$SETN = \frac{RETSW \cdot SW \cdot CWMG - SEFNH \cdot LEFCQM}{LETCQM} . \tag{40}$$

This equation takes into account the contribution of the fin, if canted, to the horizontal stabilizer effectiveness. Furthermore,

$$BETN = \sqrt{SETN \cdot AETN} \tag{41}$$

$$CETB = 2.0 \cdot \frac{BETN}{AETN \cdot (1 + UETN)} \tag{42}$$

$$CETM = \frac{2}{3} \cdot CETB \cdot \frac{1 + UETN + UETN^2}{1 + UETN} \tag{43}$$

$$XETM = \frac{CETB - CETM}{1 - UETN} \cdot 0.5 \cdot BETN \cdot \tan(QETL) + 0.25 \cdot CETM \tag{44}$$

The leading edge of the horizontal stabilizer at the root is located aft of the aircraft nose a distance

$$XETLB = XWCQM + LETCQM - XETM \ . \tag{45}$$

4.1.5. Engine Bay and Diffusers

The development of the thrust vectoring module followed closely the engine and nozzle design synthesis given by Lovell (Ref. 3). The original engine bay specification was retained, with modifications where appropriate to accomodate two-dimensional vectoring nozzles.

The engine geometry when axisymmetrical nozzles are used is defined by Fig. 25, and an engine with two-dimensional nozzles is shown in Fig. 27. The difference is in the presence of a section for transition from a circular cross-section to a rectangular one if two-dimensional nozzles are being used. A set of external variables define a reference engine in terms of the lengths, diameters and masses of the gas generator, reheat section including refuelling, nozzle and thrust reverser, if fitted. Using a scaling factor, RTP, which is also an independent variable, the reference engine is scaled to match the aircraft thrust requirements according to a set of correlations given below.

$$LP12 = LP12R \cdot RTP^{FLP1K} ,$$

$$LP22A = LP22AR \cdot RTP^{FLP2K} ,$$

$$LP2A4 = LP2A4R ,$$

$$LP2B3 = LP2B3R \cdot RTP^{FLP3K}$$

and

$$LP34 = LP34R \cdot RTP^{FLP4K} , \quad (46)$$

and therefore

$$LP22B = LP22A + LP2A4 - LP34 - LP2B3 . \quad (47)$$

If axisymmetric nozzles are used, LP23 is equal to LP22B, otherwise LP23 is equal to LP22B+LP2B3.

The overall engine length is given by

$$LPG = LP12 + LP22B + LP2B3 + LP34 . \quad (48)$$

At each reference station a diameter is found from the following relationships:

$$DP1 = DP1R \cdot \sqrt{RTP},$$

$$DP2 = DP2R \cdot \sqrt{RTP} ,$$

$$DP3 = DP3R \cdot \sqrt{RTP} \text{ and}$$

$$DP4 = DP4R \cdot \sqrt{RTP} . \quad (49)$$

When two-dimensional nozzles are being used, the reference diameter at station 2B is assumed to be the same as for station 3.

The number of engines is set by an external variable, NENG, and therefore the total nozzle exit area is given by

$$OPN = NENG \cdot \frac{\pi}{4} \cdot RTP \cdot DP4R^2 . \quad (50)$$

If an axisymmetric nozzle has been installed, then the reference engine is assumed to have circular cross sections at all of the reference stations. When two-dimensional nozzles are installed, the transition from a circular to a rectangular cross section is

assumed to occur between section 2B and section 3. In order to determine the dimensions at station 4, an aspect ratio is defined:

$$AP4 = \frac{HP4}{BP4} \tag{51}$$

and consequently the height and width may be determined by considering the cross-sectional area defined in equation (50):

$$HP4 = \sqrt{\frac{OPN}{NENG} \cdot AP4}$$

$$BP4 = \frac{HP4}{AP4} \tag{52}$$

A set of vertical and horizontal clearances are applied to the scaled engine defined above. They are defined as the sum of all the gaps between engine and fuselage including the gap between engines for a twin-engine installation. Together, they form the engine bay, which represents the minimum dimensions of the installed propulsion system. The clearances at each station are found from linear functions of the respective engine diameters. Also, they are constrained to lie within specified minimum and maximum values. Cubic splines are used to fair the joins between the limiting values in order to ensure a smooth variation of the engine clearance with engine size. Thus, the overall clearances on height are found to be

$$\begin{aligned} EHP1 &= FHP1K \cdot DP1 \quad \text{for} \quad EHP1S \le EHP1 \le EHP1H \\ EHP2 &= FHP2K \cdot DP2 \quad \text{for} \quad EHP2S \le EHP2 \le EHP2H \\ EHP3 &= FHP3K \cdot DP3 \quad \text{for} \quad EHP3S \le EHP3 \le EHP3H\,. \end{aligned} \tag{53}$$

The clearance at station 2B is assumed to be the same as at station 3. On breadth, the clearances are dependent upon the presence of twin or single engines, and may be calculated from

$$\begin{aligned} EBP1 &= \frac{FBP1K \cdot DP1}{NENG} \quad \text{for} \quad EBP1S \le EBP1 \le EBP1H \\ EBP2 &= \frac{FBP2K \cdot DP2}{NENG} \quad \text{for} \quad EBP2S \le EBP2 \le EBP2H \\ EBP3 &= \frac{FBP3K \cdot DP3}{NENG} \quad \text{for} \quad EBP3S \le EBP3 \le EBP3H\,. \end{aligned} \tag{54}$$

The factors FBPK and the limits EHPS, EHPH, EBPS and EBPH have different values for a twin- and a single-engine installation. Accordingly, the overall clearance on bay width is divided between the number of engines to obtain figures appropriate to a side-by-side installation. There are no clearances at station 4, the nozzle exit plane.

The dimensions of a two-dimensional nozzle at station 3 are found by considering the dimensions at station 4. The width of the nozzles is assumed to remain constant between section 3 and 4, and therefore the height of the nozzle at station 3 may be found from the area defined by the reference diameters in equation (49):

$$BP3 = BP4$$

$$HP3 = \frac{\frac{\pi}{4} \cdot DP3^2}{BP3} \tag{55}$$

If axisymmetric nozzles are installed, then the cross sections of the stations of a single engine installation are assumed to be elliptical in shape, with the major and minor axes fixed by the engine diameter at the respective station plus the clearances. Thus,

$$OP1B = NENG \cdot \frac{\pi}{4} \cdot (DP1 + EHP1) \cdot (DP1 + EBP1),$$

$$OP2B = NENG \cdot \frac{\pi}{4} \cdot (DP2 + EHP2) \cdot (DP2 + EBP2), \text{ and}$$

$$OP3B = NENG \cdot \frac{\pi}{4} \cdot (DP3 + EHP3) \cdot (DP3 + EBP3). \tag{56}$$

Should two-dimensional nozzles be installed, the diameter at stations 3 and 4 is replaced by the respective heights and widths of the nozzle, calculated in Equations (52) and (55). In this case, the cross-sectional area at section 3 becomes

$$OP3B = NENG \cdot [(BP3 + EBP3) \cdot (HP3 + EHP3) - 0.21 \cdot EBP3 \cdot EHP3]. \tag{57}$$

This expression was derived by considering the corners of the nozzle to be elliptical in shape, as shown in Fig. 26. The cross-sectional area at station 2B is considered to be:

$$OP2BB = NENG \cdot \frac{\pi}{4} \cdot (DP3 + EBP3)(DP3 + EHP3) \tag{58}$$

and is equal to the cross sectional area of station 3 for the axisymmetric nozzle installation.

For an engine with axisymmetric nozzles, the volume of the engine bay is found using the assumption that the height and width vary linearly between stations 1, 2, 3 and 4. Hence,

$$VP12B = \frac{LP12}{3}\cdot\left\{OP1B + OP2B + NENG\cdot\frac{\pi}{8}\cdot\left[\begin{array}{l}(DP1+EHP1)\cdot(DP2+EBP2)+\\+(DP2+EHP2)\cdot(DP1+EBP1)\end{array}\right]\right\} \quad (59)$$

$$VP23B = \frac{LP23}{3}\cdot\left\{OP2B + OP3B + NENG\cdot\frac{\pi}{8}\cdot\left[\begin{array}{l}(DP2+EHP2)\cdot(DP3+EBP3)+\\+(DP3+EHP3)\cdot(DP2+EBP2)\end{array}\right]\right\} \quad (60)$$

and

$$VP34B = \frac{LP34}{3}\cdot\left\{OP3B + OPN + NENG\cdot\frac{\pi}{8}\cdot DP4\cdot[2\cdot DP3 + EHP3 + EBP3]\right\}. \quad (61)$$

When two-dimensional nozzles are installed, volume VP12B does not change and VP22BB is set equal to VP23B. However, VP34B is now found from

$$VP34B = \frac{1}{2}\cdot(OPB3 + OPB4)\cdot LP34 \quad (62)$$

and VP2B3B is found with

$$VP2B3B = 0.5\cdot NENG\cdot LP2B3\cdot\left\{\frac{\pi}{4}(DP3+EBP3)\cdot(DP3+EHP3)+ + [(BP3+EBP3)\cdot(HP3+EHP3) - 0.21\cdot EBP3\cdot EHP3]\right\} \quad (63)$$

A linear variation of cross sectional area from station 2b to 3 is assumed. Finally, the total engine bay volume becomes

$$VPB = VP12B + VP23B + VP34B + VP2B3\ , \quad (64)$$

with VP2B3 equal to the value computed by equation 63 for two-dimensional nozzles or set to zero if axisymmetric nozzles are used.

For a twin engine installation, the engine spacing, YPCH, is found as the maximum of the distances given by the application of an engine separation factor, FYPCH, to each engine bay station in turn. Similarly, a maximum engine bay height is found by examining the installed height of each station in turn. This value, HPH, is used to determine the vertical engine position relative to the wing position.

The geometry of the intake diffusers is relatively complex, and the method used will now be described. First, a general diffuser cross section is shown in Fig. 28. An aspect ratio is defined as

$$AII = \frac{HII}{BII} \tag{65}$$

Referring to the figure, the following variables are defined:

$$HIIB = \frac{HII \cdot \cos(QID1)}{\sin\left(\frac{\pi}{2} - QID1 + QID2\right)} \tag{66}$$

$$BIIB = BII \cdot \cos(QID2) \tag{67}$$

The coordinates of the center of the parallelogram, defined as the intersection of the diagonals, are given as follows:

$$ZIDC = \frac{HIIB + BII \cdot \sin(QID2)}{2} - BII \cdot \sin(QID2) \tag{68}$$

$$YIDC = \frac{BIIB + HIIB \cdot \tan(QID1)}{2} \tag{69}$$

These relationships describe the geometry of the enclosing parallelogram. For a given station, the ratio of the enclosing area to the actual cross-sectional area is given by ROIDX. This value is assumed to vary linearly from the intake plane to a station which is located one engine diameter ahead of the engine face. At this last station, ROIDX is given by the ratio of the area of a square to the area of the inscribed circle. Thus, for the variation of ROIDX with axial distance, we have

$$ROIDX = 1 + \left(\frac{4}{\pi} - 1\right) \cdot \frac{XID}{LIDG - DIE} \tag{70}$$

Similarly, the cross-sectional area as well as the angles giving the inclination of the parallelogram are assumed to vary linearly from the intake to the diffuser exit. Thus,

$$OIX = OII + \frac{OIE - OII}{LIDG - DIE} \cdot XID \quad , \tag{71}$$

$$QIX1 = QFC3 \cdot \left(1 - \frac{XID}{LIDG - DIE}\right) \quad \text{, and} \tag{72}$$

$$QIX2 = QFC2 \cdot \left(1 - \frac{XID}{LIDG - DIE}\right) \tag{73}$$

The aspect ratio is similarly assumed to vary linearly with axial distance. At the engine face, it is equal to 1 and thus

$$AIX = AII \cdot \left(\frac{1 - AII}{XID2 - XII}\right) \cdot (X - XII) \quad . \tag{74}$$

Using the values defined above, it is possible to find the dimensions of a given diffuser station. The vertical inboard coordinate is found as

$$HIDBX = \frac{\sqrt{\frac{AIX \cdot OISX}{2}} \cdot \cos(QIX1)}{\sin\left(\frac{\pi}{2} - QIX1 + QIX2\right)} \quad \text{, with} \tag{75}$$

$$OISX = OIX(XID) \cdot ROIDX(XID) \quad . \tag{76}$$

The three-dimensional geometry of the diffusers is modelled as shown in Fig. 29. It has been divided into a forward and a rear section, with the latter extending to a station which is located one engine diameter forward of the compressor face. The Y- and Z-coordinates of the center of any given diffuser station are given by the equations

$$\begin{aligned} ZIDX &= ZI + FZIDA \cdot X^3 + FZIDB \cdot X^2 \quad \text{and} \\ YIDX &= YI + FYIDA \cdot X^3 + FYIDB \cdot X^2 \quad . \end{aligned} \tag{77}$$

For the forward section of the diffuser, X is measured rearwards from XII and

$$FZIDA = \frac{-2 \cdot (ZID1 - ZII)}{(XID1 - XII)^3} \quad \text{and}$$

$$FZIDB = \frac{3 \cdot (ZID1 - ZII)}{(XID1 - XII)^2} \quad . \tag{78}$$

Similarly, for the equation giving the Y-coordinate,

$$FYIDA = \frac{-2 \cdot (YID1 - YII)}{(XID1 - XII)^3} \quad \text{and}$$

$$FYIDB = \frac{3 \cdot (YID1 - YII)}{(XID1 - XII)^2} \quad . \tag{79}$$

In order to find the centerline coordinates of the rearward portion of the intake diffuser, the same relationships as in equations 77, 78 and 79 may be used. This time, however, X is measured from XID1, (YID1-YII) is replaced by (YID2-YID1), (ZID1-ZII) is replaced by (ZID2-ZID1) and (XID1-XII) is replaced by (XID2-XID1).

Several constraints upon the diffuser position within the fuselage and in relation to other items are employed to obtain values for the variables used above. XID1 is assumed to lie half way between XII and XID2, and XID2 itself lies a distance of one engine diameter forward of the compressor face, thus wholly defining the X-axis of the intake diffusers. Furthermore, the diffuser position is constrained by the lateral and vertical dimensions of the internal weapons bay at station XID1. Finally, the diffuser is assumed to have the same cross-sectional shape and dimensions at station XID2 and at XIE, the engine intake plane. This is necessary in order to ensure a sufficiently smooth airflow into the compressor.

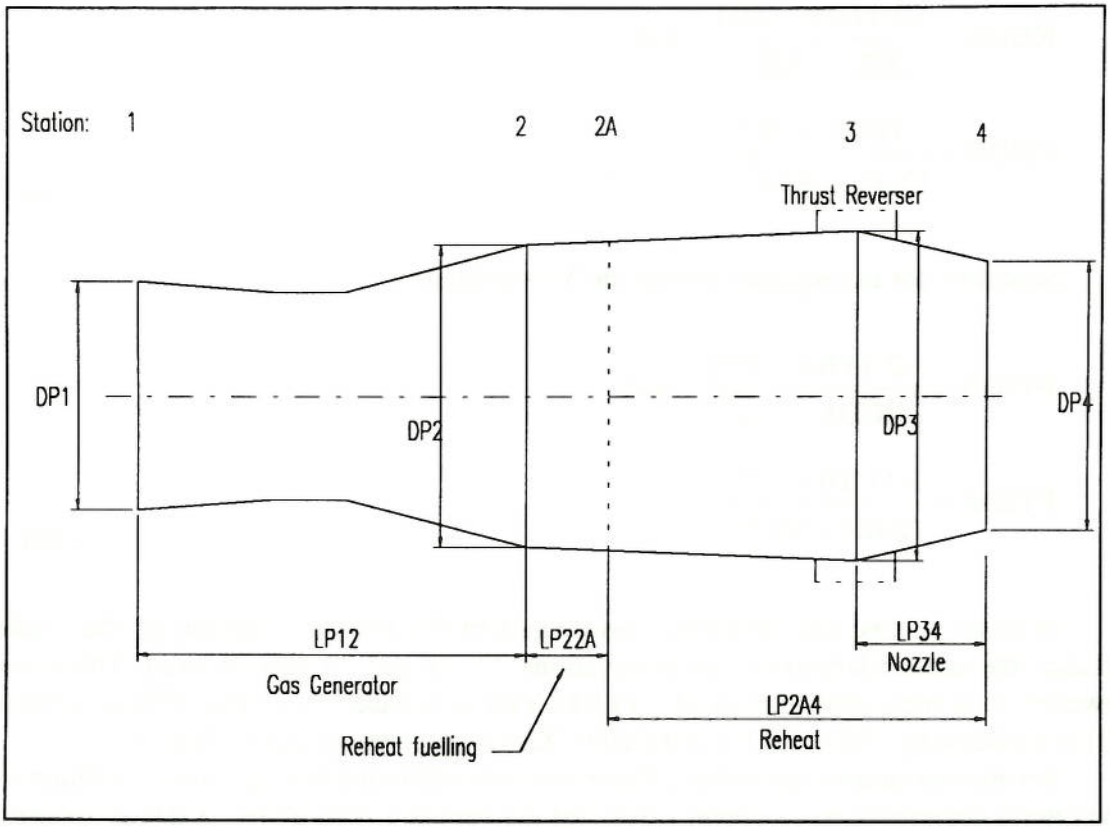

Fig. 25: Engine Bay Geometry, Axisymmetric Nozzles

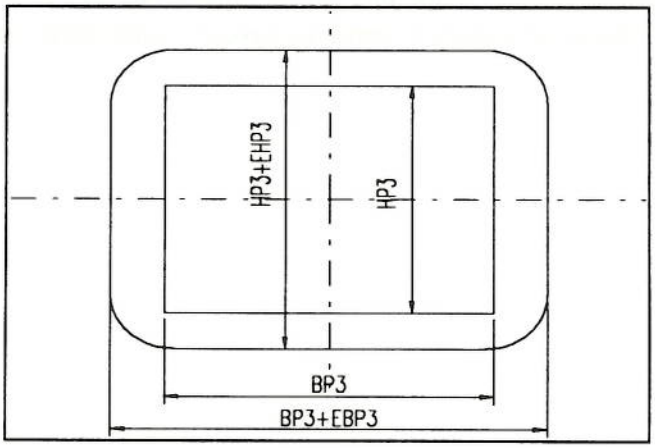

Fig. 26: Two-dimensional Nozzle Cross-Section

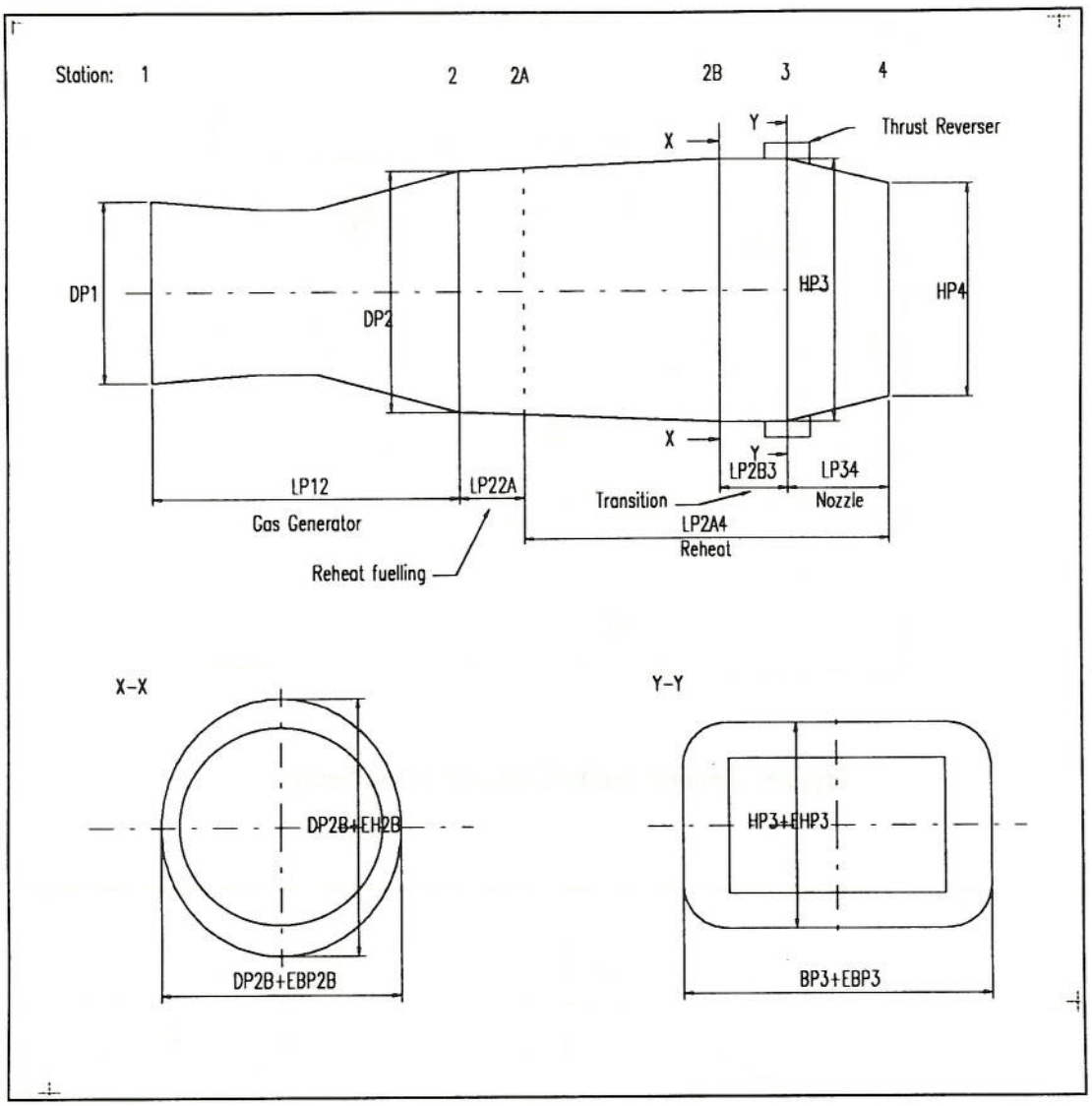

Fig. 27: Engine Geometry with Two-Dimensional Nozzles

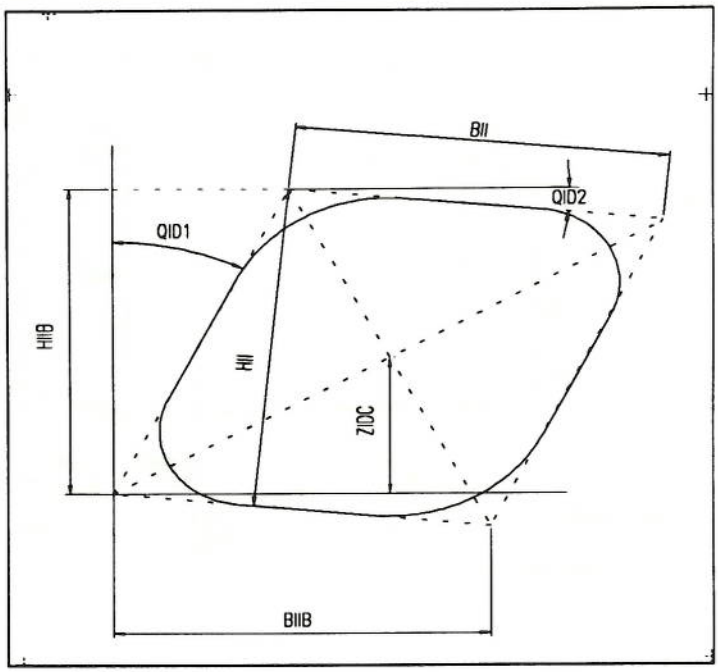

Fig. 28: General Intake Diffuser Cross Section

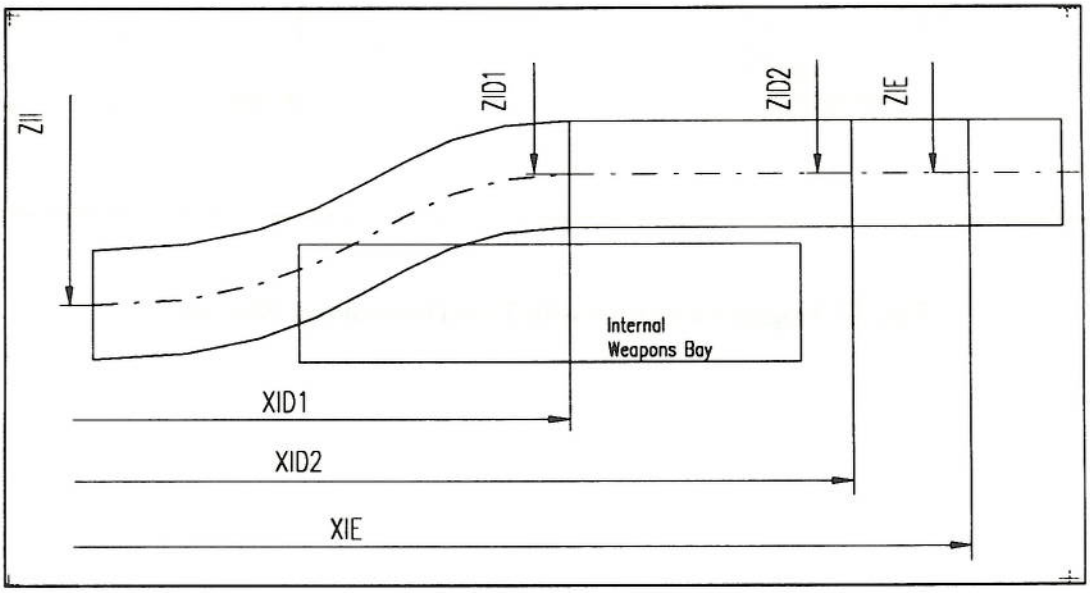

Fig. 29: Modelling of Intake Diffuser Geometry

4.1.6. FUSELAGE CROSS SECTIONS TO ENCLOSE CONTENTS

Now that the major aircraft components have been described, the synthesis of the cross sections required to enclose the fuselage contents is given. The order in which they are described below corresponds to the order in which the modules are arranged within the synthesis code.

4.1.6.1. STATION C

Station C is located aft of the pilot's head and contains the rear portion of the cockpit as well as the intake diffusers. The height of the fuselage at station C, HFC, is defined from

$$HFC = ZFLOOR + H1 - ZB1C + 0.5 \cdot HB1BI, \tag{80}$$

where

$$H1 = ZFLOOR + xcubic(XFC - XFA, FZCR, 4). \tag{81}$$

The function xcubic evaluates the cubic whose coefficients are stored in FZCR at the X value XFC-XFA.

The width of the fuselage at the cockpit side is initially set equal to the cockpit width, BCH, and the width at the bottom of the fuselage, BFCB, is constrained to be the greater of BB1BI and BCH, using the blending function. Referring to Fig. 30, two Bezier splines are used to define the top part of the fuselage (above the intakes), while the bottom part is constructed of straight line segments.

In order that the height of the intakes does not exceed the height of the fuselage minus the canopy, HIIB is found to be the lesser of HIIB defined by the intake aspect ratio AII and an expression involving the cockpit. Thus,

$$HIIB = blend(HIIB, H2 - (ZB1C - 0.5 \cdot HB1BI, 0.001, BELOW)), \tag{82}$$

with

$$H2 = ZFLOOR + HCEYE - HC7 + \tan(QCCAN) \cdot (XFC - XFB). \tag{83}$$

Then, to resize the intakes, if necessary,

$$\begin{aligned}
HII &= \frac{HIIB \cdot \sin(90° - QID1 + QID2)}{\cos(QID1)}, \\
AII &= \frac{2.0 \cdot HII^2}{OII}, \\
BII &= \frac{HII}{AII}, \text{ and} \\
BIIB &= BII \cdot \cos(QID2).
\end{aligned} \tag{84}$$

The top spline is defined by

$$\begin{aligned}
G1 &= 0.0, \\
G2 &= -\frac{1.0}{\tan(QFC1)}, \\
PFCT1(1,1) &= 0.0, \\
PFCT1(1,2) &= ZB1C - 0.5 \cdot HB1BI + HFC, \\
PFCT1(4,1) &= 0.5 \cdot BFCT, \text{ and} \\
PFCT1(4,2) &= H2 \ .
\end{aligned} \tag{85}$$

H2 has been defined in Eq. 83. The bottom spline is defined by

$$\begin{aligned}
G1 &= G2, \\
G2 &= -\tan(QID2), \\
PFCT2(1,1) &= PFCT1(4,1), \\
PFCT2(1,2) &= PFCT1(4,2), \\
PFCT2(4,1) &= 0.5 \cdot BFCB + \left[ZW - (ZB1C - 0.5 \cdot HB1BI)\right] \cdot \tan(QFC1) + BIIB \\
PFCT2(4,2) &= ZW.
\end{aligned} \tag{86}$$

The cross-sectional areas underneath the curves as well as their perimeters are summed and stored in the variables OFCS and PFC, respectively. In addition, the fuselage width at C is given by

$$BFC = 2.0 \cdot PFCT2(4,1). \tag{87}$$

The total cross sectional area required at station C is given by the value previously stored in OFCS and by

$$\begin{aligned}
OFCS = OFCS &+ 0.5 \cdot (BFCB + BFC - 2.0 \cdot BIIB - 2.0 \cdot BVI) \cdot \\
&\cdot abs(ZW - ZB1C + 0.5 \cdot HB1BI).
\end{aligned} \tag{88}$$

Also, the total perimeter is given by PFC, found above and with

$$PFC = PFC + BFCB + 2.0 \cdot \left[\frac{HIIB}{\cos(QID1)} + \frac{BIIB}{\cos(QID2)} \right]. \tag{89}$$

A net scaling factor is defined by the ratio of required cross-sectional area to the value calculated in OFCS, using

$$ROFCNS = \frac{OFC - OII - OVI}{OFCS}. \tag{90}$$

The value found is used to scale BFCT, BFCB, and HFC with

$$\begin{aligned} BFCT &= BFCT \cdot \sqrt{ROFCNS}, \\ BFCB &= BFCB \cdot \sqrt{ROFCNS}, \quad \text{and} \quad , \\ HFC &= (HFC - RCCAN) \cdot \sqrt{ROFCNS} + RCCAN. \end{aligned} \tag{91}$$

The vertical position of the cockpit floor is adjusted using

$$ZFLOOR = ZB1C - 0.5 \cdot HB1BI + HFC - H1, \tag{92}$$

where H1 has been defined in Eq. 81. Using an iterative procedure, it is possible to find the correct dimensions in order to match the actual to the required cross-sectional area.

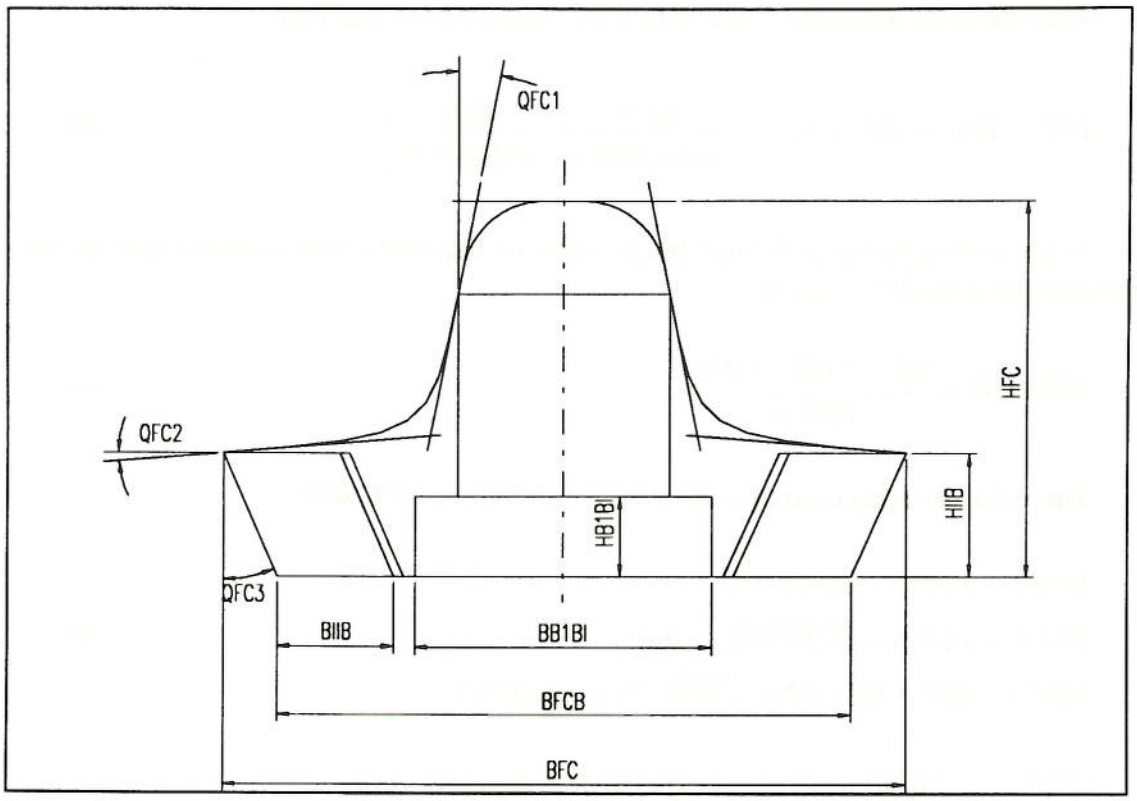

Fig. 30: Cross-Section of Fuselage at Station C

4.1.6.2. STATION A

Station A is located at the front cockpit bulkhead. Referring to Fig. 31, minimum values for HFA and BFA are found from

$$HFA = ZFLOOR + HC5 - ZFUS, \tag{93}$$

$$BFA = 2.0 \cdot YFA, \tag{94}$$

and they remain fixed throughout the scaling described below.
Also,

$$\begin{aligned} HFAT &= 0.5 \cdot (ZFLOOR + HC5 - ZSA), \\ HFAB &= 0.5 \cdot (ZSA - ZFUS) \\ BFAT &= \text{blend}\left(\frac{OFA}{HFA}, BFR, ABOVE, 0.001\right), \quad \text{and} \\ BFAB &= BFAT. \end{aligned} \tag{95}$$

Using these values, Bezier curves describe the top and bottom parts of the cross-section. For the top part,

$$
\begin{aligned}
&G1 = -\frac{1.0}{\tan(QFA1)}, \\
&G2 = -\tan(QFA2), \\
&PFAT2(1,1) = 0.5 \cdot BFAT, \\
&PFAT2(1,2) = ZSA + HFAT, \\
&PFAT2(4,1) = YFA, \quad \text{and} \\
&PFAT2(4,2) = ZSA.
\end{aligned}
\tag{96}
$$

For the bottom part,

$$
\begin{aligned}
&G2 = -G1, \\
&G1 = -G2, \\
&PFAB2(1,1) = 0.5 \cdot BFAB, \\
&PFAB2(1,2) = ZSA - HFAB, \\
&PFAB2(4,1) = YFA, \quad \text{and} \\
&PFAB2(4,2) = ZSA.
\end{aligned}
\tag{97}
$$

Next,

$$
\begin{aligned}
&G2 = -G1, \\
&G1 = 0.0, \\
&PFAT1(1,1) = 0.0, \\
&PFAT1(1,2) = ZFLOOR + HC5, \\
&PFAT1(4,1) = PFAT2(1,1), \quad \text{and} \\
&PFAT1(4,2) = PFAT2(1,2).
\end{aligned}
\tag{98}
$$

Finally,

$$
\begin{aligned}
&G1 = 0.0 \\
&G2 = -G2, \\
&PFAB1(1,1) = 0.0, \\
&PFAB1(1,2) = ZFUS, \\
&PFAB1(4,1) = PFAB2(1,1), \quad \text{and} \\
&PFAB1(4,2) = PFAB2(1,2).
\end{aligned}
\tag{99}
$$

The above series of equations appears in this order in the synthesis code.

In order to scale the cross section at A to match the fairing curve, a scaling factor is derived from the calculated area, OFAS and the required fairing curve area, OFA:

$$\text{ROFAS} = \frac{\text{OFA}}{\text{OFAS}}. \tag{100}$$

ROFAS is applied to BFAT using

$$\text{BFAT} = \text{BFAT} \cdot \sqrt{\text{ROFAS}} \tag{101}$$

and an iterative procedure is used to find the correct value for BFAT.

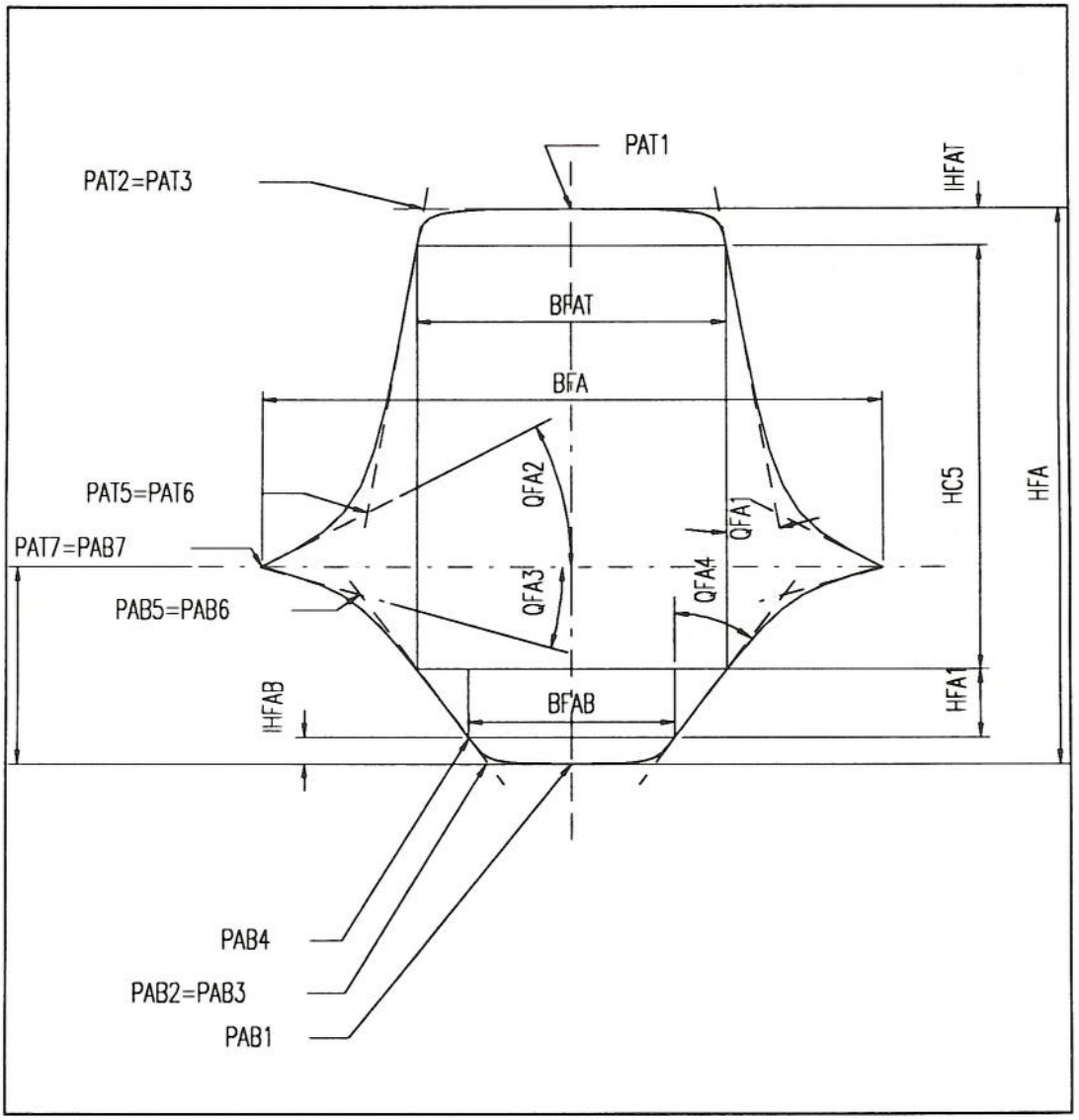

Fig. 31: Cross-Section of Fuselage Station A

4.1.6.3. STATION B

Fuselage station B is located at the pilot's eyepoint, the longitudinal position of which is derived from the cockpit geometry. Firstly,

$$BFB = 2.0 \cdot YSB\ , \tag{102}$$

which defines the width of the fuselage at B in terms of the forebody chine geometry given by YSB. Also, several width and height descriptors are given in a manner similar to station A, these being

$$\begin{aligned} BFBT &= BCH, \\ BFBB &= 0.5 \cdot \frac{BFB}{FFS}\ , \\ HFBT &= ZFLOOR + HCEYE - HC7 - ZSB\ , \text{ and} \\ HFBB &= \frac{ZSB - ZFUS}{2.0}\ . \end{aligned} \tag{103}$$

The spline used at the top of the cross-section to fit the canopy is dependent upon whether a single or a twin seat cockpit has been chosen. In the former case,

$$PFBT1(1,2) = ZFLOOR + HCEYE + HC4, \tag{104}$$

while in the latter case

$$PFBT1(1,2) = ZFLOOR + xcubic(XF - XFA, FZCF, 4). \tag{105}$$

These equations are based upon the assumption that for a single-seat cockpit the maximum canopy elevation is located above the pilot's eyepoint. Furthermore, we have

$$\begin{aligned} G1 &= 0.0, \\ G2 &= -\frac{1.0}{\tan(QFB1)}\ , \\ PFBT1(1,1) &= 0.0, \\ PFBT1(4,1) &= 0.5 \cdot BFBT, \text{ and} \\ PFBT1(4,2) &= ZC + HFBT. \end{aligned} \tag{106}$$

For the rest of the upper spline,

$$
\begin{aligned}
&G1 = G2,\\
&G2 = -\tan(QFB2),\\
&PFBT2(1,1) = PFBT1(4,1),\\
&PFBT2(1,2) = PFBT1(4,2),\\
&PFBT2(4,1) = 0.5 \cdot BFB, \text{ and}\\
&PFBT2(4,2) = ZC.
\end{aligned}
\tag{107}
$$

The lower portion of the fuselage at B has splines defined by the following values:

$$
\begin{aligned}
&G1 = 0.0\\
&G2 = \frac{1.0}{\tan(QFB1)},\\
&PFBB1(1,1) = 0.0,\\
&PFBB1(1,2) = ZFUS,\\
&PFBB1(4,1) = 0.5 \cdot BFBB, \text{ and}\\
&PFBB1(4,2) = ZC - HFBB.
\end{aligned}
\tag{108}
$$

$$
\begin{aligned}
&G1 = G2,\\
&G2 = \tan(QFB2),\\
&PFBB2(1,1) = PFBB1(4,1),\\
&PFBB2(1,2) = PFBB1(4,2),\\
&PFBB2(4,1) = 0.5 \cdot BFB, \text{ and}\\
&PFBB2(4,2) = ZC.
\end{aligned}
\tag{109}
$$

A scaling factor is formed using the area enclosed by the splines and the area required at station B found from the fairing curve, so

$$
ROFBS = \frac{OFB}{OFBS} . \tag{110}
$$

Using an iterative procedure, the square root of the scaling factor is applied to BFBT, HFBT, and BFBB, until agreement is obtained between the actual and the required cross-sectional areas:

$$
\begin{aligned}
&BFBT = BFBT \cdot \sqrt{ROFBS},\\
&HFBT = \frac{HFBT}{\sqrt{ROFBS}}, \text{ and}\\
&BFBB = BFBB \cdot \sqrt{ROFBS}.
\end{aligned}
\tag{111}
$$

As can be seen from the above, HFB and BFB remain constant during the scaling process.

4.1.6.4. STATION F

In order to define the vertical geometry of the fuselage aft of the cockpit, station F needs to be defined before stations D and E. It is located at the face of the engine compressor, which is also engine station number 1. This cross section additionally contains a part of the wing box as well as the main landing gear bays. The synthesis of station F was fairly complicated because account needed to be taken of the possible different positions of the main gear when retracted as well as the options for positioning the weapons bay. Also, the vertical position of the engine centreline is determined in this module by relating it to the main gear and weapons bay positions, depending upon the clearances necessary in order to avoid the main gear bay extending below the bottom of the fuselage as defined by the weapons bay.

First, a vertical position of the engine, denoted by ZPCH, is found by relating the geometry to the datum position given in ZDATWB, which is the bottom of the weapons bay, given by

$$ZDATWB = ZB1C - 0.5 \cdot HB1BI. \tag{112}$$

If the weapons bay is located between the diffusers and the main gear is stowed verticall, the engine is assumed to be located between the main gear bay and the weapons bay, and ZPCH is found under the assumption that sufficient clearance exists between the fuselage underside and the engine to pass the wing structure around the bay. Thus,

$$ZPCH = ZDATWB + 0.5 \cdot HWBF \cdot FHWBF + 0.5 \cdot (DP1 + EHP1). \tag{113}$$

Alternatively, if the main gear is stowed horizontally, the engine bay is located above the main gear bay, and its width is added to equation 113.

If the weapons bay is located underneath the diffusers, no account needs to be taken of the main gear position for determining ZPCH, so

$$ZPCH = ZDATWB + HB1BI + 0.5 \cdot FHWBF \cdot HWBF + 0.5 \cdot (DP1 + EHP1). \tag{114}$$

In order to fit the splines in a uniform fashion for all four of the above cases, the following variables are defined.

If the weapons bay is located between the diffusers,

$$BFFT1 = YPCH + DP1 + EBP1, \text{ and}$$
$$BFFT2 = DP1 + EBP1. \tag{115}$$

Additionally, if the main gear is stowed vertically, then

$$\text{BFFB} = \text{YPCH} + 2.0 \cdot \text{BUMG} + \text{DP1} + \text{EBP1}, \text{ and}$$
$$\text{ZFFTP} = \text{blend}\begin{pmatrix} \text{ZPCH} + 0.5 \cdot (\text{DP1} + \text{EHP1}) + 0.5 \cdot \text{FHWBF} \cdot \text{HWBF}, \\ \text{ZDATWB} + \text{DUMG} + \text{HWBF} \cdot \text{FHWBF}, 0.001, \text{ABOVE} \end{pmatrix}. \quad (116)$$

Otherwise,

$$\text{BFFB} = \text{YPCH} + \text{blend}(\text{DUMG}, \text{DP1} + \text{EBP1}, 0.001, \text{ABOVE}) \text{ and}$$
$$\text{ZFFTP} = \text{ZPCH} + 0.5 \cdot (\text{DP1} + \text{EHP1}) + 0.5 \cdot \text{HWBF} \cdot \text{FHWBF}. \quad (117)$$

In these equations, ZFFTP denotes the z-coordinate of the fuselage perimeter located above the propulsion bay, while ZFFTC denotes the corresponding z-coordinate at the fuselage centreline. Also, DUMG denotes the diameter of the main wheel bay, including clearances.

If the weapons bay is located underneath the diffusers, then

$$\text{ZFFTP} = \text{ZPCH} + 0.5 \cdot \text{FHWBF} \cdot \text{HWBF} + 0.5 \cdot (\text{DP1} + \text{EHP1}), \text{ and}$$
$$\text{BFFB} = \text{blend}(\text{YPCH} + \text{DP1} + \text{EBP1}, \text{BB1BI}, 0.001, \text{ABOVE}) + \quad (118)$$
$$+ 0.5 \cdot \text{HWBF} \cdot \text{FHWBF}.$$

Also, if the main gear is stowed vertically, then

$$\text{BFFT1} = \text{YPCH} + \text{DP1} + \text{EBP1} + 2.0 \cdot \text{BUMG}, \text{ and}$$
$$\text{BFFT2} = \text{DP1} + \text{EBP1} + \text{BUMG}. \quad (119)$$

Otherwise,

$$\text{BFFT1} = \text{YPCH} + \text{DP1} + \text{EBP1} \text{ and}$$
$$\text{BFFT2} = \text{DP1} + \text{EBP1}. \quad (120)$$

The relationship for BFFB in Equation 118 ensures that the fuselage is wide enough to accomodate the greater of the widths obtained from the weapons bay and the propulsion bay. Also, BUMG denotes the width of the main gear bay including clearances.

Some variables are the same for all of the above cases, these being

$$\text{ZFFTC} = \text{ZW} + 0.5 \cdot \text{FHWBF} \cdot \text{HWBF},$$
$$\text{HFFC} = \text{ZFFTC} - \text{ZDATWB}, \text{ and} \quad (121)$$
$$\text{RHHV} = \frac{\text{ZFFTC} - \text{ZW}}{\text{HFFC}}.$$

HFFC is the fuselage height at station F at the centreline, while RHHV denotes the ratio of the distance between the wing centreline and the top of the fuselage at the centreline to the fuselage height. The latter value is needed for the definition of the aftbody shape in the case of twin engines being installed.

After the above variables have been defined, spline curves are fitted according to the following relationships. First, a fuselage width is defined using

$$\mathrm{BFF} = \mathrm{FFS}\cdot\left[\mathrm{BFFB} + 2.0\cdot(\mathrm{ZW} - 0.5\cdot\mathrm{HWBF} - \mathrm{ZDATWB})\cdot\tan(\mathrm{QFS})\right]. \quad (122)$$

Then, two temporary variables, Z1 and Z2, are calculated from

$$\mathrm{Z1} = \mathrm{blend}\begin{pmatrix}\mathrm{ZDATWB} + \mathrm{WHEEL} + \mathrm{FHWBF}\cdot\mathrm{HWBF}, \\ \mathrm{ZW} + 0.5\cdot\mathrm{HWBF}, 0.001, \mathrm{ABOVE}\end{pmatrix} - (\mathrm{ZW} + 0.5\cdot\mathrm{HWBF}) \quad (123)$$

and

$$\mathrm{Z2} = \mathrm{Z1}\cdot\frac{\mathrm{BFF} - \mathrm{BFFT1}}{\mathrm{BFF} - \mathrm{BFFB}}\ . \quad (124)$$

The splines are then calculated in the following order, using definitions

$$\begin{aligned}
&\mathrm{G1} = 0.0, \\
&\mathrm{G2} = -\frac{1.0}{\tan(\mathrm{QFF1})}, \\
&\mathrm{PFFT1}(1,1) = 0.5\cdot\mathrm{YPCH}, \\
&\mathrm{PFFT1}(1,2) = \mathrm{ZFFTP}, \\
&\mathrm{PFFT1}(4,1) = 0.5\cdot\mathrm{BFFT1}, \\
&\mathrm{PFFT1}(4,2) = 0.5\cdot(\mathrm{ZW} + 0.5\cdot\mathrm{HWBF} + \mathrm{Z2} + \mathrm{ZFFTP}),
\end{aligned} \quad (125)$$

and

$$\begin{aligned}
&\mathrm{G1} = \mathrm{G2}, \\
&\mathrm{G2} = -2.0\cdot\frac{\mathrm{Z1}}{\mathrm{BFF} - \mathrm{BFFB}}, \\
&\mathrm{PFFT2}(1,1) = \mathrm{PFFT1}(4,1), \\
&\mathrm{PFFT2}(1,2) = \mathrm{PFFT1}(4,2), \\
&\mathrm{PFFT2}(4,1) = 0.5\cdot\mathrm{BFF}, \\
&\mathrm{PFFT2}(4,2) = \mathrm{ZW} + 0.5\cdot\mathrm{HWBF}
\end{aligned} \quad (126)$$

for the upper outer section of the cross-section, and

$$\begin{aligned}
&G1 = 0.0,\\
&G2 = \frac{1.0}{\tan(QFF1)},\\
&PFFT3(1,1) = PFFT1(1,1),\\
&PFFT3(1,2) = PFFT1(1,2),\\
&PFFT3(4,1) = \text{blend}(0.5 \cdot BFFT1 - BFFT2, 0.0, 0.01, \text{ABOVE}),\\
&PFFT3(4,2) = 0.5 \cdot (PFFT1(1,2) + ZFFTC),
\end{aligned} \tag{127}$$

as well as

$$\begin{aligned}
&G1 = G2,\\
&G2 = 0.0,\\
&PFFT4(1,1) = PFFT3(4,1),\\
&PFFT4(1,2) = PFFT3(4,2),\\
&PFFT4(4,1) = 0.0, \text{ and}\\
&PFFT4(4,2) = ZFFTC
\end{aligned} \tag{128}$$

for the upper centre section. In Equations 127 and 128, ZFFTC is constantly modified as the scaling to match the fairing curve progresses, in order to maintain the correct fuselage shape:

$$ZFFTC = \text{blend}(ZFFTC, ZZ1, 0.001, \text{ABOVE}), \tag{129}$$

with

$$ZZ1 = PFFT3(4,2) - G2 \cdot PFFT3(4,1). \tag{130}$$

For the lower section (underneath the wing centreline), we have a spline defined by

$$\begin{aligned}
&G1 = \frac{1.0}{\tan(QFF1)},\\
&G2 = 0.0,\\
&PFFB1(1,1) = 0.5 \cdot BFFB,\\
&PFFB1(1,2) = ZDATWB,\\
&PFFB1(4,1) = 0.5 \cdot BFF, \text{ and}\\
&PFFB1(4,2) = ZW - 0.5 \cdot HWBF.
\end{aligned} \tag{131}$$

After the areas enclosed by the splines and their perimeters have been found and stored in OFFS and PFF, respectively, any additional sections of the cross-sectional area are found, using

$$\begin{aligned} OFFS = OFFS + 2.0 \cdot [PFFB1(4,1) - PFFB1(1,1)] \cdot 0.5 \cdot HWBF + \\ + BFFB \cdot (ZW - ZDATWB) \end{aligned} \tag{132}$$

and

$$PFF = PFF + 2.0 \cdot HWBF + BFFB. \tag{133}$$

A scaling factor is defined using the actual and required cross-sectional areas less the cross section of the engine stream tube, so

$$ROFFS = \frac{OFF - NENG \cdot \frac{\pi}{4} \cdot DP2^2}{OFFS - NENG \cdot \frac{\pi}{4} \cdot DP2^2} . \tag{134}$$

ROFFS is applied to ZFFTP, BFFT1, and BFFB using

$$\begin{aligned} ZFFTP &= ZFFTP \cdot \sqrt{ROFFS}, \\ BFFT1 &= BFFT1 \cdot \sqrt{ROFFS}, \text{ and} \\ BFFB &= BFFB \cdot \sqrt{ROFFS}. \end{aligned} \tag{135}$$

BFFT2 is recalculated using

$$BFFT2 = BFFT1 - YPCH. \tag{136}$$

The curve fitting is repeated until the actual corresponds to the required cross-sectional area. HFF is found as the greater of HFFC and ZFFTP-ZDATWB.

4.1.6.5. STATION D

Station D is located at the front of the outer weapons bays. The height at the centreline is defined using a curve fit between stations C and F, and remains constant during the iteration to match the minimum required area to the fairing curve.

The width at the bottom of the fuselage is given as

$$BFDB = 2.0 \cdot YID + BID + 2.0 \cdot BB2BI, \tag{137}$$

where YID is the y-coordinate of the diffusers at station D and BID is the corresponding diffuser width.

Also,

$$\begin{aligned} &HFDC = ZW + 0.5 \cdot HWD - ZB1C + 0.5 \cdot HB1BI, \\ &BFD = BFDB + 2.0 \cdot HFDC \cdot \tan(QFD3), \\ &BFDT = BFCT, \\ &HFDT = .5 \cdot (BFD - BFDT) \cdot \tan(QFD2) + HFDC, \end{aligned} \tag{138}$$

where HWD is the height of the wing box at the fuselage side at D, so that finally the height of the fuselage at D is

$$HFD = ZFD - ZB1C + 0.5 \cdot HB1BI. \tag{139}$$

ZFD is the z-coordinate of the fuselage spine at station D, found from the curve fit mentioned above.

Once again a series of Bezier fits are defined using

$$\begin{aligned} &G1 = 0.0, \\ &G2 = -\frac{1.0}{\tan(QFD1)}, \\ &PFDT1(1,1) = 0.0, \\ &PFDT1(1,2) = ZB1C - 0.5 \cdot HB1BI + HFD, \\ &PFDT1(4,1) = 0.5 \cdot BFDT, \text{ and} \\ &PFDT1(4,2) = ZB1C - 0.5 \cdot HB1BI + HFDT \end{aligned} \tag{140}$$

for the upper spline, and

$$\begin{aligned} &G1 = G2, \\ &G2 = -\tan(QFD2), \\ &PFDT2(1,1) = PFDT1(4,1), \\ &PFDT2(1,2) = PFDT1(4,2), \\ &PFDT2(4,1) = 0.5 \cdot BFD, \text{ and} \\ &PFDT2(4,2) = ZB1C - 0.5 \cdot HB1BI + HFDC. \end{aligned} \tag{141}$$

The rest of the cross-sectional area is found using OFDS from the splines in Equations 140 and 141 and the folowing expression:

$$OFDS = OFDS + 0.5 \cdot (BFD + BFDB) \cdot HFDC + BFDT \cdot (HFDT - HFDC) \tag{142}$$

The rest of the perimeter is similarly found, using

$$PFD = PFD + BFDB + 2.0 \cdot \frac{HFDC}{\cos(QFD3)} \quad . \tag{143}$$

The scaling factor, ROFDS, is found from

$$ROFDS = \frac{OFD - OIXD}{OFDS - OIXD}, \tag{144}$$

where OIXD is the cross-sectional area of the intake diffusers at station D. The square root of the scaling factor is applied as follows:

$$\begin{aligned} BFDT &= BFDT \cdot \sqrt{ROFDS}, \\ BFDB &= BFDB \cdot \sqrt{ROFDS}, \end{aligned} \tag{145}$$

and BFD is recalculated using the expression in Equation 138.

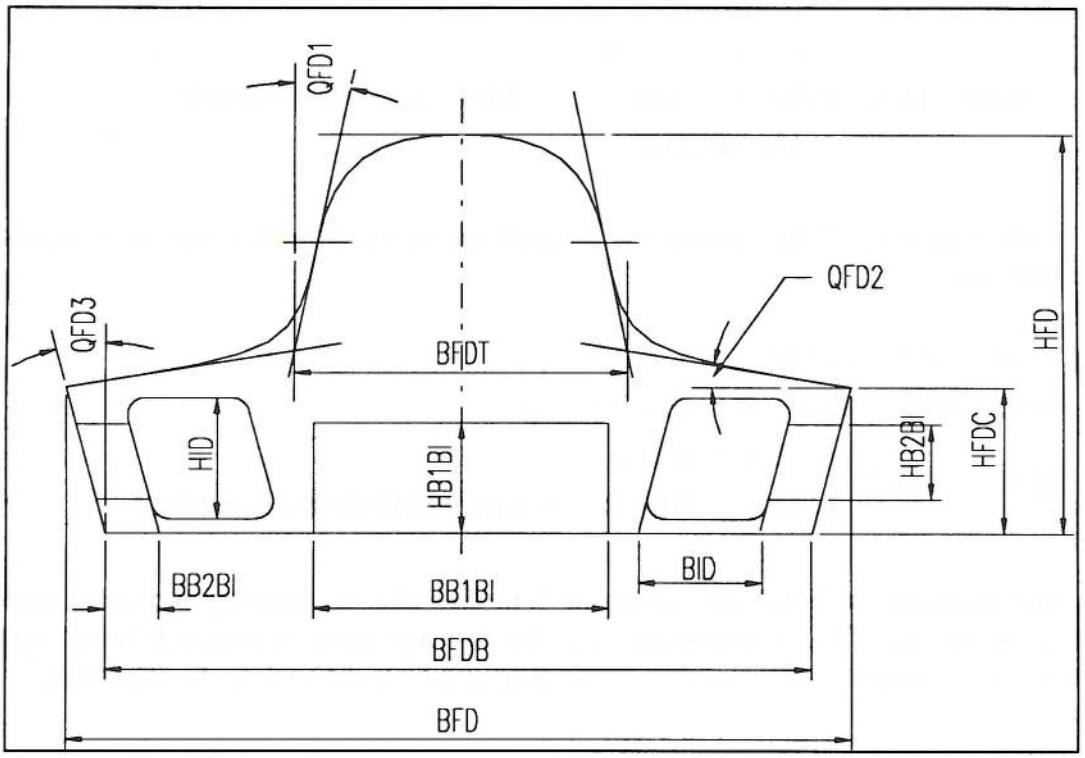

Fig. 32: Fuselage Station D

4.1.6.6. STATION E

Station E is located at the front of the main gear bay, and its minimum dimensions depend, as for station F, upon the way the main gear is stowed. If the wheel is retracted vertically, then

$$BFE1 = BIE + BUMW \cdot FBUMW, \tag{146}$$

where BIE is the width of the diffuser at station E, and

$$BFEB = YIXE + BIE + 2.0 \cdot BUMW \cdot FBUMW, \tag{147}$$

where YIXE is the y-coordinate of the diffuser centreline at station E. Also,

$$ZFEBP = \text{blend}\begin{pmatrix} ZB1C - 0.5 \cdot HB1BI, \\ ZIXE - 0.5 \cdot HIE - 0.5 \cdot HWBE, 0.001, BELOW \end{pmatrix}, \tag{148}$$

which denotes the Z-coordinate of the fuselage underneath the intake diffuser. If, on the other hand, the main wheel is stowed horizontally, then

$$\begin{aligned} BFE1 &= \text{blend}(BIE, BUMW \cdot FBUMW, 0.001, ABOVE), \\ BFEB &= 2.0 \cdot (YIXE - 0.5 \cdot BIE + BFE1), \text{ and} \\ ZFEBP &= \text{blend}\begin{pmatrix} ZB1C - 0.5 \cdot HB1BI, \\ ZIXE - 0.5 \cdot HIE - 0.5HWBE - BUMW \cdot FBUMW, \\ 0.001, BELOW \end{pmatrix}. \end{aligned} \tag{149}$$

In this equation, ZIXE denotes the z-coordinate of the diffuser centreline at station E. Furthermore,

$$\begin{aligned} HFEC &= ZW - ZFEBP, \\ HFE &= ZFE - (ZB1C - 0.5 \cdot HB1BI), \text{ and} \\ HFET &= \text{blend}\begin{pmatrix} ZB1C - 0.5 \cdot HB1BI, \\ ZIXE - 0.5 \cdot HIE - 0.5 \cdot HWBE - ZFEBP, 0.001, ABOVE \end{pmatrix}. \end{aligned} \tag{150}$$

The procedure to fit the area at station E to the value required by the fairing curve begins by fixing ZFETC, the z-coordinate of the fuselage spine at station E based upon the curve fit between C and F and then fitting Bezier splines defined by the following:

$$\begin{aligned} G1 &= 0.0, \\ G2 &= -\frac{1.0}{\tan(QFE1)}, \\ PFET1(1,1) &= YIXE, \\ PFET1(1,2) &= ZFEBP + HFET, \\ PFET1(4,1) &= 0.5 \cdot BFE1 + PFET1(1,1), \text{ and} \\ PFET1(4,2) &= ZFEBP + 0.5 \cdot (HFET + HFEC + 0.5 \cdot HWBE). \end{aligned} \tag{151}$$

Now, a fuselage width for station E can be defined as

$$\mathrm{BFE} = \mathrm{FFS}\cdot \mathrm{blend}\begin{pmatrix} \mathrm{BFEB} + 2.0\cdot\tan(\mathrm{QFE4})\cdot \mathrm{HFEC}, 2.0\cdot \mathrm{PFET}(4,1) + \\ +2.0\cdot\tan(\mathrm{QFE1})\cdot\left(\mathrm{PFET1}(4,2) - \mathrm{ZW} + 0.5\cdot\mathrm{HWBE}\right), \\ 0.001, \mathrm{ABOVE} \end{pmatrix}. \quad (152)$$

Next,

$$\begin{aligned} &\mathrm{G1} = \mathrm{G2}, \\ &\mathrm{G2} = -\tan(\mathrm{QFE2}), \\ &\mathrm{PFET2}(1,1) = \mathrm{PFET1}(4,1), \\ &\mathrm{PFET2}(1,2) = \mathrm{PFET1}(4,2), \\ &\mathrm{PFET2}(4,1) = 0.5\cdot\mathrm{BFE}, \text{ and} \\ &\mathrm{PFET2}(4,2) = \mathrm{ZW} + 0.5\cdot\mathrm{HWBE}. \end{aligned} \quad (153)$$

$$\begin{aligned} &\mathrm{PFET3}(1,1) = \mathrm{PFET1}(1,1), \\ &\mathrm{PFET3}(1,2) = \mathrm{PFET1}(1,2), \\ &\mathrm{PFET3}(4,1) = \mathrm{PFET1}(4,1) - \mathrm{BFE1}, \\ &\mathrm{PFET3}(4,2) = 0.5\cdot\left(\mathrm{ZFETC} + \mathrm{PFET1}(1,2)\right), \text{ and} \\ &\mathrm{G1} = 0.0. \end{aligned} \quad (154)$$

In order to obtain a practical fuselage shape at E, for this spline, if PFET3(4,2) is less than ZFETC, then

$$\mathrm{G2} = -\frac{1.0}{\tan(\mathrm{QFE1})}, \quad (155)$$

else

$$\mathrm{G2} = \frac{1.0}{\tan(\mathrm{QFE1})}. \quad (156)$$

Finally, for the top part of fuselage station E,

$$
\begin{aligned}
&G1 = G2,\\
&G2 = 0.0,\\
&PFET4(1,1) = PFET3(4,1),\\
&PFET4(1,2) = PFET3(4,2),\\
&PFET4(4,1) = 0.0, \text{ and}\\
&PFET4(4,2) = ZFETC.
\end{aligned}
\tag{157}
$$

The bottom part of the fuselage cross-section at E contains one Bezier spline defined by

$$
\begin{aligned}
&G1 = \frac{1.0}{\tan(QFE4)},\\
&G2 = \tan(QFE3),\\
&PFEB1(1,1) = 0.5 \cdot BFEB,\\
&PFEB1(1,2) = ZW - HFEC,\\
&PFEB1(4,1) = 0.5 \cdot BFE, \text{ and}\\
&PFEB1(4,2) = ZW - 0.5 \cdot HWBE,
\end{aligned}
\tag{158}
$$

and, if $ZFEBP < ZB1C - 0.5 \cdot HB1BI$, then the following is defined:

$$
\begin{aligned}
&PFEB2(1,1) = PFEB1(1,1) - BFE1,\\
&PFEB2(1,2) = PFEB1(1,2),\\
&PFEB2(4,1) = 0.5 \cdot BB1BI, \text{ and}\\
&PFEB2(4,2) = ZB1C - 0.5 \cdot HB1BI.
\end{aligned}
\tag{159}
$$

The rest of the points are not defined using the Bezier fitting routine, but are defined by

$$
\begin{aligned}
&PFEB2(2,1) = PFEB2(1,1),\\
&PFEB2(2,2) = PFEB2(4,2),\\
&PFEB2(3,1) = PFEB2(4,1), \text{ and}\\
&PFEB2(3,2) = PFEB2(4,2).
\end{aligned}
\tag{160}
$$

Following the evaluation of the cross-sectional area enclosed by these splines, a scaling factor is defined using

$$
ROFES = \frac{OFE - OIXE}{OFES - OIXE},
\tag{161}
$$

where OFE is the required area obtained from the fairing curve, OFES is the minimum area calculated from the splines, and OIXE is the cross-sectional area of the intake diffusers at station E. Using an iterative procedure, BFEB and HFET are adjusted until the desired cross-sectional area is achieved:

$$\begin{aligned} BFEB &= BFEB \cdot \sqrt{ROFES} \quad \text{and} \\ HFET &= HFET \cdot \sqrt{ROFES}. \end{aligned} \tag{162}$$

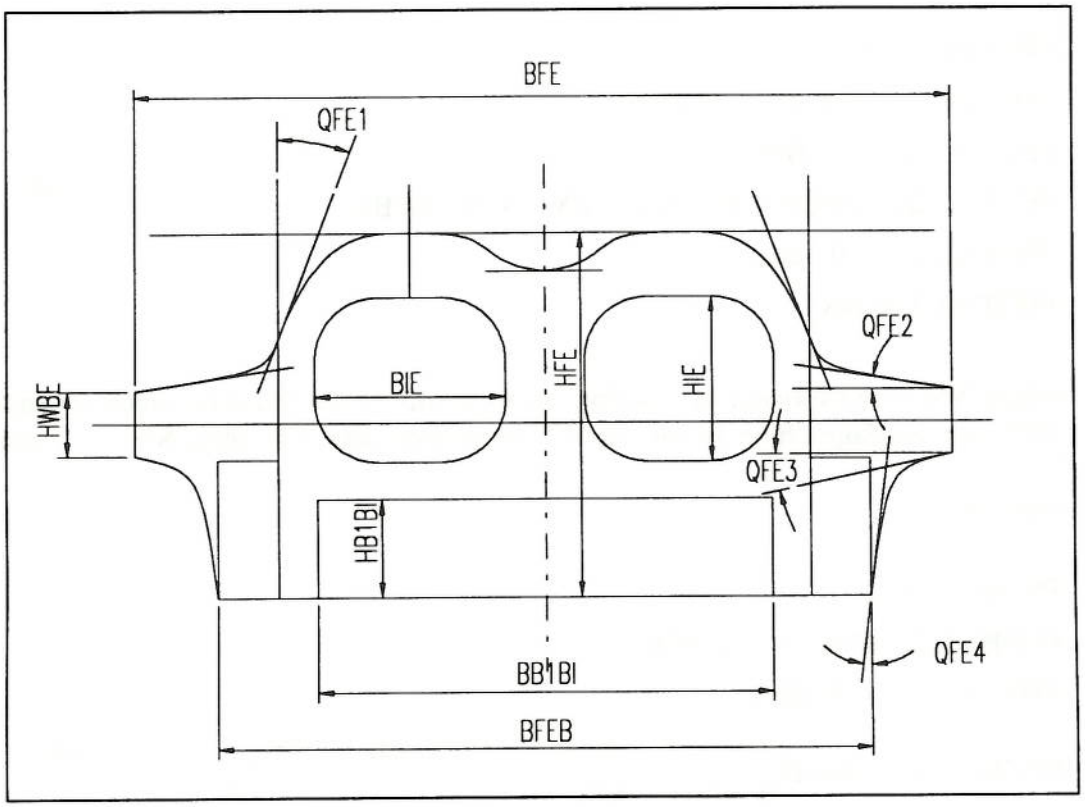

Fig. 33: Fuselage Station E

4.1.6.7. STATION G

Fuselage station G is located at the engine bay station 2, which corresponds to the rear of the gas generator. The geometry depends upon whether a single or twin engine layout is chosen. For the single engine case,

$$
\begin{aligned}
&BFG1 = DP2 + EBP2,\\
&HFG = DP2 + EHP2,\\
&HFG1 = ZPCH + 0.5 \cdot HFG - ZW,\\
&HFG2 = HFG - HFG1, \text{ and}\\
&BFG = BFG1 + 2.0 \cdot \text{blend}(HFG1, HFG2, 0.001, \text{ABOVE}) \cdot \tan(QFG1).
\end{aligned}
\tag{163}
$$

In this case, an elliptic fit has been used for the fuselage contour, so the controlling parameters are found as follows:

$$
\begin{aligned}
&PFGT1(1,1) = 0.0,\\
&PFGT1(1,2) = ZW + 0.5 \cdot HWBG,\\
&PFGT1(2,1) = 0.5 \cdot BFG,\\
&PFGT1(2,2) = ZPCH + 0.5 \cdot HFG - ZW - 0.5 \cdot HWBG,\\
&PFGT1(3,1) = 1.0, \text{ and}\\
&PFGT1(3,2) = NN,
\end{aligned}
\tag{164}
$$

where NN is an exponent as described in Appendix (), the value of which depends upon FFS, the fuselage chine factor. If FFS is greater than 1.0, then NN=-1.5, else NN=0.0.

Furthermore,

$$
\begin{aligned}
&PFGB1(1,1) = 0.0,\\
&PFGB1(1,2) = ZW - 0.5 \cdot HWBG,\\
&PFGB1(2,1) = 0.5 \cdot BFG,\\
&PFGB1(2,2) = \text{blend}\begin{pmatrix} ZW - 0.5 \cdot HWBG - ZPCH + 0.5 \cdot HFG, \\ 0.0, 0.001, \text{ABOVE} \end{pmatrix},\\
&PFGB1(3,1) = 1.0, \text{ and}\\
&PFGB1(3,2) = NN.
\end{aligned}
\tag{165}
$$

After the area enclosed by the superellipse has been evaluated, a net scaling factor is defined using

$$
ROFGS = \frac{OFG - \frac{\pi}{4} \cdot DP2^2}{OFGS - \frac{\pi}{4} \cdot DP2^2}, \tag{166}
$$

where DP2 is the diameter of the propulsion bay at station G, OFG is the cross-sectional area required by the fairing curve, and OFGS is the minimum area as calculated

from the superellipses defined above. The scaling is accomplished with an iterative procedure using

$$\begin{aligned} &HFG = HFG \cdot \sqrt{ROFGS} \quad \text{and} \\ &BFG1 = BFG1 \cdot \sqrt{ROFGS}. \end{aligned} \tag{167}$$

If twin engines are chosen, a slightly more complicated shape results, as shown in Fig. 34. Thus, BFG2, HFG, HFG1, HFG2, BFG1, and BFG are defined as in Equation 163. There are now three elliptical fits, the one defined by Equation 168 being the outboard fit at the top of the fuselage section:

$$\begin{aligned} &PFGT1(1,1) = 0.5 \cdot YPCH, \\ &PFGT1(1,2) = ZW + 0.5 \cdot HWBG, \\ &PFGT1(2,1) = 0.5 \cdot (BFG - YPCH), \\ &PFGT1(2,2) = ZPCH + 0.5 \cdot HFG - ZW - 0.5 \cdot HWBG, \\ &PFGT1(3,1) = 1.5, \quad \text{and} \\ &PFGT1(3,2) = NN. \end{aligned} \tag{168}$$

Furthermore, for the top inboard section

$$\begin{aligned} &PFGT2(1,1) = PFGT1(1,1), \\ &PFGT2(1,2) = ZW + RHHV \cdot HFGC, \\ &PFGT2(2,1) = 0.5 \cdot BFG2, \\ &PFGT2(2,2) = ZPCH + 0.5 \cdot HFG - PFGT2(1,2), \\ &PFGT2(3,1) = 1.0, \quad \text{and} \\ &PFGT2(3,2) = NN, \end{aligned} \tag{169}$$

Where RHHV was calculated in Equation 121 and HFGC is determined from the rear fuselage layout.

For the bottom section of station G, a flat underside is assumed at the centre, with the outer elliptic fit similar to the one for a single-engine case. Thus,

$$\begin{aligned} &PFGB1(1,1) = 0.5 \cdot YPCH, \\ &PFGB1(1,2) = ZW - 0.5 \cdot HWBG, \\ &PFGB1(2,1) = 0.5 \cdot (BFG - YPCH), \\ &PFGB1(2,2) = \text{blend}(Z1, Z2, 0.01, \text{ABOVE}), \\ &PFGB1(3,1) = 1.0, \quad \text{and} \\ &PFGB1(3,2) = NN, \end{aligned} \tag{170}$$

with

$$Z1 = ZW - 0.5 \cdot HWBG - ZPCH + 0.5 \cdot HFG$$
$$\text{and} \qquad (171)$$
$$Z2 = HFGC \cdot (1.0 - RHHV).$$

In this case, the scaling factor ROFGS is calculated using

$$ROFGS = \frac{OFG - \frac{\pi}{2} \cdot DP2^2}{OFGS - \frac{\pi}{2} \cdot DP2^2} \qquad (172)$$

and the scaling is accomplished via iteration by applying the square root of ROFGS in turn to

$$HFG = HFG \cdot \sqrt{ROFGS},$$
$$HFGC = HFGC \cdot \sqrt{ROFGS}, \text{ and} \qquad (173)$$
$$BFG2 = BFG2 \cdot \sqrt{ROFGS}.$$

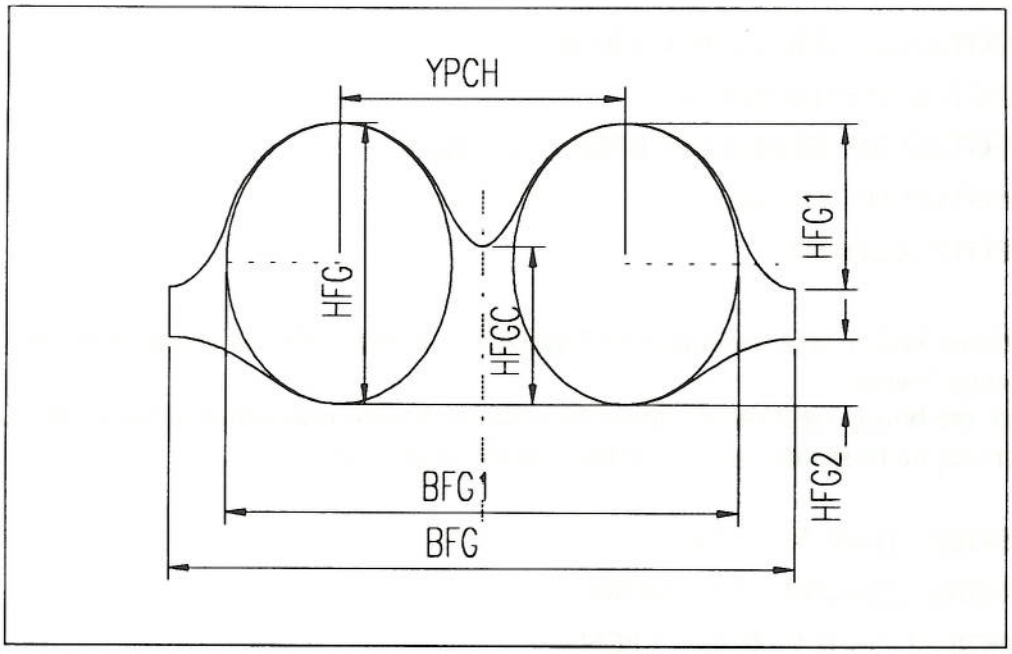

Fig. 34: Fuselage Station G for Twin-Engine Case

4.1.6.8. STATION H

Fuselage station H is located at engine station 3, which is also the entrance to the nozzle. Therefore, its shape depends not only on whether one or two engines are present, but also upon the type of exhaust nozzle chosen, two-dimensional or axisymmetric. The curve fits are again elliptical in form. To begin with, a value for NN is defined using the same criteria as for station G. Then, for axisymmetric nozzles and a single engine, several reference width and height values are calculated:

$$\begin{aligned}
&\mathrm{BFH1} = \mathrm{DP3} + \mathrm{EBP3},\\
&\mathrm{HFH} = \mathrm{DP3} + \mathrm{EHP3},\\
&\mathrm{HFH1} = \mathrm{ZPCH} + 0.5 \cdot \mathrm{HFH} - \mathrm{ZW},\\
&\mathrm{HFH2} = \mathrm{HFH} - \mathrm{HFH1}, \text{ and}\\
&\mathrm{BFH} = \mathrm{BFH1} + 2.0 \cdot \mathrm{blend}(\mathrm{HFH1}, \mathrm{HFH2}, 0.001, \mathrm{ABOVE}) \cdot \tan(\mathrm{QFH1}).
\end{aligned} \tag{174}$$

The elliptical curve fits are made to the upper and lower section. For the top part,

$$\begin{aligned}
&\mathrm{PFHT1}(1,1) = 0.0,\\
&\mathrm{PFHT1}(1,2) = \mathrm{ZW} + 0.5 \cdot \mathrm{HWBH},\\
&\mathrm{PFHT1}(2,1) = 0.5 \cdot \mathrm{BFH},\\
&\mathrm{PFHT1}(2,2) = \mathrm{ZPCH} + 0.5 \cdot \mathrm{HFH} - \mathrm{ZW} - 0.5 \cdot \mathrm{HWBH},\\
&\mathrm{PFHT1}(3,1) = 1.0, \text{ and}\\
&\mathrm{PFHT1}(3,2) = \mathrm{NN}.
\end{aligned} \tag{175}$$

For the lower section,

$$\begin{aligned}
&\mathrm{PFHB1}(1,1) = 0.0,\\
&\mathrm{PFHB1}(1,2) = \mathrm{ZW} - 0.5 \cdot \mathrm{HWBH},\\
&\mathrm{PFHB1}(2,1) = 0.5 \cdot \mathrm{BFH},\\
&\mathrm{PFHB1}(2,2) = \mathrm{blend}\begin{pmatrix} \mathrm{ZW} - 0.5 \cdot \mathrm{HWBH} - \mathrm{ZPCH} + 0.5 \cdot \mathrm{HFH}, \\ 0.0, 0.001, \mathrm{ABOVE} \end{pmatrix},\\
&\mathrm{PFHB1}(3,1) = 1.0, \text{ and}\\
&\mathrm{PFHB1}(3,2) = \mathrm{NN}.
\end{aligned} \tag{176}$$

For the scaling factor,

$$\mathrm{ROFHS} = \frac{\mathrm{OFH} - \frac{\pi}{4} \cdot \mathrm{DP3}^2}{\mathrm{OFHS} - \frac{\pi}{4} \cdot \mathrm{DP3}^2} \tag{177}$$

and it is applied in turn to HFH and BFH1 such that

$$\begin{aligned} &HFH = HFH\sqrt{ROFHS} \\ &\text{and} \\ &BFH1 = BFH1\sqrt{ROFHS}. \end{aligned} \tag{178}$$

For a twin-engined aircraft with axisymmetric nozzles,

$$\begin{aligned} &BFH2 = DP3 + EBP3, \\ &HFH = DP3 + EHP3, \\ &HFH1 = ZPCH + 0.5 \cdot HFH - ZW, \\ &HFH2 = HFH - HFH1, \\ &BFH1 = YPCH + BFH2, \quad \text{and} \\ &BFH = BFH1 + 2.0 \cdot \text{blend}(HFH1, HFH2, 0.001, ABOVE) \cdot \tan(QFH1). \end{aligned} \tag{179}$$

Then,

$$\begin{aligned} &PFHT1(1,1) = 0.5 \cdot YPCH, \\ &PFHT1(1,2) = ZW + 0.5 \cdot HWBH, \\ &PFHT1(2,1) = 0.5 \cdot (BFH - YPCH), \\ &PFHT1(2,2) = ZPCH + 0.5 \cdot HFH - ZW - 0.5 \cdot HWBH, \\ &PFHT1(3,1) = 1.5, \quad \text{and} \\ &PFHT1(3,2) = NN \end{aligned} \tag{180}$$

for the top outer section, and

$$\begin{aligned} &PFHT2(1,1) = PFHT1(1,1), \\ &PFHT2(1,2) = ZW + RHHV \cdot HFHC, \\ &PFHT2(2,1) = 0.5 \cdot BFH2, \\ &PFHT2(2,2) = ZPCH + 0.5 \cdot HFH - PFHT2(1,2), \\ &PFHT2(3,1) = 1.0, \quad \text{and} \\ &PFHT2(3,2) = NN \end{aligned} \tag{181}$$

as well as, for the outer bottom section,

$$
\begin{aligned}
&\text{PFHB1}(1,1) = 0.5 \cdot \text{YPCH},\\
&\text{PFHB1}(1,2) = \text{ZW} - 0.5 \cdot \text{HWBH},\\
&\text{PFHB1}(2,1) = 0.5 \cdot (\text{BFH} - \text{YPCH}),\\
&\text{PFHB1}(2,2) = \text{blend}(\text{Z1}, \text{Z2}, 0.001, \text{ABOVE}),\\
&\text{PFHB1}(3,1) = 1.0 \quad \text{and}\\
&\text{PFHB1}(3,2) = \text{NN},
\end{aligned}
\tag{182}
$$

with

$$
\begin{aligned}
&\text{Z1} = \text{ZW} - 0.5 \cdot \text{HWBH} - \text{ZPCH} + 0.5 \cdot \text{HFH}\\
&\text{and}\\
&\text{Z2} = \text{HFHC} \cdot (1.0 - \text{RHHV}).
\end{aligned}
\tag{183}
$$

A scaling factor is once again defined using

$$
\text{ROFHS} = \frac{\text{OFH} - \frac{\pi}{2}\text{DP3}^2}{\text{OFHS} - -\frac{\pi}{2}\text{DP3}^2}
\tag{184}
$$

and is applied to

$$
\begin{aligned}
&\text{HFH} = \text{HFH}\sqrt{\text{ROFHS}},\\
&\text{HFHC} = \text{HFHC}\sqrt{\text{ROFHS}}, \quad \text{and}\\
&\text{BFH2} = \text{BFH2}\sqrt{\text{ROFHS}}.
\end{aligned}
\tag{185}
$$

In the case of one engine with rectangular (two-dimensional) nozzles,

$$
\begin{aligned}
&\text{BFH1} = \text{BP3} + \text{EBP3},\\
&\text{HFH} = \text{HP3} + \text{EHP3},\\
&\text{HFH1} = \text{ZPCH} + 0.5 \cdot \text{HFH} - \text{ZW},\\
&\text{HFH2} = \text{HFH} - \text{HFH1}, \quad \text{and}\\
&\text{BFH} = \text{BFH1} + 2.0 \cdot \text{blend}(\text{HFH1}, \text{HFH2}, 0.001, \text{ABOVE}) \cdot \tan(\text{QFH1}).
\end{aligned}
\tag{186}
$$

Then, superellipses are fit to the upper and lower sections defined by

$$
\begin{aligned}
&\text{PFHT1}(1,1) = 0.5 \cdot \text{BFH1},\\
&\text{PFHT1}(1,2) = \text{ZW} + 0.5 \cdot \text{HWBH},\\
&\text{PFHT1}(2,1) = 0.5 \cdot \text{BFH},\\
&\text{PFHT1}(2,2) = \text{ZPCH} + 0.5 \cdot \text{HFH} - \text{ZW} - 0.5 \cdot \text{HWBH},\\
&\text{PFHT1}(3,1) = 1.0, \quad \text{and}\\
&\text{PFHT1}(3,2) = \text{NN}
\end{aligned}
\tag{187}
$$

for the upper section an

$$
\begin{aligned}
&\text{PFHB1}(1,1) = 0.5 \cdot \text{BFH1},\\
&\text{PFHB1}(1,2) = \text{ZW} - 0.5 \cdot \text{HWBH},\\
&\text{PFHB1}(2,1) = 0.5 \cdot \text{BFH},\\
&\text{PFHB1}(2,2) = \text{blend}\begin{pmatrix}\text{ZW} - 0.5 \cdot \text{HWBH} - \text{ZPCH} + 0.5 \cdot \text{HFH},\\ 0.0, 0.001, \text{ABOVE}\end{pmatrix},\\
&\text{PFHB1}(3,1) = 1.0, \quad \text{and}\\
&\text{PFHB1}(3,2) = \text{NN}
\end{aligned}
\tag{188}
$$

for the lower section.
The scaling factor is defined as

$$
\text{ROFHS} = \frac{\text{OFH} - \text{BP3} \cdot \text{HP3}}{\text{OFHS} - \text{BP3} \cdot \text{HP3}},
\tag{189}
$$

and it is applied to

$$
\begin{aligned}
&\text{HFH} = \text{HFH}\sqrt{\text{ROFHS}}\\
&\text{and}\\
&\text{BFH1} = \text{BFH1}\sqrt{\text{ROFHS}}.
\end{aligned}
\tag{190}
$$

Similary, for a twin-engined aircraft with axisymmetric nozzles,

$$
\begin{aligned}
&\text{BFH2} = \text{BP3} + \text{EBP3},\\
&\text{HFH} = \text{HP3} + \text{EHP3},\\
&\text{HFH1} = \text{ZPCH} + 0.5 \cdot \text{HFH} - \text{ZW} - 0.5 \cdot \text{HWBH},\\
&\text{HFH2} = \text{HFH} - \text{HFH1} - \text{HWBH},\\
&\text{BFH1} = \text{YPCH} + \text{BFH2}, \quad \text{and}\\
&\text{BFH} = \text{BFH1} + 2.0 \cdot \text{blend}(\text{HFH1}, \text{HFH2}, 0.001, \text{ABOVE}) \cdot \tan(\text{QFH1}).
\end{aligned}
\tag{191}
$$

Then, for the outer upper curve fit,

$$\begin{aligned}
&PFHT1(1,1) = 0.5 \cdot (YPCH + BFH2),\\
&PFHT1(1,2) = ZW + 0.5 \cdot HWBH,\\
&PFHT1(2,1) = 0.5 \cdot (BFH - YPCH - BFH2),\\
&PFHT1(2,2) = ZPCH + 0.5 \cdot HFH - ZW - 0.5 \cdot HWBH,\\
&PFHT1(3,1) = 1.5, \text{ and}\\
&PFHT1(3,2) = NN
\end{aligned} \tag{192}$$

and for the upper inboard curve fit,

$$\begin{aligned}
&PFHT2(1,1) = PFHT1(1,1) - BFH2,\\
&PFHT2(1,2) = ZW + RHHV \cdot HFHC,\\
&PFHT2(2,1) = PFHT1(2,1)\\
&PFHT2(2,2) = ZPCH + 0.5 \cdot HFH - PFHT2(1,2),\\
&PFHT2(3,1) = 1.0, \text{ and}\\
&PFHT2(3,2) = NN.
\end{aligned} \tag{193}$$

Then, the lower section is given by

$$\begin{aligned}
&PFHB1(1,1) = PFHT1(1,1),\\
&PFHB1(1,2) = ZW - 0.5 \cdot HWBH,\\
&PFHB1(2,1) = 0.5 \cdot (BFH - YPCH - BFH2),\\
&PFHB1(2,2) = \text{blend}(Z1, Z2, 0.001, \text{ABOVE}),\\
&PFHB1(3,1) = 1.0, \text{ and}\\
&PFHB1(3,2) = NN,
\end{aligned} \tag{194}$$

with Z1 and Z2 calculated using Equation 183. The scaling factor is defined as

$$ROFHS = \frac{OFH - 2.0 \cdot HP3 \cdot BP3}{OFHS - 2.0 \cdot HP3 \cdot BP3} \tag{195}$$

and is applied as in Equation 185.

4.1.7. THE ENTIRE AIRCRAFT

After having defined the geometry and layout of the major aircraft components as well as the cross-sections of several fuselage reference stations, there remain a number of relationships to be defined which will ensure the correct packaging of the items presented above. Firstly, the longitudinal positioning of the fuselage stations will be described.

The total aircraft length is determined from the maximum of the nozzle length and the location of the trailing edge of either the tailplane or the fin, whichever is the greater. Thus, the empennage is allowed to extend beyond the rear of the aircraft. Based upon the options for flying surface arrangement detailed in Table 2, then

$$LT = \max(XEFLB + CEFB, CETLB + CETB, XFN). \tag{196}$$

However, this length can only be determined after the empennage has been sized, which in turn depends upon the size of fuselage station C.

Next, the aircraft length up to the nozzle exit plane, XFN, is divided into 9 reference stations, the geometry of which has been defined above. For the purpose of integrating the fuselage perimeter to obtain the surface area of the fuselage, the intervals between the reference stations have been divided into a number of intermediate stations, 38 in total. This subdivision will now be described.

The length of the radome, XFR, was given in Equation 5. It is divided into two equally spaced sections of length $\frac{XFR}{2}$. Behind the radome, a radar avionics bay of length LAR as well as the front part of a general avionics bay of length LAX1 are located, so that station A is located at a distance

$$XFA = XFR + LAR + LAX1 \tag{197}$$

from the aircraft nose. The distance between radome and front cockpit bulkhead has been divided into 5 equally spaced sections.

The axial location of station B is determined from the position of the pilot's eyepoint, so

$$XFB = XFA + LCEYE1. \tag{198}$$

The intakes are positioned aft of the pilot's head, and so XFC is equal to XII and

$$XII = XFB + (HC4 + HCEYE) \cdot \tan(QCSEAT). \tag{199}$$

The description of the boundary layer diverter is the same as given by Lovell. Because of the presence of the intakes at XFC, a jump in the cross-sectional area distribution occurs, a discontinuity which is dealt with by defining two fuselage stations at the same longitudinal location (see Ref. 3).

A minimum cockpit floor height is now defined by relating it to the pilot's forward vision requirement. Thus,

$$ZFLOOR = XFA \cdot \tan(QCEYE1) - HC5, \tag{200}$$

assuming that the nose is not drooped to aid in achieving this requirement.

After defining the forward fuselage in the manner described above, station C can now be sized, followed by the definition of the front fuselage chine, assumed to proceed laterally along the nose from the radome to the intake position. Thus,

$$\begin{aligned} &XSI = XII \\ &\text{and} \\ &ZSI = ZW + BIIB \cdot \tan(QWL). \end{aligned} \tag{201}$$

At the intermediate positions (stations A and B as well as the radome), the z-coordinates of the chine are found to be

$$ZSA = (XFA - XFR) \cdot \frac{ZSI}{XSI - XFR} \text{ and} \tag{202}$$

$$ZSB = (XFB - XFR) \frac{ZSI}{XSI - XFR}. \tag{203}$$

Also, for the y-coordinates of the chine, we have

$$YSI = 0.5 \cdot BFC - BIIB \tag{204}$$

and hence

$$YSA = YFR + (XFA - XFR) \cdot \frac{YSI - YFR}{XSI - XFR} \text{ and} \tag{205}$$

$$YSB = YFR + (XFB - XFR) \cdot \frac{YSI - YFR}{XSI - XFR}. \tag{206}$$

Fuselage station D has been described above, and its location is set by using the independent variable XB2C, which is the x-coordinate of the outer weapons bay centre of gravity. Therefore,

$$XFD = XB2C - 0.5 \cdot LB2BI. \tag{207}$$

The fuselage stations coincident with the propulsion bay are defined as per Lovell's report (Ref. 3):

$$\begin{aligned} XFF &= XFN - LPG, \\ XFG &= XFF + LP12, \text{ and} \\ XFH &= XFF + XFF + LP12 + LP23. \end{aligned} \tag{208}$$

The contour of the lower front fuselage between the weapons bay and the radome is found by fitting a Bezier spline between station B and the radome, defined as follows:

$$\begin{aligned} ZFUS(1,1) &= XFR, \\ ZFUS(1,2) &= ZSR - 0.5 \cdot (DAR + EDAR), \\ ZFUS(4,1) &= XFB, \\ ZFUS(4,2) &= ZB1C - 0.5 \cdot HB1BI, \\ G1 &= \frac{ZFUS(1,2)}{ZFUS(1,1)}, \text{ and} \\ G2 &= 0.0. \end{aligned} \tag{209}$$

Having defined the layout of the front fuselage, stations A and B are now synthesized, followed by the definition of the net wing as described by Lovell (Ref. 3) and the determination of the fuel mass in the net wing, used to find an initial landing reference mass for use in the gear sizing and definition of station E, which is positioned at the front of the main gear bay. If the main gear is retracted forward, then

$$XUMB = XWCQM + RLUPCW \cdot CWMA + ELUP - LUMB. \tag{210}$$

Otherwise,

$$XUMB = XWCQM + RLUPCW \cdot CWMA - ELUP. \tag{211}$$

Consequently, XFE=XUMB.

Having now defined all of the axial positions of the fuselage stations, the intake duct geometry is defined using the relationships above, followed by the synthesis of the fuselage cross-sections D through H. The contour of the fuselage spine between C and F is described using a conic-cubic curve fit whose coefficients are stored in the aray FZFCF.

Next, the fuselage wetted area and volume are found by simply integrating along the x-axis the perimeters and cross-sectional areas found during the sizing of the stations. The volume integration follows the method given by Lovell (Ref. 3), as does the volume accounting and mass estimation, with slight modifications outlined below.

4.2. Weapons Bay Mass Estimation

According to the program objectives, modifications were to be undertaken to Lovell's mass estimation methods in order to account for the presence of a weapons bay, while the overall mass estimation methodology remained the same and can be found in

Ref. 3. Two methods were available for this calculation, the first having been developed from work done by Burt and Phillips (Ref. 52) while the second was provided by the DRA.

The first method consists of an estimation of the effect on the aircraft of four parts: the mass of the doors, the mass of the surroundings, including the landings and hinges of the doors, the mass of the weapons bay roof and, finally, the mass of the launcher. The last item is currently an external variable, while the method for predicting the mass of the first three is presented in the following paragraphs.

The mass of the doors is given by the equation

$$MBBID = PNDKG \cdot FMBBI1 \cdot OBBI^{FMBBI2} \cdot VD^{FMBBI3} \qquad (212)$$

where OBBI is the area of the weapons bay door in sq. ft., VD is the design dive speed in knots, and PNDKG is a conversion factor from pounds into kilograms. Factors FMBBI1=0.03644, FMBBI2=0.91863, and FMBBI3=0.78258. This relationship was derived from a curve fit to the chart in Burt and Phillips, using a program for nonlinear regression obtained from Ref. 53 and modified for the multi-variate case. The results of this analysis are shown in Fig. 35. If the doors open into the fuselage, then they will be lighter than if they open into the airstream, but the hinges and mountings will be heavier, the net effect being a reduction in the door mass of 95%.

The mass of the surroundings is given by an equation relating the weapons bay width and length, shown in Equation 213, to the average mass per sq. ft. of the fuselage shell skin-stringer combination, shown in Equation 215.

$$FMBI = OBBI + LBBI + 5.0 \cdot BBBI \qquad (213)$$

The additional mass has contributions from several terms. The first allows for the redistribution of the direct loads. According to Burt and Phillips, the effects of using longerons instead of the original skin approximately cancel each other out, so that the weight of the replacement material is the same as that of the uncut shell.

The second term caters for the redistribution of shear loads, now being carried by extra plating and frames fore and aft of the cutout. In the case of a weapons bay, it is assumed that the roof takes the larger share of the shear loads, and thus this term is replaced by the relationship shown in Fig. 36, relating the weapons bay area in sq. ft. to the roof weight. The graph was approximated using the equation

$$MBBIR = PNDKG \cdot FMBBI4 \cdot OBBI^{FMBBI5}. \qquad (214)$$

where MBBIR is the weight of the roof in kg, PNDKG is again a conversion factor, and OBBI is the area of the weapons bay door in sq.ft. In this equation, FMBBI4=2.00508 and FMBBI5=1.05409.

The last term in Equation 213 caters for the material for the landings. In summary, then, the weight of the material for surrounds excluding the term for the shear loads is given by $MFXAVG \cdot FMBI$, where MFXAVG is the average weight of the skin stringer combination per m^2. The cutout is assumed to be rectangular, and the weight of the

surrounding material is then in kg. The average skin weight is derived from the relationship given by Lovell (Ref. 3) based upon the British Aerospace method by dividing the mass of the fuselage shell by the wetted area of the fuselage:

$$MFXAVG = FMF2\left[0.07232(VD-180)^{0.9} + \frac{0.0000002602 \cdot XFN \cdot ULTN \cdot TPGD^{0.8}}{BFCDH + HFCDH} + 3.7\right] \quad (215).$$

In this equation, FMF2 is a materials factor and ULTN is the ultimate load factor.

In addition to the material needed to carry the fuselage loads around the weapons bay, reinforcements will be needed to carry the missile including its launcher and redistribute the loads into the fuselage structure. While it could be assumed that the missiles will be mounted to existing frames, resulting in only a very small increment in weight, Burt and Phillips suggest using an increment of 30 lb. per 1000 lb. of missile weight. However, they warn that this increment is very approximate and may be significantly in error for loads greater than 10,000 lb. Such loads are unlikely to be carried on the type of aircraft under consideration in this research program. Thus the given increment was adopted.

In summary, the mass effect of the weapons bay is given by

$$EMFBI = MBBID + MBBIR + MFXAVG \cdot FMBI + 0.03 \cdot (MBI + MLI), \quad (216)$$

where MBI and MLI are, respectively, the masses of the internal stores and of the launchers.

The method available from the DRA for estimating the mass effects of a weapons bay is similar to the method of Burt and Phillips in the sense that the mas increment is broken down into contributions from the door, the door mechanism, the weapons support structure, and the fuselage cutout, but the expression for calculating the total door mass includes a function of AMMX, the maximum airframe Mach number.

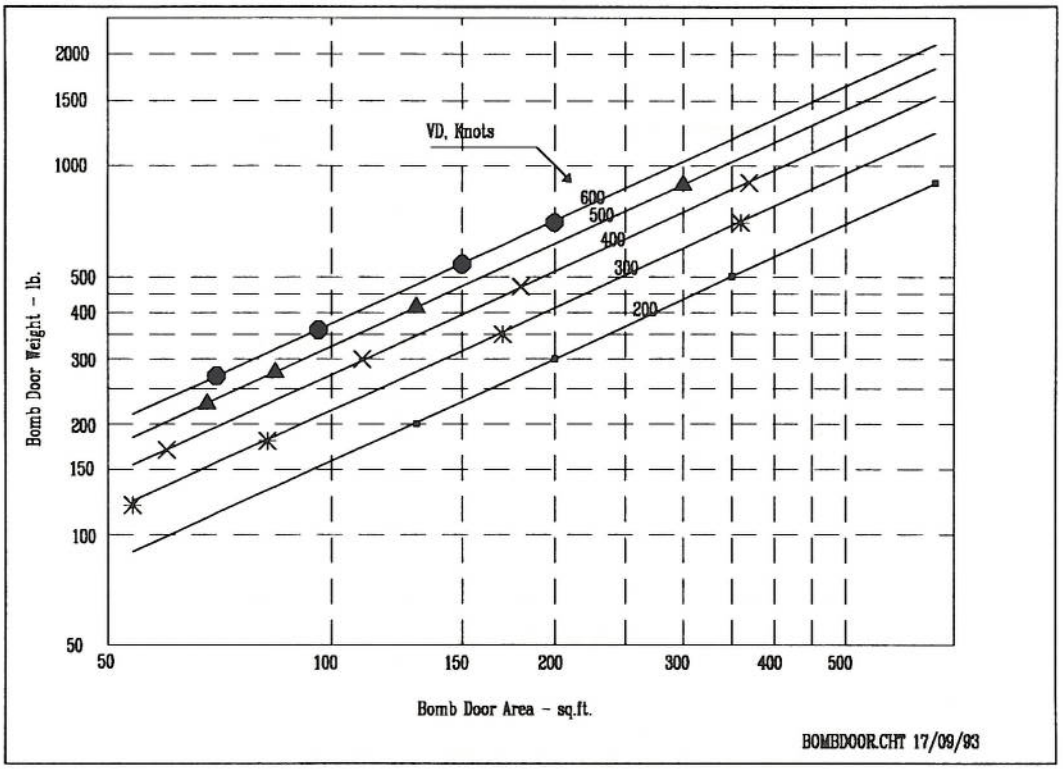

Fig. 35: Bomb Door Weight vs. Area

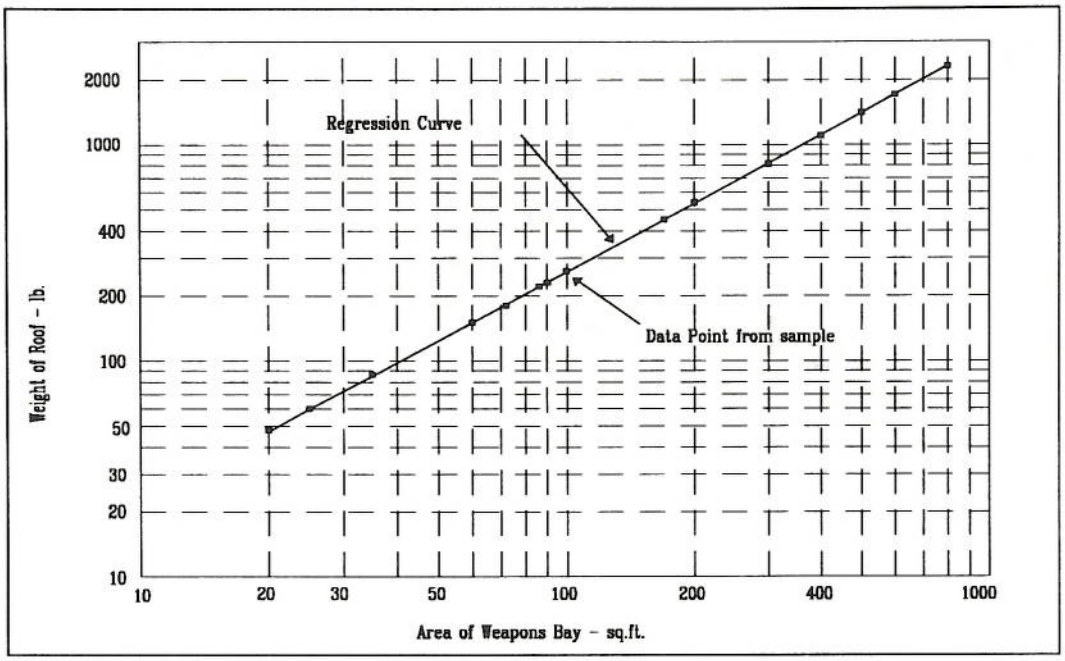

Fig. 36: Weight of the Bomb Bay Roof

5. DISCUSSION

Conceptual design of aircraft involves a compromise between the need for methods allowing quick analyses of aircraft characteristics, often linked together in computerized prototyping tools, and the desire to obtain at as early a stage in the design process as possible the most accurate results conceivable. Traditionally, this has been a very demanding task. While empirically derived algorithms are often simple enough to evaluate with hand-held calculators, the results thus obtained may be significantly in error, particularly when the methods are applied to aircraft configurations which considerably differ from the ones used to compile the formulae. On the other hand, more sophisticated and, in theory, more accurate techniques such as aerodynamic panel, computational fluid dynamics or finite element methods usually suffer from prohibitively high computational cost. The analysis of a single aerodynamic or structural load case may take many hours of processing time, and this does not even take into account the time needed to perform a full scale optimization. Moreover, these methods often require detailed structural or geometric configuration information not available at an early stage in the design.

With this background in mind, the aerodynamic and mass estimation methods given by Lovell (Ref. 3) were assessed in terms of accuracy, applicability, and flexibility. One of the objectives was to determine whether the equations were applicable to the baseline aircraft described in Section 3, designed to closely match Lovell's original concept for swept wing combat aircraft. The results thus obtained were used to recommend modifications to the original synthesis code, which linked the findings of the aerodynamics and mass estimation assessment with the baseline aircraft.

Because of the important role that the aerodynamic prediction methods play in the aircraft conceptual design process, it was appropriate to examine their accuracy by comparing them to experimental data, if available. A number of configurations were chosen which most closely resembled the types of aircraft under consideration. Some of the more important features were a blended shape suitable to a reduced radar cross section design as well as good supersonic cruise characteristics and a relatively simple, straight tapered wing planform. It was not always possible to satisfy all of these conditions simultaneously.

Not surprisingly, it was found that for the subsonic friction drag, transonic and supersonic wave drag, and drag due to lift estimations the given equations (Ref. 3) were sufficiently accurate for use at the conceptual design stage. After all, as demonstrated in Section 2, the methods described by Lovell are based upon empirical studies of experimental data from a variety of aircraft types, many of which are no doubt similar to the configuration used here. Furthermore, methods such as the DATCOM (Ref. 7), used to support Lovell's work, are widely accepted as standards for conceptual design and can safely be assumed to have been compiled with valid data.

On the other hand, it must be pointed out that the more an aircraft concept deviates from ones used in Lovell's report, the less accurate the results become. For example, in the case of DATCOM, the configurations to which the method is applicable generally have a circular or nearly circular fuselage. This premise no longer holds true for stealthy aircraft, as demonstrated in Section 3, and the handbook mentions a variety of

references dealing with the situation of having a non-circular fuselage cross section. There is no conclusive evidence from them as to the quantitative effects upon aerodynamic characteristics, but it can be said that, in general, the greater the ratios either of fuselage width to fuselage height or of fuselage diameter to wing span the greater the impact of the fuselage on the overall lift characteristics of the aircraft. The exact nature of this increase will depend quite significantly upon the shape of the forebody, especially at higher angles of attack, where the shedding of vortices begins to play an important role in the aircraft lift characteristics.

It has emerged from the analysis of the aerodynamics methods that the fuselage shape has a much more significant impact upon the aerodynamics at lifting conditions than upon the drag, with the exception, perhaps, of the induced drag. Clearly, more attention should have been paid during the original code development by Lovell to the prediction of the lift curve slope with respect to angle of attack, and the analysis in Section 2.1.4 has demonstrated the inability of linear theory as proposed by Lovell to deal with the transonic and low supersonic lift cases. While it might be said that at the relatively low angles of attack under consideration during this investigation the exactness of the lift curve shape is not a significant problem, it was shown how the lift curve slope was crucial to the estimation of aircraft angle of attack, which is in turn used for further point performance evaluations and mission analyses, all of which are constraints upon the design variables when an optimizer is linked to the synthesis code.

A similarly detailed analysis of the mass estimation methods was not possible because of the extremely limited amount of data available in the literature and because insufficient time was allocated to this task. Therefore, the work concentrated on examining mass estimation methods for the effect of internal weapons bays, supported by two different sets of equations as given in Section 4.2, one of which was obtained from the Defence Research Agency, the other one being from a Royal Aircraft Establishment report by Burt and Phillips (Ref. 52). An initial comparison showed that the two methods appear to give similar results. This could be due to the fact that the more recent Defence Research Agency method is based in part upon data used to produce the Burt and Phillips method, but the lack of empirical data to validate the results makes any meaningful conclusions very difficult. Nonetheless, S. Simm of the Defence Research Agency has done some studies which show that their method is very good at predicting the correct mass penalty.

As mentioned in Section 2, the basic mass formula for the fuselage is a result of a British Aerospace study for specific aircraft types only. Since the design synthesis by Lovell was developed in the 1980's, it is safe to assume that it reflects the types of aircraft under development at that time, such as the Jaguar or the Tornado, which have well-defined, circular to rectangular cross sections, and is applicable only with caution to other shapes, such as diamond or hexagonal, and only within limits. This conclusion was confirmed by J. Donaldson of the Ministry of Defence, who is in the process of obtaining an updated study from British Aerospace based on more current aircraft types.

Using the information gleaned from the literature search, the baseline aircraft was defined to contain as many as possible of the general features of stealth technology. They include an option for twin canted fins, canted fuselage sides, curved engine intakes to shield the compressor face, aligned leading edges of wing, tailplane and fin, and a chine-shaped forebody, which is also beneficial to high-angle-of-attack characteristics.

Although the method was developed so as to comply as much as possible with the design synthesis of D. Lovell, some of the fuselage cross-section definitions need careful testing in the overall aircraft geometry algorithm to ensure their robustness. For example, it can be seen from the spline definitions in Section 4.1.6 that the choice of vertical fuselage sides will lead to division by zero in, for example, Eq. 85 because in this case QFC1=0. Also, the use of conics for the definition of fuselage coordinates as described in Section 4.1.7 may cause problems when the equations used to find the coefficients contain poles, and Ref. 21 suggests the use of cubics in this case. Even so, depending upon the boundary conditions, cubics may have unwanted inflection points which would not be present when lofting is accomplished by hand. One way around this problem would be the use of splines, which are mathematically much more robust and simpler to calculate.

The current method of defining the vertical location of the wing should also be reassessed with the objective of permitting more variation. By using the engine intake information at station C as the location descriptor, the wing is unnecessarily fixed to the size of the intake. A more suitable method might be to define the fuselage geometry at a fixed axial location and then define the wing vertical coordinate as a percentage of the fuselage height at that station, either as a fixed design parameter or as an external variable to be optimized. In this way a larger variety of configurations, from low to high wing, could be synthesized.

During the development of the fuselage synthesis method as well as the preparation of the computer code care was taken to cater for the requirements of linking the design synthesis with the Defence Research Agency's numerical optimizer. Steps taken included the modularization of the code, allowing the synthesis modules to be called as subroutines, as well as ensuring that the results of the calculations are continuous in the design space, if necessary by using the blending function described by Lovell (Ref. 3). Further testing will be necessary to develop constraints appropriate to this type of aircraft. For example, the scaling of cross-sections might be left to the optimization routine to deal with. Another suggestion is to quantify the degree of engine compressor face masking by the intakes using the separation distance between engine and intake centrelines. Also, the fuselage sides should be canted at an angle close to or equal to that of the fins, and the leading and trailing edges of the wing, tailplane and fin should be aligned when viewed in planform.

6. CONCLUSIONS

An analysis of the aerodynamic and mass properties estimation methods as proposed by D. Lovell was performed as a preliminary step in enhancing the design synthesis of swept wing combat aircraft to include stealth technology. It was found that, in general, the empirically derived aerodynamics prediction equations were adequate and applicable to the more advanced types of aircraft under consideration, especially when the already fairly large uncertainties inherent in the method are taken into account. The lift curve slope estimation method was found to be inadequate, and would need further work, beginning with a sensitivity study to quantify the impact of accurate lift values on the overall design outcome, followed by a choice of method to implement. Furthermore, it was found that the use of the fairing curve as proposed by Lovell (Ref. 3) created difficulties when applied to the synthesis code, and further work is recommended to develop more robust methods of obtaining fuselage cross sections matching a given area distribution. One suggestion would be to determine the fuselage dimensions using geometric constraints derived from the components only, subsequently varying their size and position until a given smooth area distribution is approximated.

A baseline aircraft was defined which takes into account common features of stealthy aircraft, such as twin canted fins and fuselage sides, a relatively flat shape, options for two-dimensional, vectoring engine exhaust nozzles and curved intake ducts to hide the engine face. The extensive use of splines enables a precise geometrical description of the fuselage shape to be made. Weapons may be carried internally, distributed between a maximum of three weapons bays. It is thought that the new design synthesis allows greater flexibility in the choice of aircraft component layouts and geometry descriptions, which could be enhanced by further options allowing overwing or underwing intakes as well as a more precise definition of the size, shape and layout of the landing gear, fuel tanks and gun bay.

Because of the inclusion of thrust vectoring as an option, it is recommended that a more detailed method for the sizing of the control surfaces be implemented. Also, further work is necessary on the centre of gravity calculation, for which a more accurate determination of the fuel distribution within the fuselage might be necessary.

The development of the synthesis code was a complex task due to the large amount of new information necessitating inclusion in the new algorithms. More time should have been allocated to this task, and further work will certainly be necessary to ensure the robustness of the code. Also, extra tasks would need to be carried out in order to provide some desirable features, such as a graphical output and menu-driven input, but the overall code structure is very straightforward due to its modularity so that future modifications or enhancements will be fairly uncomplicated.

In summary, the work undertaken for this research program has produced a detailed survey of the aerodynamics prediction algorithms as well as the development of weapons bay mass estimation methods. A survey of the available unclassified literature on stealth has lead to the definition of a baseline aircraft, with recommendations on enhancements and implementation of modifications to the original design synthesis for swept wing combat aircraft. Further work will be necessary to fully evaluate the merits of the new synthesis code and to validate and enhance further the prediction algorithms

both for mass and aerodynamics, but it is expected that this research program has yielded a useful tool for design analysis and trade-off studies of aircraft incorporating stealth technology.

7. NOTATION

Variable	Description	Eq.	pg.	type[2]
AEFN	Fin aspect ratio	34	47	ev
AETN	Aspect ratio of net tailplane	41	48	ev
AII	Aspect ratio of intake	65	53	ev
AIX	Aspect ratio of diffuser at a given station x	74	54	dv
AMMX	Maximum airframe design Mach number		90	ev
AP4	Ratio of nozzle height to width at exit	51	50	dv
BB1BI	Width overall of internal weapons bay 1	27	45	dv
BB1I	Total width of each store in bay 1	27	45	ev
BB1K	Clearance on width of stores in bay 1	27	45	ev
BB2BI	Width overall of internal weapons bay 2	28	46	dv
BB2I	Total width of each store in bay 2	28	46	ev
BB2K	Clearance on width of stores in bay 2	28	46	ev
BBBI	General width of a weapons bay	213	89	dv
BCH	Minimum width of standard cockpit	13	43	ev
BEFN	Fin span	39	47	dv
BETN	Net span of tailplane (exposed)	41	48	dv
BFA	Width of fuselage at station A	94	62	dv
BFAB	Width of bottom part of fuselage at station A	95	62	dv
BFAT	Width of top part of fuselage at station A	95	62	dv
BFB	Width of fuselage at station B	102	65	dv
BFBB	Width of bottom part of fuselage at station B	103	65	dv
BFBT	Width of fuselage station B at cockpit side	103	65	dv
BFC	Width of fuselage at station C	87	60	dv
BFCDH	Maximum fuselage width	215	90	dv
BFD	Width of fuselage at station D	138	72	dv
BFDB	Width of underside of fuselage station D	137	71	dv
BFDT	Width of fuselage station D, top part, for spline definition	138	72	dv
BFE	Width overall at fuselage station E	152	75	dv
BFE1	Auxiliary height for definition of fuselage splines at station E	146	74	dv
BFEB	Width of fuselage underside at station E	147	74	dv
BFF	Width of fuselage at station F	122	69	dv
BFFB	Width of fuselage underside at station F	116	68	dv
BFFT	Auxiliary width values for defining splines around eng. bay at statn. F	115	67	dv
BFG	Width of fuselage at station G	163	78	dv
BFG1	Width of engine plus clearance at fuselage station G	163	78	dv
BFH	Width of fuselage at station H	174	81	dv
BFH1	Width of engine plus clearance at fuselage station H	174	81	dv
BID	Width of the diffuser at fuselage station D	137	71	dv
BIE	Width of the intake diffuser at fuselage station E	146	74	dv
BII	Width of intake	65	53	dv
BIIB	Width of intake projected into horizontal	67	53	dv
BP3	Width of two-dimensional nozzle at nozzle entrance	55	51	dv
BP4	Width of two-dimensional nozzle at exit	52	50	dv
BUMG	Width of main undercarriage wheel including clearances	116	68	dv
BUMW	Width of main undercarriage wheel	146	74	dv
CEFB	Fin root chord	34	47	dv
CEFM	Mean aerodynamic chord of fin	35	47	dv
CETB	Chord of tailplane at body side	42	48	dv
CETM	Mean aerodynamic chord of tailplane	43	48	dv
CWMA	Aerodynamic mean chord of wing	210	88	dv

[2]This column was compiled by considering three types of variable: 1. ev (external variables) are set as input data. 2. dv (dependent variables) are assigned a value as a result of a calculation within the synthesis code. 3. iv (independent variables) are set as input values, but may be modified by an optimizer linked to the synthesis code.

CWMG	Geometric mean chord of the wing	40	47	dv
DAR	Diameter of the radar dish	2	41	ev
DFC	Equivalent fuselage diameter at station C	31	46	dv
DIE	Diameter of the intake at the exit	70	53	dv
DP1	Diameter of engine at compressor front face	49	49	dv
DP1R	Diameter of reference engine at compressor front face	49	49	ev
DP2	Diameter of engine at front of reheat fuelling section	49	49	dv
DP2R	Diameter of reference engine at front of reheat fuelling section	49	49	ev
DP3	Diameter of engine at entrance to nozzle	49	49	dv
DP3R	Diameter of reference engine at entrance to nozzle	49	49	ev
DP4	Diameter of engine at nozzle exit	49	49	dv
DP4R	Diameter of reference engine at nozzle exit	49	49	ev
DUMG	Diameter of main undercarriage wheel including clearances	116	68	dv
EBP1	Engine bay width clearance at the compressor face	54	50	dv
EBP1H	Maximum value of engine bay width clearance at the compressor face	54	50	ev
EBP1S	Minimum value of engine bay width clearance at the compressor face	54	50	ev
EBP2	Engine bay width clearance at entrance to reheat fuelling	54	50	dv
EBP2H	Maximum value of width clearance at entrance to reheat fuelling	54	50	ev
EBP2S	Minimum value of width clearance at entrance to reheat fuelling	54	50	ev
EBP3	Engine bay width clearance at entrance to nozzle	54	50	dv
EBP3H	Maximum value of width clearance at entrance to nozzle	54	50	ev
EBP3S	Minimum value of width clearance at entrance to nozzle	54	50	ev
EDAR	Clearance on the diameter of the radar dish	2	41	ev
EHC5	Distance between the seat back and the rear cockpit bulkhead	9	43	ev
EHP1	Engine bay height clearance at the compressor face	53	50	dv
EHP1H	Maximum value of engine bay height clearance at the compressor face	53	50	ev
EHP1S	Minimum value of engine bay height clearance at the compressor face	53	50	ev
EHP2	Engine bay height clearance at entrance to reheat fuelling	53	50	dv
EHP2H	Maximum value of height clearance at entrance to reheat fuelling	53	50	ev
EHP2S	Minimum value of height clearance at entrance to reheat fuelling	53	50	ev
EHP3	Engine bay height clearance at entrance to nozzle	53	50	dv
EHP3H	Maximum value of height vlearance at entrance to nozzle	53	50	ev
EHP3S	Minimum value of height clearance at entrance to nozzle	53	50	ev
ELCT	Increment in length between front and rear cockpit	19	44	ev
ELUP	Dist. between main undercarriage pintle and rear or front of u/c bay	210	88	ev
EMFBI	Mass increment due to internal weapons bays	216	90	dv
FBP1K	Factor on engine diameter at the compressor face for width clearance	54	50	ev
FBP2K	Factor on engine diameter at reheat fuelling for width clearance	54	50	ev
FBP3K	Factor on engine diameter at nozzle entrance for width clearance	54	50	ev
FBUMW	Clearance factor on the main undercarriage wheel width	146	74	dv
FFS	Factor on the fuselage width for the chine	2	41	ev
FHP1K	Factor on engine diameter at the compressor face for height clearance	53	50	ev
FHP2K	Factor on engine diameter at reheat fuelling for height clearance	53	50	ev
FHP3K	Factor on engine diameter at nozzle entrance for height clearance	53	50	ev
FHWBF	Factor on height of wing box to allow for carry-through structure	113	67	ev
FLP1K	Factor in correlation for scaling of LP12R	46	49	ev
FLP2K	Factor in correlation for scaling of LP22AR	46	49	ev
FLP3K	Factor in correlation for scaling of LP2B3R	46	49	ev
FLP4K	Factor in correlation for scaling of LP34R	46	49	ev
FMBBI1	Factor in correlation for the weapons bay door mass	212	89	ev
FMBBI2	Exponent in correlation for the weapons bay door mass	212	89	ev
FMBBI4	Factor in correlation of weapons bay roof mass	214	89	ev
FMBBI5	Factor in correlation of weapons bay roof mass	214	89	ev
FMBI	Factor for the mass of the weapons bay structural surroundings	213	89	dv
FMF2	Materials factor on average skin/stringer combination weight	215	90	dv
FMBBI3	Exponent in correlation for the weapons bay door mass	212	89	ev
FYID	Coefficient in calculation of y-coordinate of diffuser centreline	79	55	dv
FZCR	Array of coefficients for cubic of top of rear canopy section	81	59	dv
FZID	Coefficient in calculation of z-coordinate of diffuser centreline	78	55	dv
G1	Gradient used in calculation of curve fits			dv
G2	Gradient used in calculation of curve fits			dv
GCCANR	Gradient in the calculation of the canopy z-coordinate cubic	18	44	dv
GOF1	Gradient of fuselage cross-sectional area distribution at radome	5	42	ev

HB1BI	Height overall of internal weapons bay 1	27	45	dv
HB1I	Total height of each store in bay 1	27	45	ev
HB1K	Clearance on height of stores in bay 1	27	45	ev
HB2BI	Height overall of internal weapons bay 2	28	46	dv
HB2I	Total height of each store in bay 2	28	46	ev
HB2K	Clearance on height of stores in bay 2	28	46	ev
HC1	Distance between thighpoint and eyepoint in standard cockpit	7	42	ev
HC2	Distance between thighpoint and heel point in standard cockpit	6	42	ev
HC3	Distance between thigh point and seat back in standard cockpit	6	42	ev
HC4	Distance between eyepoint and canopy in standard cockpit`	15	43	ev
HC5	Front bulkhead height above cockpit floor	10	43	dv
HC6	Clearance in cockpit for ejection seat escape path	11	43	ev
HC7	Height of pilot's eyepoint above cockpit side	13	43	dv
HCCANS	Maximum height of cockpit canopy above cockpit floor	15	43	dv
HCEYE	Height of the pilot's eyepoint above the cockpit floor	7	42	dv
HCSEAT	Pilot's seating point height above floor measured along the seat back	6	42	ev
HCT	Increment in height between front and rear cockpit	20	44	dv
HFA	Height of fuselage at station A	93	62	dv
HFAB	Height used to define bottom splines at station A	95	62	dv
HFAT	Height used to define top spline at station A	95	62	dv
HFBB	Height of bottom part of fuselage at station B	103	65	dv
HFBT	Height of fuselage side (cockpit side) above chine at station B	103	65	dv
HFC	Height of fuselage at station C	80	59	dv
HFCDH	Maximum fuselage height	215	90	dv
HFD	Height of fuselage at station D	139	72	dv
HFDC	Height of fuselage station D from top of wing box to underside	138	72	dv
HFDT	Height of fuselage top part for spline definition	138	72	dv
HFE	Height of fuselage station E	150	74	dv
HFEC	Height of fuselage station E from underside to wing centreline	150	74	dv
HFET	Height of fuselage station E, top part	150	74	dv
HFFC	Fuselage height at centreline, station F	121	68	dv
HFG	Overall height of fuselage station G	163	78	dv
HFG1	Height of fuselage station G above wing plane	163	78	dv
HFG2	Height of fuselage station G below wing plane	163	78	dv
HFGC	Height of fuselage station G at centreline	169	79	dv
HFH	Overall height of fuselage station H	174	81	dv
HFH1	Height of fuselage station H above wing plane	174	81	dv
HFH2	Height of fuselage station H below wing plane	174	81	dv
HIDBX	Height of diffuser at a given station x	75	54	dv
HIE	Height of intake diffuser at fuselage station E	148	74	dv
HII	Height of intake	65	53	dv
HIIB	Projection of the intake intake height HII into vertical plane	66	53	dv
HP3	Height of two-dimensional nozzle at nozzle entrance	55	51	dv
HP4	Height of two-dimensional nozzle at exit	52	50	dv
HWBE	Height of wing box at fuselage station E	148	74	dv
HWBF	Height of wing box at station F	113	67	dv
HWBG	Height of wing or tailplane box at fuselage station G	164	78	dv
HWBH	Height of taiplane or wing box at fuselage station H	175	81	dv
HWD	Height of the wing box at fuselage station D	138	72	dv
LB1BI	Length overall of internal weapons bay 1	27	45	dv
LB1I	Total length of each store in bay 1	27	45	ev
LB1K	Clearance on length of stores in bay 1	27	45	ev
LB2BI	Length overall of internal weapons bay 2	28	46	dv
LB2I	Total length of each store in bay 2	28	46	ev
LB2K	Clearance on length of stores in bay 2	28	46	ev
LBBI	General length of a weapons bay	213	89	dv
LCCANS	Length of cockpit canopy minus windscreen	16	43	dv
LCEYE1	Horizontal distance between cockpit front bulkhead and pilot's eyepoint	8	43	dv
LCEYE2	Distance of rear pilot's eyepoint from front cockpit bulkhead	22	44	dv
LCFL1	Floor length of front cockpit	9	43	dv
LCFL2	Floor length of rear cockpit	21	44	dv
LCT	Distance of rear cockpit aft of front cockpit bulkhead	19	44	dv
LCWSC	Length of windscreen from front bulkhead	12	43	dv

LEFCQM	Fin moment arm measured from wing mean quarter chord point	31	46	ev
LETCQM	Tailplane moment arm between mean ¼ chord points of wing and tail	40	47	ev
LIDG	Total length of intake diffuser	70	53	dv
LP12	Length of engine gas generator	46	49	dv
LP12R	Length of engine gas generator for reference engine	46	49	ev
LP22A	Length of reheat fuelling section of engine	46	49	dv
LP22AR	Length of reheat fuelling section of reference engine	46	49	ev
LP22B	Engine length between gas generator and transition section	47	49	dv
LP2A4	Length of reheat burning section of engine	46	49	dv
LP2A4R	Length of reheat burning section of reference engine	46	49	ev
LP2B3	Length of transition section for two-dimensional nozzles	46	49	dv
LP2B3R	Length of reference transition section for two-dimensional nozzles	46	49	ev
LP34	Nozzle length	46	49	dv
LP34R	Reference nozzle length	46	49	ev
LPG	Overall length of engine including nozzle	48	49	dv
LT	Total length of aircraft	196	86	dv
LUMB	Length of main undercarriage bay	210	88	dv
MBBID	Mass of the internal weapons bay doors	212	89	dv
MBBIR	Mass of weapons bay roof to carry shear loads	214	89	dv
MBI	Total mass of internal stores in a given bay	216	90	dv
MFXAVG	Average weight of skin/stringer combination of fuselage	215	90	dv
MLI	Total mass of launchers in a given bay	216	90	dv
NBB1I	Number of store stations in width of internal bay 1	27	45	ev
NBB2I	Number of store stations in width of internal bay 2	28	46	ev
NENG	Number of engines (1 or 2)	50	49	ev
NFIN	Number of fins (1 or 2)	34	47	ev
NHB1I	Number of store stations vertically in internal bay 1	27	45	ev
NHB2I	Number of store stations vertically in internal bay 2	28	46	ev
NLB1I	Number of store stations lengthwise in internal bay 1	27	45	ev
NLB2I	Number of store stations lengthwise in internal bay 2	28	46	ev
NWEPB	Number of internal weapons bays		45	ev
OB1BI	Area of cavity for internal weapons bay 1	29	46	dv
OB2BI	Area of cavity for internal weapons bay 2	29	46	dv
OBBI	General area of a weapons bay cavity	213	89	dv
OF1	Cross-sectional area of fuselage at rear of radome	4	41	dv
OFA	Cross-sectional area required by fairing curve at station A	100	64	dv
OFAS	Cross-sectional area at station A	100	64	dv
OFB	Area required by fairing curve at station B	110	66	dv
OFBS	Area at fuselaeg station B	110	66	dv
OFC	Cross-sectional area at station C required by fairing curve	90	61	dv
OFCS	Cross-sectional area at station C	88	60	dv
OFD	Cross-sectional area required by fairing curve at fuselage station D	144	73	dv
OFDS	Cross-sectional area at fuselage station D	142	72	dv
OFE	Cross-sectional area required by fairing curve at fuselaege station E	161	76	dv
OFES	Cross-sectional area at fuselage station E	161	76	dv
OFF	Cross-sectional area required by fairing curve at station F	134	71	dv
OFFS	Cross-sectional area at fuselage station F	132	71	dv
OFG	Cross-sectional area required by fairing curve at fuselage station G	166	78	dv
OFGS	Cross-sectional area at fuselage station G	166	78	dv
OFH	Cross-sectional area required by fairing curve at fuselage station H	177	81	dv
OFHS	Cross-sectional area of fuselage station H	177	81	dv
OIE	Cross-sectional area of intake exit	71	54	dv
OII	Cross-sectional area of intake streamtube	71	54	dv
OISX	Area of enclosing parallelogram at diffuser station x	76	54	dv
OIX	Cross-sectional area of inlet at a given x-position	71	54	dv
OIXD	Cross-sectional area of intake diffusers at fuselage station D	144	73	dv
OIXE	Cross-sectional area of intake diffusers at fuselage station E	161	76	dv
OP1B	Cross-sectional area of engine bay at compressor face	56	51	dv
OP2B	Cross-sectional area of engine bay at entrance to reheat fuelling	56	51	dv
OP2BB	Cross-sectional area of engine bay at entrance to transition section	58	51	dv
OP3B	Cross-sectional area of engine bay at nozzle entrance	56	51	dv
OPN	Nozzle exit area	50	49	dv
OVI	Cross sectional area of boundary layer diverter at station C	90	61	dv

PFAB1	Array containing Bezier control points for bottom spline 1 at B	99	63	dv
PFAB2	Array containing Bezier control points for bottom spline 2 at B	97	63	dv
PFAT1	Array containing Bezier conrtol points for top spline 1 at A	98	63	dv
PFAT2	Array containing Bezier control points for top spline 2 at A	96	63	dv
PFBB1	Array containing Bezier control points for bottom spline 1 at station B	108	66	dv
PFBB2	Array containing Bezier control points for bottom spline 2 at station B	109	66	dv
PFBT1	Array containing Bezier control points for top spline 1 at station B	104	65	dv
PFBT2	Array containing Bezier control points for top spline 2 at station B	107	66	dv
PFC	Perimeter of fuselage at station C	89	61	dv
PFCT1	Array containing Bezier control points for top spline at station C	85	60	dv
PFCT2	Array containing Bezier control points for bottom spline at station C	85	60	dv
PFD	Perimeter of fuselage at station D	143	73	dv
PFDT1	Array containing Bezier control points for top spline 1 at station D	140	72	dv
PFDT2	Array containing Bezier control points for top slpine 2 at station D	141	72	dv
PFEB1	Array containing Bezier control points for bottom spline 1 at station E	158	76	dv
PFEB2	Array containing Bezier control points for bottom spline 2 at station E	159	76	dv
PFET1	Array containing Bezier control points for top spline 1 at station E	151	74	dv
PFET2	Array containing Bezier control points for top spline 2 at station E	153	75	dv
PFET3	Array containing Bezier control points for top spline 3 at station E	154	75	dv
PFET4	Array containing Bezier control points for top spline 4 at station E	157	76	dv
PFF	Perimeter of fuselage at station F	133	71	dv
PFFB1	Array containing Bezier control points for bottom spline 1 at station F	131	70	dv
PFFT1	Array containing Bezier control points for top spline 1 at station F	125	69	dv
PFFT2	Array containing Bezier control points for top spline 2 at station F	126	69	dv
PFFT3	Array containing Bezier control points for top spline 3 at station F	127	70	dv
PFFT4	Array containing Bezier control points for top spline 4 at station F	128	70	dv
PFGB1	Array containing the coeff. of a superellipse at station G	165	78	dv
PFGT1	Array containing the coeff. of a superellipse at station G	164	78	dv
PFGT2	Array containing the coeff. of a superellipse at station G, twin-engine	169	79	dv
PFHB1	Array containing coefficients of superellipse at fuselage station H	176	81	dv
PFHT1	Array containing coefficients of superellipse at fuselage station H	175	81	dv
PFHT2	Array containing coefficients of a superellipse at fuselage station H	181	82	dv
PFR	Perimeter of fuselage at rear of radome	3	41	dv
PFRT	Array holding the Bezier coefficients at rear of radome	2	41	dv
PNDKG	Conversion factor from pounds into kilogram	212	89	ev
QCEYE1	Pilot's downward vision angle in standard cockpit	10	43	ev
QCEYE2	Pilot's upward vision angle in standard cockpit	11	43	ev
QCEYE3	Pilot's side and downward vision angle	13	43	ev
QCEYE4	Rear cockpit forward downward vision angle	20	44	ev
QCFOOT	Angle between the line joining the thigh-heel points and the horizontal	6	42	dv
QCSEAT	Angle of back of ejection seat	6	42	ev
QCWSC	Windscreen inclination angle	14	43	dv
QEF	Fin cant angle (for twin fins)	32	46	ev
QEFL	Fin leading edge sweep	37	47	ev
QETL	Tailplane leading edge sweep	44	48	ev
QFC1	Angle of fuselage side at station C, top section	85	60	ev
QFD1	Angle between fuselage side and vertical at station D	140	72	ev
QFD2	Angle of fuselage side above wing plane with horizontal at station D	138	72	ev
QFD3	Angle between fuselage side at bottom to vertical, fuselage station D	138	72	ev
QFE1	Angle between fuselage side and vertical at E, top part	152	75	ev
QFE2	Angle between fuselage and horizontal, top part	153	75	ev
QFE3	Angle between fuselage side and horizontal at E, bottom part	158	76	dv
QFE4	Angle between fuselage side and vertical at E, bottom part	152	75	ev
QFG1	Angle between fuselage side and vertical at fuselage station G	163	78	ev
QFH1	Angle between fuselage side and vertical at fuselage station H	174	81	ev
QFS	Angle to the vertical of the fuselage side	2	41	ev
QID1	Angle between vertical and intake side	66	53	ev
QID2	Angle between horizontal and bottom of intake	66	53	ev
QIX1	Angle between side of diffuser and vertical at station x	72	54	dv
QIX2	Angle between bottom of diffuser and the horizontal at station x	73	54	dv
RCCAN	Radius of cockpit canopy	91	61	ev
REFSW	Vertical tail volume coefficient	31	46	dv
RETSW	Horizontal tail volume coefficient	40	47	ev

RHHV	Ratio of fuselage sections above and below wing plane at centreline	121	68	dv
RLUPCW	Undercarriage c.g. pos. aft of mean ¼ chord point as fract. of AMC	210	88	ev
ROFAS	Scaling factor on cross-sectional area at station A	100	64	dv
ROFBS	Scaling factor on fuselage cross-sectional area at station B	110	66	dv
ROFCNS	Scaling factor on net cross-sectional area at station C	90	61	dv
ROFDS	Scaling factor on cross-sectional area at fuselage station D	144	73	dv
ROFES	Scaling factor on cross-sectional area at fuselage station E	161	76	dv
ROFFS	Scaling factor on cross-sectional area at fuselage station F	134	71	dv
ROFGS	Scaling factor on cross-sectional area at fuselage station G	166	78	dv
ROFHS	Scaling factor on cross sectional area at fuselage station H	177	81	dv
ROIDX	Ratio of the area of the enclosing parallelogram to the intake area	70	53	dv
RTEF	Fin thickness to chord ratio	39	47	ev
RTP	Engine scale factor	46	49	iv
SEFN	Fin planform area	32	46	dv
SEFNH	Projection of fin planform area into horizontal plane	33	46	dv
SEFNV	Projection of the fin planform area into the vertical plane	31	46	dv
SETN	Planform area of horizontal stabilizer	40	47	dv
SW	Gross wing area	40	47	iv
TPGD	Maximum sea-level static thrust of the engine with reheat	215	90	dv
UEFF	Factor for the utilization of fin volume for fuel storage	39	47	ev
UEFN	Fin taper ratio	34	47	ev
UETN	Taper ratio of net tailplane	42	48	ev
ULTN	Ultimate load factor	215	90	dv
VB1BI	Volume of internal weapons bay 1	30	46	dv
VB2BI	Volume of internal weapons bay 2	30	46	dv
VD	Design dive speed in knots	212	89	ev
VEFF	Volume of fin	39	47	dv
VFR	Volume of radome	5	42	dv
VP12B	Volume of engine gas generator	59	52	dv
VP23B	Volume of engine reheat fuelling and burning section	60	52	dv
VP2B3B	Volume of transition section from to two-dimensional exhaust nozzle	63	52	dv
VP34B	Volume of engine exhaust nozzle	61	52	dv
VPB	Volume of entire engine	64	52	dv
WFR	Wetted area of radome	5	42	dv
XEFLB	Distance of fin leading edge at fin root aft of aircraft nose	38	47	dv
XEFM	Distance along x-axis of fin mean ¼ chord point from fin leading edge	37	47	dv
XETLB	Distance of tailplane leading edge at tailplane root aft of aircraft nose	45	48	dv
XETM	Distance along x-axis of tailplane mean ¼ chord point from tailplane l.e.	44	48	dv
XFA	X-coordinate of fuselage station A	197	86	dv
XFB	X-coordinate of fuselage station B	198	86	dv
XFC	X-coordinate of fuselage station C	81	59	dv
XFD	X-coordinate of fuselage station D	207	87	dv
XFE	X-coordinate of fuselage station E		88	dv
XFF	X-coordinate of fuselage station F	208	88	dv
XFG	X-coordinate of fuselage station G	208	88	dv
XFH	X-coordinate of fuselage station H	208	88	dv
XFN	Distance of nozzle exit plane aft of aircraft nose	196	86	iv
XFR	X-coordinate of fuselage station containing radar dish	5	42	dv
XID	X-coordinate of any diffuser station measured from intake front	70	53	dv
XID1	X-coordinate of diffuser centreline at end of forward section	78	55	dv
XID2	X-coordinate of diffuser centreline at end of aft section	78	55	dv
XII	X-coordinate of intake, measured from aircraft nose	199	86	dv
XSI	X-coordinate of rear of front fuselage chine	201	87	dv
XUMB	X-coordinate of front of main undercarriage bay	210	88	dv
XWCQM	Distance of wing mean quarter chord point from aircraft nose	31	46	ev
YFA	Y-coordinate of chine at station A	94	62	dv
YID	Y-coordinate of diffuser centreline a station D	137	71	dv
YID1	Y-coordinate of diffuser centreline at end of forward section	78	55	dv
YID2	Y-coordinate of diffuser centreline at end of aft section	78	55	dv
YIDC	Y-coordinate of intake centre measured from lower inboard corner	69	53	dv
YIDX	Y-coordinate of diffuser centreline at any station x	77	54	dv
YIXE	Horizontal separation distance between intake diffusers at station E	147	74	dv
YPCH	Separation distance between engine centrelines	115	67	dv

YSA	Y-coordinate of fuselage chine at station A	205	87	dv
YSB	Y-coordinate of fuselage chine at station B	206	87	dv
YSI	Y-coordinate of the rear of the front fuselage chine	204	87	dv
ZB1C	Z-coordinate of centre of gravity of weapons bay 1	80	59	iv
ZCCANR	Z-Coordinate of canopy top at aircraft centreline	17	44	dv
ZDATWB	Datum Z-coordinate used in dimensioning of fuselage station F	112	67	dv
ZEFM	Distance along z-axis of mean aerodynamic chord from fin root	36	47	dv
ZFD	Z-coordinate of the fuselage top at station D, centreline	139	72	dv
ZFE	Z-coordinate of fuselage top centreline at station E	150	74	dv
ZFEBP	Z-coordinate of fuselage underside at station E, at diffuser centreline	148	74	dv
ZFETC	Z-coordinate of fuselage spine at station E	157	76	dv
ZFFTC	Z-coordinate of fuselage top at station F, centreline	121	68	dv
ZFFTP	Z-coordinate of fuselage top above propulsion bay at station F	116	68	dv
ZFLOOR	Z-coordinate of cockpit floor	200	86	dv
ZFUS	Array for z-coordinate of fuselage underside between A and C	93	62	dv
ZID1	Z-coordinate of diffuser centreline at end of forward section	78	55	dv
ZID2	Z-coordinate of diffuser centreline at end of aft section	78	55	dv
ZIDC	Z-coordinate of intake centre measured from lower inboard corner	68	53	dv
ZIDX	Z-coordinate of diffuser centreline at any station x	77	54	dv
ZIXE	Z-coordinate of diffuser centreline at fuselage station E	149	74	dv
ZPCH	Z-coordinate of engine bay	113	67	dv
ZSA	Z-coordinate of chine at station A	202	87	dv
ZSB	Z-coordinate of fuselage chine at station B	203	87	dv
ZSI	Z-coordinate of rear of front fuselage chine	201	87	dv
ZW	Z-coordinate of wing	86	60	dv

8. REFERENCES

1. *Jane's All the World's Aircraft 1989-90*. Jane's Information Group Ltd., 1989.
2. Kehayas, N.: ASTOVL Combat Aircraft Design Synthesis and Optimization. PhD Thesis, Cranfield Institute of Technology, 1992.
3. Lovell, D.A.: The Application of Multivariate Optimization to Combat Aircraft Design. RAE TR 88003, January 1988.
4. Serghides, V.C.: Design Synthesis for Canard-Delta Combat Aircraft. PhD Thesis, Cranfield Institute of Technology, 1987.
5. Eminton, E. and W.T. Lord: Note on the Numerical Evaluation of the Wave Drag of Smooth Slender Bodies Using Optimum Area Distributions for Minimum Wave Drag. *Journal of the Royal Aeronautical Society*, January 1956, Vol. 60, pp. 61-63.
6. Barger, R.L.: A Method for Designing Blended Wing-Body Configurations for Low Wave Drag. NASA TP 3261, Sept. 1992.
7. *United States Air Force Stability and Control DATCOM (Data Compendium)*. McDonnell-Douglas Corp., October 1960.
8. Nicolai, L.M. *Fundamentals of Aircraft Design*. METS, Inc., USA, 1984.
9. Pitts, W.C., J.N. Nielsen and G.E. Kaattari: Lift and Center of Pressure of Wing-Body-Tail Combinations at Subsonic, Transonic, and Supersonic Speeds. NACA Report 1307, 1957.
10. Vukelich, S.R. and J.E. Williams jr.: Wing-Body Carryover at Supersonic Speeds With Finite Afterbodies. AIAA 81-4413, *AIAA Journal*, Vol 19, No. 5, May 1981, pp 661-664.
11. Erickson, G.E. and J.M. Brandon: On the Nonlinear Aeodynamic and Stability Characteristics of a Generic Chine-Forebody Slender Wing Fighter Configuration. AIAA 87-2617, 1987.
12. Jorgensen, L.H.: Inclined Bodies of Various Cross Sections at Supersonic Speeds. NASA MEMO 10-3-58A, November 1958.
13. Bielat, R.P., D.E. Harrison and D.A. Coppolino: An Investigation at Transonic Speeds of the Effects of Thickness Ratio and of Thickened Root Sections on the Aerodynamic Characteristics of Wings with 47° Sweepback, Aspect Ratio 3.5 and Taper Ratio 0.2 in the Slotted Test Section of the Langley 8-Foot High-Speed Tunnel. NACA RM L51I04a.
14. Dollyhigh, S.M.: Subsonic and Supersonic Longitudinal Stability and Control Charatceristics of an Aft Tail Fighter Configuration with Cambered and Uncambered Wings and Uncambered Fuselage. NASA TM X-3078, August 1974.

15. Morris, O.A.: Subsonic and Supersonic Characteristics of a Supersonic Cruise Fighter Model With a Twisted and Cambered Wing With 74° Sweep. NASA TM X-3530, August 1977.

16. Dollyhigh, S.M.: Experimental Aerodynamic Characteristics at Mach Numbers From 0.60 to 2.70 of Two Supersonic Cruise Fighter Configurations. NASA TM 78764, February 1979.

17. Hicks, R.E. and E.J. Hopkins: Effects of Spanwise Variation of Leading Edge Sweep on the Lift, Drag, and Pitching Moment of a Wing-Body Combination at Mach Numbers from 0.7 to 2.94. NASA TN D-2236, April 1964.

18. Shrout, B.L.: Aerodynamic Characteristics at Mach Numbers from 0.6 to 2.16 of a Supersonic Cruise Fighter Configuration with a Design Mach Number of 1.8. NASA TM X-3559, September 1977.

19. Schlichting, H. and E. Truckenbrodt: *Aerodynamik des Flugzeuges*. 2nd Edition, Springer-Verlag, 1967, Vols. 1 and 2.

20. Sears, W.R.: On Projectiles of Minimum Wave Drag. *Quarterly of Applied Mathematics,* Vol. 4, No. 4, 1946, pp. 361-366.

21. Skrobanski, J.J. and D.A. Lovell: A Conic-Cubic Method for Curve Fitting and Function Interpolation. RAE Technical Memo Aero 2025, August 1985.

22. Nicolai, L.M. and F. Sanchez: Correlation of Wing-Body Combination Lift Data. *Journal of Aircraft,* Vol. 10, No. 2, February 1973, pp. 126-128.

23. Aircrew Station Geometry for Military Aircraft. MIL-STD-1333B, U.S. Dept. of Defense, Wasington D.C., 9 January 1987.

24. Dimensions, Basic, Cockpit, Stick Controlled, Fixed-Wing Aircraft. Military Statndard MS33574 Rev. B, U.S. Dept. of Defense, 25 August 1987.

25. U.K. Ministry of Defence DEF STAN 00-970: Chapter 104, View and Clear Vision.

26. Staton, R.N.: Fuselage Basic Shell Weight Prediction. SAWE Paper 1019, May 1974.

27. Knott, E.F.; J.E. Shaeffer and M.T. Tuley: *Radar Cross Section. Its Prediction and Measurement*. Artech House Inc., 1985.

28. Ruck, G.T.; D.E. Barrick, W.D. Stuart, and C.K. Kirchbaum: *Radar Cross Section Handbook*. Plenum Press, New York, 1970, Vols. 1 and 2.

29. Fuhs, A.E.: *The No-See-Um Book: Radar Cross Section Lectures*. American Institute of Aeronautics and Astronautics, New York, 1982.

30. James, R.M.: Slenderness Approximations in RCS Estimation - The Simplest 2-D Case. IEEE Transactions on Antennas and Propagation, Vol. 40, No. 2, February 1992, pp. 149-155.

31. Klement, D.: Streuung an komplizierten Objekten: Berechnung des Radarrückstrahlverhaltens von metallischen Körpern mit Hilfe der physikalischen Optik. DFVLR FB 85-22, March 1985.

32. Shelton, jr., R.: *Team Stealth F-117*. Airlife Publishing Ltd, England, 1993.

33. *The World's Great Stealth and Reconnaissance Aircraft.* Aerospace Publishing, England, 1991.

34. Boileau, jr., O.C.: B-2 Stealth Bomber. The Royal Aeronautical Society's 37th R.J. Mitchell Lecture, Southampton, March 1993.

35. Burns, J.W.: Introduction to Stealth Technology and Aircraft Weight Penalties. SAWE Journal, Fall 1993, pp. 40-58.

36. Howe, D.: Introduction to the Basic Technology of Stealth Aircraft. ASME Paper 90-GT-116 (Part 1) and 90-GT-116 (Part 2), presented at the Gas Turbine and Aeroengine Congress and Exposition, June 11-14, 1990.

37. Lindsey, G.: The Tactical and Strategic Significance of Stealth Technology. Centre québécois de relations internationales, 1989.

38. SWEPT/STEALTH Program Setup Meeting Notes, March 29, 1993 (unpublished).

39. Gal-Or, B.: Fundamentals and Similarity Transformations of Vectored Aircraft. *Journal of Aircraft*, Vol. 31, No. 1, Jan.-Feb. 1994, pp. 181-187.

40. Poisson-Quinton, Ph.: Einige physikalische Betrachtungen über das Ausblasen an Tragflügeln. *Jahrbuch der Wissenschaftlichen Gesellschaft für Luftfahrt e.V.*, 1956, pp. 29-51.

41. Siestrunck, R.: General Theory of the Jet Flap in Two-Dimensional Flow. *Boundary Layer and Flow Control, its Principles and Applications,* (G.V. Lachmann, ed.), 1961, Vol. 1, pp. 342-364.

42. Herrick, P.W.: Air Combat Payoffs of Vectoring/Reversing Exhaust Nozzles. AIAA 88-3239, AIAA/ASME/SAE/ASEE 24th Joint Propulsion Conference, July 11-13, 1988, Boston, Massachusetts.

43. Kitowski, J.V.: Fighter Airframe/Propulsion Integration - A General Dynamics Perspective. AIAA-92-3332, 1992.

44. Mace, J. and G. Nyberg: Fighter Airframe/Propulsion Integration - A McDonnell Douglas Aircraft Perspective. AIAA-92-3333, 1992.

45. Cain, A.B. and P.M. Doane: A Methodology for the Analysis and Modelling of Thrust Vectoring Usage. AIAA-92-0389, 30th Aerospace Sciences Meeting and Exhibit, January 6-9, 1992, Reno, Nevada.

46. Capone, F.J.: Effects of Nozzle Exit Location and Shape on Propulsion-Induced Aerodynamic Characteristics Due to Vectoring Twin Nozzles at Mach Numbers from 0.4 to 1.2. NASA TM X-3313, January 1976.

47. Stevens, H.L., E.B. Thayer and J.F. Fullerton: Development of the Multi-Function 2-D/C-D Nozzle. AIAA-81-1491. AIAA/SAE/ASME 17th Joint Propulsion Conference, July 27-29, 1981, Colorado Springs, Colorado.

48. Whitford, R.: *Design for Air Combat.* Jane's Information Group, Ltd., 1987.

49. Mangold, P.: Some Aerodynamic/Flight Mechanic Aspects for the Design of Future Combat Aircraft. ICAS-82-1.1.3. In *Proceedings of the 13th Congress of the ICAS*, Seattle, WA, Aug. 22-27, 1982, Vol. 1, pp. 34-43.

50. Wilson, B.: Lecture Notes on Lessons Learned: Navy Advanced Tactical Fighter. Lecture given at Cranfield Institute of Technology,

51. Foley, J.D., A. van Dam, S.K. Feiner, J.F. Hughes: *Computer Graphics Principles and Practice*. Addison-Wesley Publising Company, 1990.

52. Burt, M.E. and J. Phillips: Prediction of Fuselage and Hull Structure Weight. RAE Report Structures 122, April 1952.

53. Press, W.H., B.P. Flannery, S.A. Teukosky, et.al.: *Numerical Recipes: The Art of Scientific Computing (FORTRAN version)*. Cambridge University Press, 1989.

54. Ravi, R. and W.H. Mason: Chine-Shaped Forebody Effects on Directional Stability st High-α. *Journal of Aircraft,* Vol. 31, No. 3, May-June 1994, pp. 480-487.

9. BIBLIOGRAPHY

9.1. GENERAL

Baals, D.D., A.W Robins, R.V. Harris: Aerodynamic Design Integration of Supersonic Aircraft. AIAA-68-1018, 1968.

Bocvarov, S., E.M. Cliff and F.H. Lutze: Significance of the Dihedral-Effect for a Combat Aircraft in Rapid Fuselage Reorientation Maneuvers. AIAA-92-4490-CP, in 1992 AIAA Atmospheric Flight Mechanics Conference, Part 1.

Huenecke, K.: *Modern Combat Aircraft Design*. Airlife Publishing Ltd., 1987.

Morris, S.J. and I.L. Kroo.: Aircraft Design Optimization With Multidisciplinary Performance Criteria. In AIAA/ASME/ASCE/AHS/ASC 30th Structural Dynamics and Materials Conference, Part 2, pp. 909-919, 1989.

Nastase, A.: Optimum-optimorum Integrated Wing-Fuselage Configuration for Supersonic Transport Aircraft of Second Generation. ICAS-86-1.3.6 (ICAS Proceedings, 15th International Congress, pp. 324-342, 1986).

9.2. AERODYNAMICS

Adams, Mac.C.: Determination of Boattail Bodies of Revolution for Minimum Wave Drag. NACA-TN-2550, August, 1951.

Bangert, L.S. and G.T. Carson: Effect of Afterbody Geometry on Aerodynamic Characteristics of Isolated Nonaxisymmetric Afterbodies at Transonic Mach Numbers. NASA TP 3236, September, 1992.

Barbantini, E., A. Ferretti and A. Gatti: Mass Flow Effects on the Low Speed Characteristics of an Advanced Combat Aircraft. in AGARD-CP-498, Oct. 1991.

Barger, R.L.: An Analytical Procedure for Computing Smooth Transitions Between Two Specified Cross Sections With Applications to Blended Wing-Body Configurations. NASA TP 2012, 1982.

Barger, R.L.: A Procedure for Designing Forebodies With Constraints on Cross Section Shape and Axial Area Distribution. NASA TP 1881, 1981.

Barger, R.L. and M.S. Adams: Automatic Computation of Wing Fuselage Intersection Lines and Fillet Inserts With Fixed Area Constraint. NASA TM 4406, March 1993.

Barger, R.L. and M.S. Adams: Fuselage Design for a Specified Mach-Sliced Area Distribution. NASA TP 2975.

Bielat, R.P.: A Transonic Wind-Tunnel Investigation of the Aerodynamic Characteristics of Three 4-Percent-Thick Wings of Sweepback Angles 10.8°, 35°, and 47°, Aspect Ratio 3.5, and Taper Ratio 0.2 in Combination with a Body. NACA RM L52B08.

Bielat, R.P., D.E. Harrison and D.A. Coppolino: An Investigation at Transonic Speeds of the Effects of Thickness Ratio and of Thickened Root Sections on the

Aerodynamic Characteristics of Wings with 47° Sweepback, Aspect Ratio 3.5 and Taper Ratio 0.2 in the Slotted Test Section of the Langley 8-Foot High-Speed Tunnel. NACA RM L51I04a.

Darden, C.M.: Sonic Boom Minimization With Nose Bluntness Relaxation. NASA TP 1348, January 1979.

Dollyhigh, S.M.: Experimental Aerodynamic Characteristics at Mach Numbers From 0.60 to 2.70 of Two Supersonic Cruise Fighter Configurations. NASA TM 78764, February 1979.

Dollyhigh, S.M., W.J. Monta and G. Sangiorgio: Longitudinal Aerodynamic Characteristics at Mach 0.60 to 2.86 of a Fighter Configuration With Strut Braced Wing. NASA TP 1102, December 1977.

Dollyhigh, S.M., O.A. Morris and M.S. Adams: Experimental Effect of Fuselage Camber on Longitudinal Aerodynamic Characteristics of a Series of Wing-Fuselage Configurations at a Mach Number of 1.41. NASA TM X-3411, October 1976.

Driver, C: Aerodynamic Characteristics at Supersonic Speeds of a Series of Wing-Body Combinations Having Cambered Wings with an Aspect Ratio of 3.5 and a Taper Ratio of 0.2. Effect at Mach = 2.01 of Nacelle Shape and Position on the Aerodynamic Characteristics in Pitch of Two Wing-Body Combinations with 47° Sweptback Wings. NACA RM L52F03.

Hamilton, C.V.: Aerodynamic Characteristics at Supersonic Speeds of a Series of Wing-Body Combinations Having Cambered Wings with an Aspect Ratio of 3.5 and a Taper Ratio of 0.2. Effects of Sweep Angle and Thickness Ratio on the Static Lateral Stability Characteristics at M = 2.01. NACA RM L52E23, 1952.

Hamwi, S.: Approximate Method for Predicting the Lifting Characteristics of Wing-Body Combinations. PhD Thesis, Cranfield Institute of Technology, 1989.

Harris, R.V.: A Numerical Technique for Analysis of Wave Drag at Lifting Conditions. NASA TN D-3586, October 1966.

Hasel, L.E. and J.R. Sevier, Jr.: Aerodynamic Characteristics at Supersonic Speeds of a Series of Wing-Body Combinations Having Cambered Wings with an Aspect Ratio of 3.5 and a Taper Ratio of 0.2. Effect at M = 1.60 of Nacelle Shape and Position on the Aerodynamic Characteristics in Pitch of Two Wing-Body Combinations with 47° Sweptback Wings. NACA RM L51K14a.

Hicks, R.E. and E.J. Hopkins: Effects of Spanwise Variation of Leading Edge Sweep on the Lift, Drag, and Pitching Moment of a Wing-Body Combination at Mach Numbers from 0.7 to 2.94. NASA TN D-2236, April 1964.

Holdaway, G. and J.A. Mellenthin: Investigation at Mach Numbers of 0.2 to 3.50 of Blended Wing-Body Combinations of Sonic Design with Diamond, Delta, and Arrow Plan Forms. NASA TM X-372.

Holdaway, G. and J.A. Mellenthin: Investigation at Mach Numbers of 0.60 to 3.50 of Blended Wing-Body Combinations With Cambered and Twisted Wings With Diamond, Delta and Arrow Planforms. NASA TM X-390, October 1960.

Holdaway, G. and J.A. Mellenthin: Evaluation of Blended Wing-Body Combinations With Curved Planforms at Mach Numbers up to 3.50. NASA TM X-379, October 1960.

Hopkins, E.J., R.M. Hicks and R.L. Carmichael: Aerodynamic Characteristics of Several Cranked Leading-Edge Wing-Body Combinations at Mach Numbers from 0.4 to 2.94. NASA TN D-4211, October 1967.

Jones, R.T.: Theory of Wing Body Drag at Supersonic Speeds. NACA Report 1284, 1956

Joosen, C.J.J. and H.A. Sytsma: Application of the NLR Panel Method to a Swept-Wing/Body Combination with Part-Span Flaps at Low Speeds and Comparison with Experimental Results. NLR TR 80030 U.

Kaufman, L.G. and R.L. Clark: Mach 0.6 to 3.0 Flows over Rectangular Cavities. AFWAL-TR-82-3112, May 1983.

Lomax, H. and L. Studer: Chordwise and Compressibility Corrections to Slender-Wing Theory. NACA Report 1105, 1952.

Malmuth, N., C.C. Wu and J.D. Cole: Transonic Wave Drag Estimation and Optimization Using the Nonlinear Area Rule. Journal of Aircraft, Vol. 24, No. 3, March 1987.

Maughmer, M.D.: An Experimental Investigation of Wing/Fuselage Integration Geometries. AIAA-87-2937, September 1987.

McLemore, H.C. and L.P. Parlett: Low Speed Wind Tunnel Tests of a 1/10-Scale Model of a Blended-Arrow Supersonic Cruise Aircraft. NASA TN D-8410, June 1977.

Middleton, W.D. and H.W. Carlson: Numerical Method of Estimating and Optimizing Supersonic Aerodynamic Characteristics of Arbitrary Planform Wings. Journal of Aircraft, Vol. 2, No. 4, July-August 1965, pp. 261-265.

Middleton, W.D. and J.L. Lundry: A System for Aerodynamic Design and Analysis of Supersonic Aircraft. Part 1: General Description and Theoretical Development. NASA CR 3351, Dec. 1980.

Robins, A.W., M. Lamb and D.S. Miller: Aerodynamic Characteristics at Mach Numbers of 1.5, 1.8 and 2.0 of a Blended Wing-Body Configuration with and without Integral Canards. NASA TP 1427, May 1979.

Robinson, R.B.: Aerodynamic Characteristics at Supersonic Speeds of a Series of Wing-Body Combinations Having Cambered Wings with an Aspect Ratio of 3.5 and a Taper Ratio of 0.2. Effects of Sweep Angle and Thickness Ratio on the Aerodynamic Characteristics in Pitch at M = 2.01. NACA RM L52E09.

Robinson, R.B. and C. Driver: Aerodynamic Characteristics at Supersonic Speeds of a Series of Wing-Body Combinations Having Cambered Wings with an Aspect Ratio of 3.5 and a Taper Ratio of 0.2. Effects of Sweepback Angle and Thickness Ratio on the Aerodynamic Characteristics in Pitch at M = 1.60. NACA RM L51K16a.

Shrout, B.L.: Aerodynamic Characteristics at Mach Numbers from 0.6 to 2.16 of a Supersonic Cruise Fighter Configuration with a Design Mach Number of 1.8. NASA TM X-3559, September 1977.

Spearman, M.L. and J.H. Hilton, Jr.: Aerodynamic Characteristics at Supersonic Speeds of a Series of Wing-Body Combinations Having Cambered Wings with an Aspect Ratio of 3.5 and a Taper Ratio of 0.2. Effects of Sweep Angle and Thickness Ratio on the Static Lateral Stability Characteristics at M=1.60. NACA RM L51K15a.

Walkley, K.B. and G.E. Smith: Wave Drag Analysis of Realistic Fighter Aircraft Using a Full Potential Method. AIAA-86-2627.

9.3. AIRFRAME

Anderson, B.W.: Factors Affecting the Design of Military Aircraft Structures in Carbon Fibre Reinforced Composites. in 6th International Conference on Fracture Research (Fracture 84), Pergamon Press, Oxford, 1986, pp. 607-622.

Avery, J.G., T.R. Porter and R.W. Walter: Designing Aircraft Structure for Resistance and Tolerance to Battle Damage. AIAA Paper 72-773, 1972.

Burt, M.E.: Structural Weight Estimation for Novel Configurations. RAE Report Structures 270, December 1961.

Burt, M.E.: Effects of Design Speed and Normal Acceleration on Aircraft Structure Weight. ARC CP 490, 1960.

Elgee, D., S. Johnston and B. Ginty: Design and Manufacture of SPF Aluminum Components for Military Aircraft. Superplasticity in Aerospace - Aluminum, Cranfield Press, Cranfield, 1985, Ch. 23, pp. 407-423.

Florentine, R.A.: Characteristics of 3D Braided Composites: Status of Structure-Property Design Data for Magnaweave-Reinforced Carbon-Epoxy Aircraft Composites. 21st International SAMPE Technical Conference, September 15-28, 1989.

Lemmer, L. and G. Kagerbauer: The Design Development of the Monolithic CFRP Centre Fuselage Skin of the European Fighter Aircraft. 37th International SAMPE Symposium, March 9-12, 1992, pp. 747-759.

Macci, S.H.M.: Aircraft Wing Weight Prediction. MSc Thesis, Cranfield Institute of Technology, 1988.

Middleton, D.H. (ed.): Composite Materials in Aircraft Structures. Longman Scientific and Technical, 1990.

Ripley, R.E.: A Method of Fuselage Structure Weight Prediction. RAE Report Structures 93, November 1950.

Ripley, R.E.: A Simple Method for Tail Unit Structure Weight Prediction. RAE Report Structures 94, November 1950.

Ripley, R.E.: A Method of Wing Weight Prediction. RAE Report Structures 109, May 1951.

Soovere, J.: The Effect of Acoustic Thermal Environments on Advanced Composite Fuselage Technology. AIAA-83-0955.

Zamani, M.M. et. al.: Design Considerations for Superplastically Formed Complex Aircraft Structures. 31st International SAMPE Symposium, April 7-10, 1986.

9.4. PROPULSION

Bissinger, N.C., T.J. Benson and R.G. Bradley: AGARD WG13 "Aerodynamics of High Speed Air Intakes": Assessment of CFD Results. in AGARD-CP-498, October 1991.

Bowers, D.L. and J.A. Langhrey: Survey on Techniques Used in Aerodynamic Nozzle/Airframe Integration. in AGARD-CP-498.

Gal-Or, B.: Vectored Propulsion, Supermaneuverability and Robot Aircraft. Springer-Verlag, 1990.

Goldsmith, E.L.: Some Aspects of Intake Design, Performance and Integration with the Airframe. in AGARD-CP-498, October 1991.

Herrick, P.W.: Fighter/Aircraft Propulsion Integration. AIAA-86-2658, 1986.

Hinz, W.W. and Miller, E.H.: Propulsion Integration of a Supersonic Cruise Strike Fighter. AIAA-79-0100, 1979.

Intake Aerodynamics. Von Karman Institute Lecture Series, 1988-04, Vol. 1+2, Rhode Saint Genese, Belgium, February 1988.

Joubert, H. and J.L. Eyrand: Analyse en Vol de la Compatibilité Entrée d'Air-Moteur. in AGARD-CP-498, October 1991.

Liston, G.W. and L.L. Small: Fighter Airframe/Propulsion Integration - A Wright Laboratory Perspective. AIAA-92-3337.

Mace, P., P. Smerecniak, G. Krekeler, D. Bowers, M. MacLean and E. Thayer: Advanced Thrust Vectoring Nozzles for Supercruise Fighter Aircraft. AIAA-89-2816, July 1989.

Maggio, R.: Water Tunnel Studies of Inlet/Airframe Interference Phenomena. in AGARD-CP-498, October 1991.

Mattingley, J.: Easy Method of Matching Fighter Engine to Airframe for Use in Aircraft Engine Design Courses. AIAA-89-2260, 25th Joint Propulsion Conference, July 10-12, 1989.

Mishler, R. and T. Wilkinson: Emerging Airframe/Propulsion Integration Technologies at General Electric. AIAA-92-3335, July 1992.

Meyer, W., W. Pazur and L. Fottner: The Influence of Intake Swirl Distortion on the Steady-State Performance of a Low Bypass, Twin-Spool Engine. in AGARD-CP-498, October 1991.

Aerodynamics of Power Plant Installation. AGARD-CP-301, 1981.

Putnam, L.E. and C.E. Mercer: Pitot-Pressure Measurements in Flow Fields Behind a Rectangular Nozzle with Exhaust Jet for Free-Stream Mach Numbers of 0.00, 0.60, and 1.20. NASA TM 88990, 1986.

Mackrodt, P.A., E.L. Goldsmith, I. MacGregor, J. Leynaert, F. Garçon and J. Brill: Comparative Performance Tests of a Pitot-Inlet in Several European Wind-Tunnels at Subsonic and Supersonic Speed. in AGARD-CP-498, October 1991.

9.5. STEALTH

Brown, A.C.: Fundamentals of Low Radar Cross-Sectional Aircraft Design. Journal of Aircraft, Vol. 30, No. 3, May-June 1993, pp. 289-290.

Fulgham, D.A.: Signature Reduction Key to A-10 Survival. Aviation Week and Space Technology, June 7, 1993, pp. 135-136.

Coatings Fool Radar, Human Eye. Aviation Week and Space Technology, June 7, 1993, pp 136-137.

Trueman, C.W., S.J. Kubina, S.R. Mishra and C. Larose: RCS of Four Fuselage-Like Scatterers at HF Frequencies. IEEE Transactions on Antennas and Propagation, Vol. 40, No. 2, February 1992, pp. 236-240.

Wilson, B.: Lecture Notes on F20 and NATF. Lecture held at Cranfield Institute of Technology on May 21, 1993.

10. APPENDIX A: BEZIER SPLINES

This appendix describes the methodology used to fit Bezier splines to the fuselage cross-sections defined in Section 4.1.6. The relationships presented below were derived from a representation of Bezier splines given by Foley et. al. in Ref. 51.

Firstly, an array was defined as given in Table A1 which contains the four Bezier control points.

Point	x-coordinate	z-coordinate
1	SPL(1,1)	SPL(1,2)
2	SPL(2,1)	SPL(2,2)
3	SPL(3,1)	SPL(3,2)
4	SPL(4,1)	SPL(4,2)

Table A1: Definition of Array for Bezier Spline

Figure A1 shows how the points defined in Table A1 are calculated. Points 2 and 3 would generally be located separately, but for ease of computation, it was decided to collocate them.

In the design synthesis code, two routines are defined: one to fit the Bezier spline given points 1 and 4 as well as the gradients of the lines joining 1 with 2 and 4 with 3, stored in G1 and G2, respectively, and another routine to evaluate the area enclosed between the reference axes and the Bezier curve. The latter routine differentiates between the area located above or below the curve, depending upon whether the Bezier is located below or above the x-axis.

More specifically, the subroutine BEZFIT obtains as paramers the array SPL as well as the gradients G1 and G2, and calculates the intermediate control points 2 and 3 from the following set of equations.

First, a check is made to prevent division by zero:

$$\mathrm{DELTA} = \mathrm{G1} - \mathrm{G2} \tag{220}$$

If DELTA is not equal to zero, then

$$\mathrm{XX1} = \frac{\mathrm{Y2} - \mathrm{Y1} + \mathrm{G1} \cdot \mathrm{X1} - \mathrm{G2} \cdot \mathrm{X2}}{\mathrm{DELTA}} \tag{221}$$

and

$$\mathrm{YY1} = \mathrm{G1} \cdot (\mathrm{XX1} - \mathrm{X1}) + \mathrm{Y1}, \tag{222}$$

where X1 is equivalent to SPL(1,1), Y1 is equivalent to SPL(1,2), X2 is equivalent to SPL(4,1) and Y2 is equivalent to SPL(4,2). If DELTA is equal to zero, then

$$XX1 = \frac{X2 - X1}{2.0}$$

and (223)

$$YY1 = \frac{Y2 - Y1}{2.0} \quad .$$

The values stored in XX1 and YY1 correspond to the x and y coordinates, respectively, of points 2 and 3.

In order to evaluate the area underneath the Bezier curve, the interval from X1 to X2 is divided into n equally spaced steps of size Δ:

$$\Delta = \frac{1.0}{n} \quad . \tag{224}$$

A series of function evaluations is made for each of the n steps using the Bezier polynomial defined in Equation 225:

$$X(t) = (1-t)^3 \cdot X_1 + 3t(1-t)^2 \cdot X_2 + 3t^2(1-t) \cdot X_3 + t^3 \cdot X_4 \quad . \tag{225}$$

Variable t is a value between 0 and 1 found by multiplying the ith step of the Bezier evaluation with Δ:

$$t = i \cdot \Delta. \tag{226}$$

Equation 225 can be evaluated for the y-coordinate by substituting X_1 through X_4 with Y_1 through Y_4. In this case, X_1 corresponds to SPL(1,1), X_4 corresponds to SPL(4,1), and so on. The actual area calculation is performed using a simple trapezoidal integration scheme, as shown schematically in Fig. A1, where dA is the increment in area.

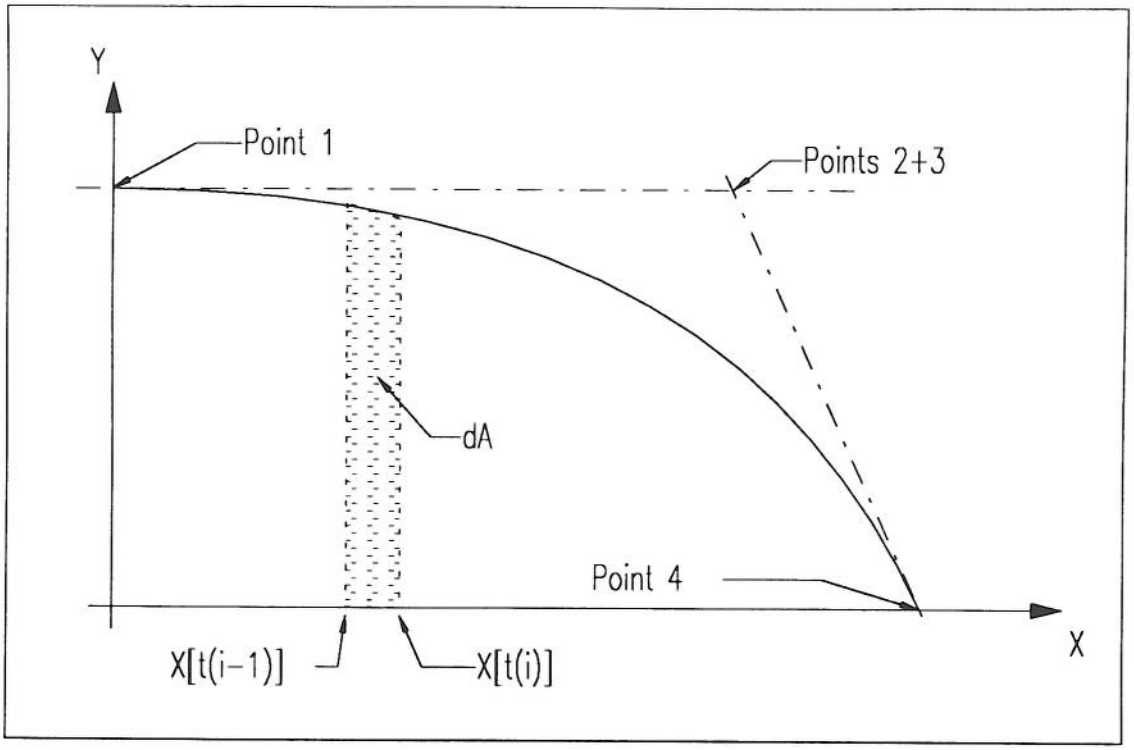

Fig. A1: Geometry Definition for Bezier Splines

11. APPENDIX B: SUPERELLIPSE

This appendix describes the algorithm used to fit a superellipse to a given fuselage station.

As described in the main text of this report, a fuselage station making use of superellipses is divided into sections such that the coefficients describe the curve in one quadrant of the Cartesian coordinate system only. The basic superellipse equation is

$$\left(\frac{x}{a}\right)^{2+m}+\left(\frac{y}{b}\right)^{2+n}=1\,, \tag{227}$$

and the corresponding geometrical interpretation is given by Fig. B1 below. In Equation 227, m and n are parameters which control the shape of the curve in the 1st quadrant of the coordinate system. More information can be found in Ref. 54.

An array was defined which contains the coefficients a, b, m, and n of the superellipse as well as the location of the origin. a and b, the semiaxes of the ellipse, are chosen to match the geometry requirements of each individual fuselage station. Table B1 shows how the coefficients are allocated to the array variable fields within the program code.

Field	Function
(1,1)	X-coordinate of origin
(1,2)	Y-coordinate of origin
(2,1)	semiaxis A (x-axis)
(2,2)	semiaxis B (y-axis)
(3,1)	m in exponent of x-coordinate
(3,2)	n in exponent of y-coordinate

Table B1: Definition of superellipse array

In order to evaluate the area enclosed by the curve and the vertical and horizontal axis as well as the perimeter of the superellipse section, Equation 227 is rewritten to obtain

$$y=b\cdot\left[1-\left(\frac{x}{a}\right)^{2+m}\right]^{\frac{1}{2+n}}. \tag{228}$$

By dividing the x-axis into a series of equally spaced intervals, a simple numerical, trapezoidal integration scheme is used to evaluate the enclosed area and the perimeter.

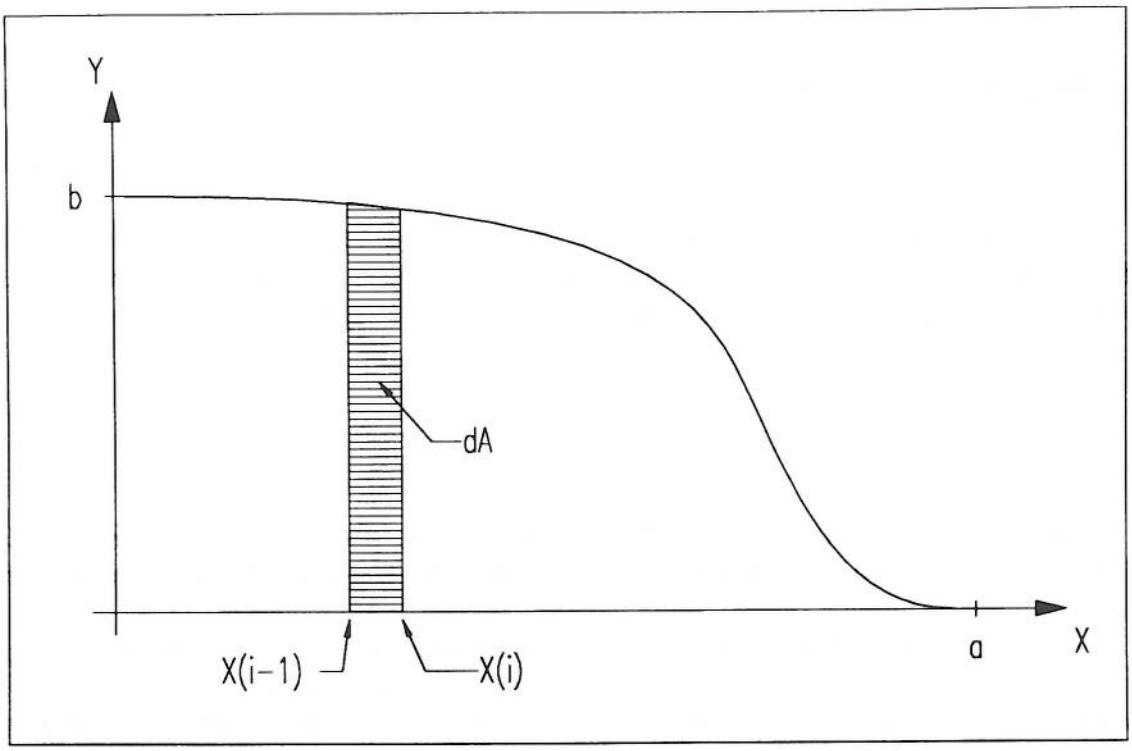

Fig. B1: Schematic Definition of Superellipse Geometry

Overall Security Classification of page | UNCLASSIFIED

1. Originator's report number.

College of Aeronautics Report No. 9402

2. Originator's Name and Location.

Cranfield University
College of Aeronautics
Dept. of Aerospace Technology
Cranfield Bedford MK43 0AL
United Kingdom

3. Contract number and period covered.

FRN1c/405, April 1993 until September 1994

4. Sponsor's name and location.

Aircraft System Performance Dept.
Defence Research Agency
Farnborough, United Kingdom

5. Report Classification

Unclassified

6. Date/Pagination/Refs.

October 1994 / 129 / 54

7a. Report Title:

Design Synthesis for Swept-Wing Combat Aircraft Incorporating Stealth Technology

7b. Security classification of title:

Unclassified

8. Author:

Frank Siegers

9. Descriptors/Key Words:

Combat Aircraft - Design Synthesis - Stealth

10. Abstract:

Changes in the military procurement environment have meant that combat aircraft must often meet a much wider range of threats and requirements. Apart from the multi-mission role expected of them, stealth technology has become one of the more important drivers behind the aircraft design process. This raises the need for more up-to-date analysis tools which take into account the advanced features of such aircraft. As part of a wider-ranging investigation into the effects of stealth technology on aircraft characteristics, Cranfield University has developed a design synthesis tool which allows the incorporation and analysis of stealth features into aircraft design trade-off studies. A literature survey was conducted in order to select aircraft parameters related to stealth and to determine the feasibility of incorporating them into the preliminary design process. As a supporting measure, an analysis of an existing aircraft design tool was conducted, focusing primarily on the mass and aerodynamics estimation methods. A baseline aircraft was developed by recommending and implementing modifications to the original design synthesis tool.

10a. Security classification of abstract: Unclassified